Article

Upper Triassic Carbonate Records: Insights from the Most Complete Panthalassan Platform (Lime Peak, Yukon, Canada)

Nicolò Del Piero [1,*], Sylvain Rigaud [1], Camille Peybernes [1], Marie-Beatrice Forel [2], Nicholas Farley [1] and Rossana Martini [1]

[1] Department of Earth Sciences, University of Geneva, 13 Rue des Maraichêrs, 1205 Geneva, Switzerland; sylvain.rigaud@hotmail.fr (S.R.); camille.peybernes@unige.ch (C.P.); nicholas.farley@unige.ch (N.F.); rossana.martini@unige.ch (R.M.)

[2] Centre de Recherche en Paléontologie—Paris (CR2P), Muséum National d'Histoire Naturelle, 8 rue Buffon, 75005 Paris, France; marie-beatrice.forel@mnhn.fr

[*] Correspondence: nicolo.delpiero@aol.com

Abstract: Upper Triassic carbonate platforms from the Panthalassa Ocean remain less-understood and less-studied than their Tethyan equivalents. This imbalance is largely due to the poorer preservation state of Panthalassan carbonate rock successions in terms of rock quality and depositional geometries, which prevents good appreciation of depositional systems. In this context, carbonate exposures from Lime Peak (Yukon, Canada) represent an outstanding exception. There, the remains of an Upper Norian Panthalassan carbonate platform are well-exposed, show remarkably preserved depositional geometries and overall superior rock preservation. In this work, we analyse the carbonates from the Lime Peak area with particular attention to the vertical and lateral distribution of biotic assemblages and microfacies at the platform scale. Results demonstrate that the Lime Peak platform was surrounded by a basin with an aphotic sea bottom. The carbonate complex developed in warm waters characterized by high carbonate saturation. The area was also defined by moderate to high nutrient levels: this influenced the type of carbonate factory by favouring microbialites and sponges over corals. During its growth, Lime Peak was influenced by tectono-eustatism, which controlled the accommodation space at the platform top, primarily impacting the internal platform environments and the stability of the slope. Gaining better knowledge of the spatial distribution and dynamics of Upper Triassic organisms and sedimentary facies of Panthalassa in relation to tectono-eustatism lays the first foundations for reconstructing more robust platform models and understanding the evolution of other, more dismantled Upper Triassic Panthalassan carbonate systems through time.

Keywords: Upper Triassic; carbonate platform; Panthalassa; paleoecology; Benthic Foraminifera

1. Introduction

The study of carbonate platforms and their systems, evolution and paleobiogeography is crucial to understanding the coevolution of life and the Earth. Carbonate platforms host more than 25% of marine life [1] and are very sensitive to climatic, oceanographic and bathymetric changes. Despite their importance, our knowledge on Upper Triassic shallow-water carbonates is fragmentary, and mainly derives from the study of Tethyan carbonate systems (e.g., see [2–14]). Upper Triassic carbonate platforms from the substantially larger Panthalassan domain [15] remain understudied, providing a minor source of information for the general comprehension of Upper Triassic carbonates. Shallow-water Panthalassan carbonates were mostly born as isolated carbonate platforms in island-arc settings, micro-continents or seamounts ([16] and reference therein). Nowadays, the remnants of these carbonate platforms are largely found in accretionary complexes along the Circum-Pacific region ([16] and reference therein) in the form of small fragments within allochthonous breccias or conglomerates, or as larger but intensely deformed and dislocated blocks in the midst of sedimentary mélanges. In such a context, the overall level of preservation of

these carbonates is extremely low due to their common dismantling prior to and during their accretion (e.g., see [17,18]) and subsequent tectonic and metamorphic complications along their accretionary path and thereafter [19,20]. These characteristics, together with the fact that outcrops of Panthalassan carbonates are often in remote locations, explain why they remain largely understudied compared to their Tethyan counterparts. With the objective of closing this knowledge gap, the REEFCaDe (REEF and Carbonate Development) scientific project was launched at the University of Geneva fourteen years ago. Over this timeframe, various Upper Triassic Panthalassan localities were investigated in the Russian Far East [17,21], Japan [18,22–30], the United States [30–41], Mexico [42–44] and Canada [45–47]. Several aspects of the taxonomy, paleoecology, stratigraphy and distribution of diverse organisms in Panthalassa, including foraminifera (e.g., [26,30,35–40,46]), calcareous algae [48], ostracods [47], halobiid bivalves [41,45] and reef biota [22], have been clarified in the framework of this long-term effort.

The carbonate rocks of the Lime Peak area (Yukon, Canada; Figure 1) were first described by Tempelman-Kluit [49], who recognized the reef-related nature of some bodies whose age was later constrained to the early to late Norian by conodont biostratigraphy [50]. Following up these first investigations, the area was later the object of a PhD thesis during the first half of the 1980s. This PhD work [51] led to several publications that focused on multiple facets of these carbonates, including their sedimentology, palaeontology and micropalaeontology [50–61]. Continuing these first investigations, Yarnell et al. [53] described the paleontological assemblages of several localities of the Whitehorse region, including Lime Peak, and later Yarnell [54] evaluated the importance of such assemblages in terms of paleogeography. More recently, several publications have focused on the micropaleontology of the Lime Peak area, describing the ostracods assemblages [47], the calcareous algae [48] and a new species of agglutinated foraminifera (*Taanella yukonensis*) that is very common in the deposits of the area [46].

Among the Upper Triassic localities of the Panthalassa, Lime Peak stands out since the carbonate rocks outcropping here are relatively well-preserved and show remarkable vertical and lateral (locally exceeding the kilometre) continuity (Figure 1D). In particular, this last characteristic makes Lime Peak one of the few places in the world where the original depositional geometries of Upper Triassic carbonate bodies can be studied. The sedimentological investigations carried out during the 1980s emphasised facies description and reconstruction of the depositional history of the Lime Peak complex [51,52,55]. This work focuses on Lime Peak's nicely preserved geometries to study in detail the vertical and platform-to-basin distribution of carbonate facies and platform-dwelling organisms. We particularly focus on foraminiferal assemblages and reef biotas, which have already been proven to be important palaeoecological and biostratigraphic tools (e.g., see [17]). Implications in term of carbonate factory, palaeoecology and paleogeography are discussed below.

2. Geological Context

The North American Cordillera is more than 70% composed of an amalgamation of allochthonous crustal fragments and oceanic remnants that have been distinctly mapped as coherent tectonostratigraphic terranes [62–65]. Most of these terranes were originally formed in the Panthalassa Ocean and were accreted onto the North American craton during the Mesozoic ([62–64] and references therein; Figure 1A). Even though there is general agreement regarding their exotic nature with respect to the North American craton, there are still many uncertainties regarding their original paleogeographic position, ante-accretion path and the total amount of post-accretion terrane displacement [64,66–73]. Most of south-central Yukon and British Columbia is underlaid by the Intermontane terranes belt ([64,74] and references therein; Figure 1B) that represents the largest assemblage of amalgamated terranes that accreted onto the North American margin during the Mesozoic [62,64]. The core of this Intermontane terranes belt is formed by the Mesozoic rocks of Stikinia and Quesnellia, which bound the Cache Creek accretionary complex [65,74]. The Cache Creek terrane, ranging in age from Upper Palaeozoic to Lower Jurassic, is made up of a mélange of

rocks formed in variegate oceanic settings (i.e., spreading ridge, atoll, oceanic plateau and trench fill: see [75]). On the other hand, Stikinia and Quesnellia are remnants of island-arcs built in the Panthalassa Ocean during the Mesozoic [76].
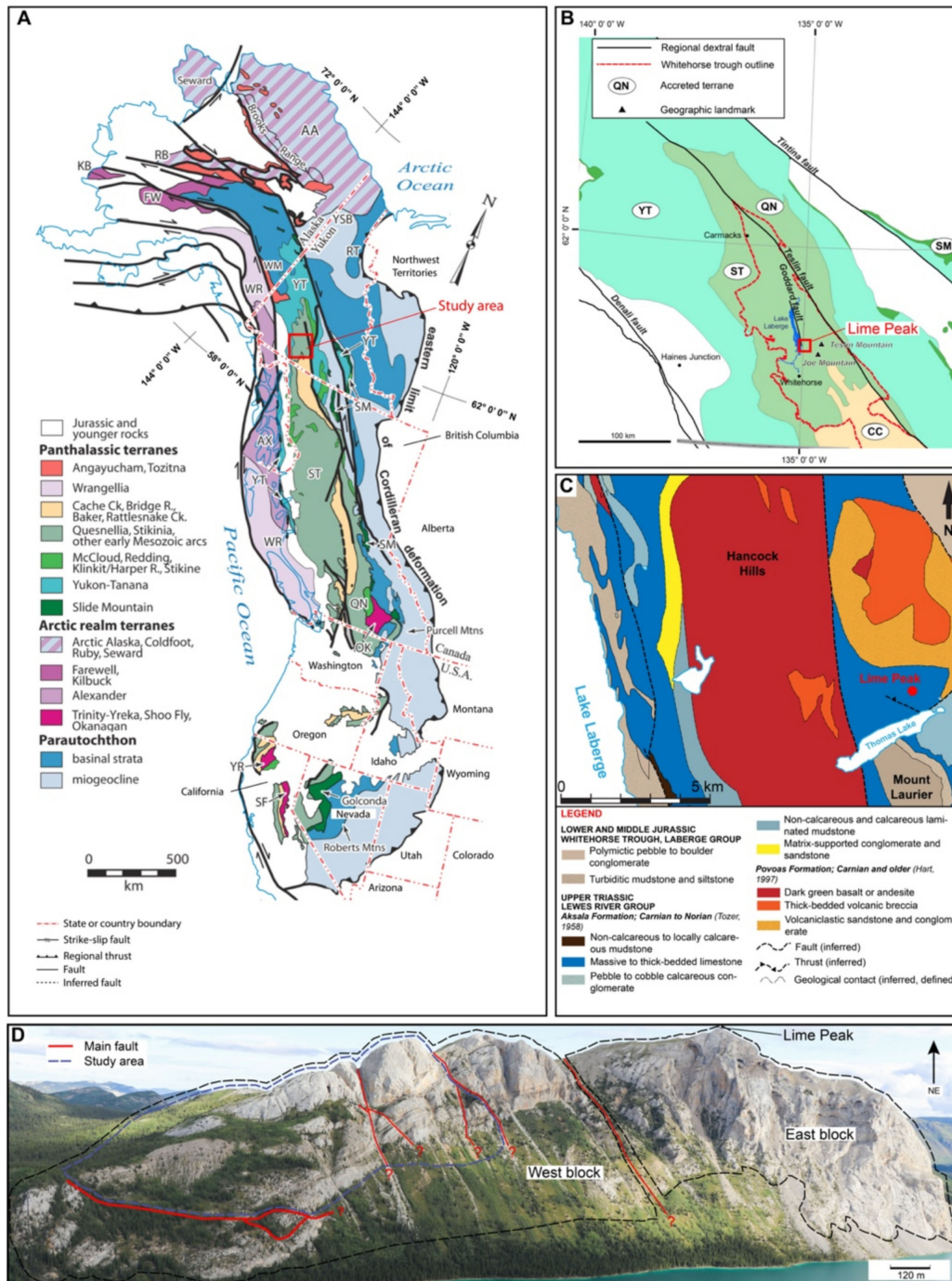

Figure 1. Geological and tectonic settings of the study area. (**A**) Terranes map of the North American Cordillera showing the study area (red square). Modified from [64]; (**B**) Intermontane terranes distribution in south-central Yukon: YT = Yukon-Tanana, ST = Stikina, QN = Quesnellia, SM = Slide Mountain, CC = Cache Creek (modified after [77]); (**C**) Geologic map of the western side of Lake Laberge where Lime Peak is located (red dot). Modified after [78]. The Carnian volcaniclastic sequence is equivalent to the Povoas Formation of [79]; (**D**) View of the southwest face of Lime Peak; the "?" indicate that the fault could not be followed in the field beyond the red line; (for a coloured version, the reader is referred to the web version of this article).

In southern Yukon, where Lime Peak is located, the stratigraphy of Stikinia is dominated by the Upper Triassic Lewes River Group (LRG). The basal part of the LRG is characterized by volcanic and volcaniclastic rocks of the Povoas Formation, mainly of Carnian age (Figure 1C). This volcanic arc assemblage, in turn, rests on older Palaeozoic rocks [80,81] of Mississippian age, which mostly consist of metamorphosed mafic volcanic rocks (e.g., the Stuhini Group; see [61]). A second volcanic arc assemblage, the Joe Mountain Formation, is exposed in the Whitehorse region. Although the nature of this Middle Triassic volcanic suite is still partially obscure, recent geochemical investigations [82] linked this unit to other Middle Triassic volcanic assemblages exposed in other parts of the Intermontane belt. The two arc systems are thought to have been in close relationship by the Late Triassic, as they are both overlaid by carbonate deposits of the Aksala Formation [82]. These Carnian–Norian carbonates were deposited during the waning stage of the Lewes River arc [78,82,83]. All Triassic strata are regionally unconformably overlaid by conglomerates, mudstones and sandstones of the Early to Middle Jurassic Laberge Group. Although the general settings in which these Upper Triassic carbonates were formed remain unclear, it is believed that they formed mostly on the eastern flank of a volcanic island arc on a pre-existing volcanic and/or volcaniclastic basement [61,78,82,84]. The depositional model for the carbonates of the Aksala Formation proposed in Morrison [85] and Hart [61] depicts the carbonate facies in three different belts in which the systems generally deepen toward the east. According to Hart [61], the central facies belt, where Lime Peak is located, was a depositional region placed at some distance from the coast on the shelf and was dominated by back-reef, reef and fore-reef depositional environments (see Figure 26 in [61]). Recent mapping work on the east side of Lake Laberge [78,82,84] investigated the stratigraphic framework of the area and was particularly helpful to unravel the stratigraphic relationship between carbonate sedimentation and volcanism. Carbonate deposition started toward the end of volcanism and was partially coeval with volcaniclastic deposition. The sedimentation was strongly influenced by the pre-existing volcanic topography together with other factors such as the importance of detrital sediment inputs [82]. The significant influence of these factors on the sedimentation is testified by the discontinuous nature of the limestone bodies, along with the diachronous onset of carbonate deposition between the different areas of the Whitehorse region (see [82]: Late Carnian to Late Norian diachronicity).

3. Area of Study, Mode of Occurrence and Lithofacies Description

3.1. Area of Study

Lime Peak is found in an isolated area (61° 03′ 59″ N 134°53′ 07″ W), which at the time of fieldwork was only accessible by helicopter. The area is located on the northern side of Thomas Lake (Figure 1C) at an elevation between circa 1000 and 1600 m. The vegetation cover, which ranges from almost absent (southeast face) to full (northwest side), mostly comprises low-growing grasses and bushes with some sporadic trees (becoming more and more abundant toward lower altitudes). The terrain ranges from moderately flat (northern part of the area) to very steep (southeast face).

3.2. Mode of Occurrence and Geometries

Exposures of Upper Triassic rocks are widespread in the Lime Peak area. In particular, the southeast face of the mountain provides an exceptional window into the Upper Triassic of the area. A major fault divides Lime Peak into two main blocks: east and west (see Figure 1D; [51]). The rock outcroppings in the east block are hardly accessible, heavily deformed and largely made up of carbonate breccias (e.g., see Enclosures 2 and 3 in [51]). Conversely, the west block is characterized by rocks that include a greater variety of carbonate lithofacies (see [51]) whose depositional relationships are still largely preserved (Figure 2A).
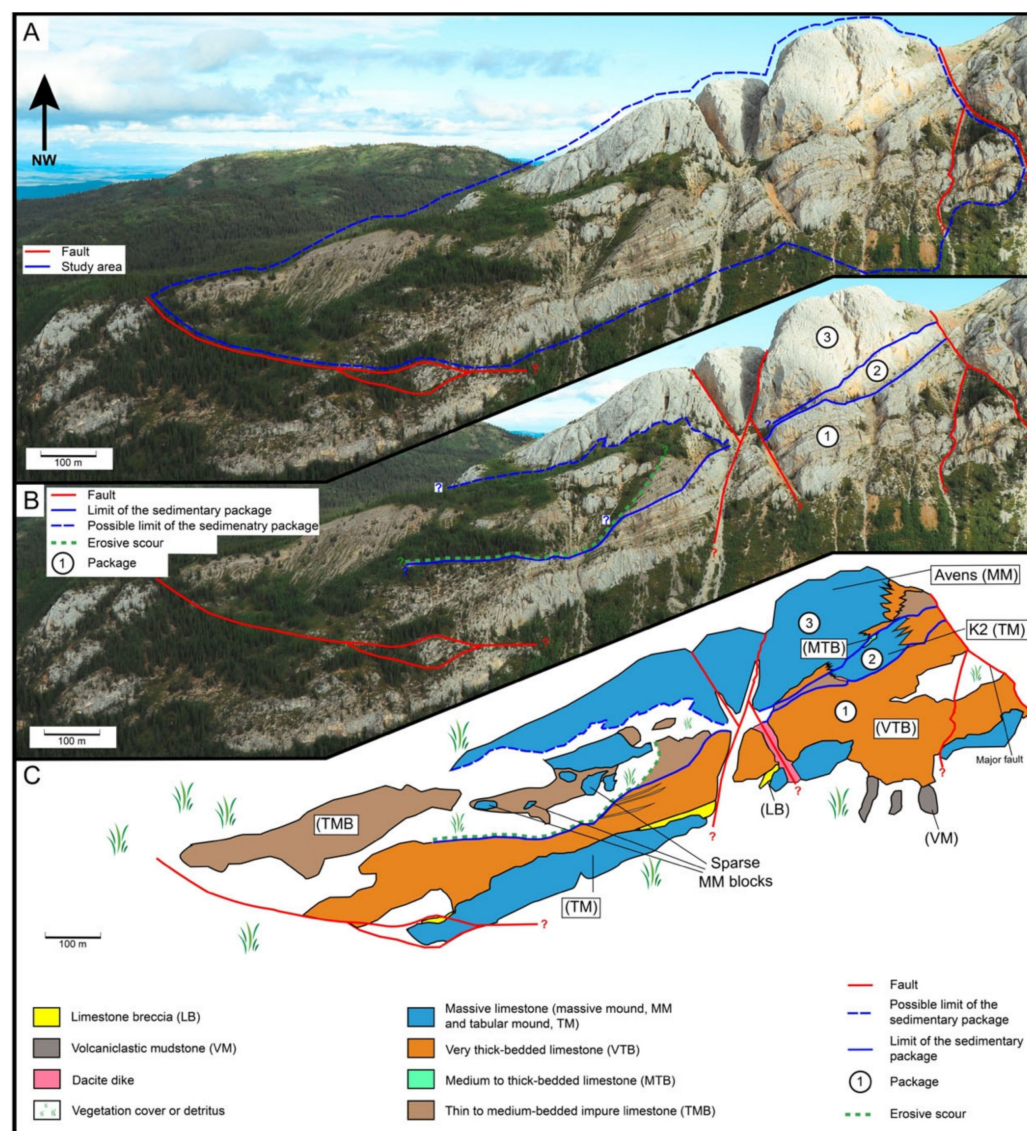
Figure 2. View of the southeast face of Lime Peak area with (**A**) focus on the study area; (**B**) focus on the three sedimentary packages; (**C**) lithofacies mapping: (1) first package, with base to top successio of: volcaniclastic red-weathering mudrocks, VM; very thick-bedded limestone, VTB; thin-to-medium-bedded impure limestone, TMB; (2) second package, characterized by a tabular mound, TM and thin-to-medium-bedded impure limestone, TMB; (3) third package, characterized by massive mound limestone, MM (nomenclature from Reid [51]); the "?" indicate that the fault could not be visually followed beyond the red line; (for a coloured version, the reader is referred to the web version of this article).

The lateral continuity is interrupted toward the eastern and western ends by two other major faults (Figure 2B). Although the amount and type of displacement caused by these faults is unknown, they juxtapose stratigraphic sequences whose primary depositional relationships were most likely different from the ones observed today. Hence, for the scope of this work, we only focus on the central part of the west block, i.e., the area where tectonic had only a minor impact and carbonate geometries are best preserved (Figures 1D and 2A).

The carbonate sequence on this part of the southwest face can be divided into three different sedimentary packages (Figure 2B). The first sedimentary package includes the lowermost part of the carbonate sequence and is defined by a pronounced pinch-out geometry toward the west: reaching almost 250 m in the eastern end; the stratigraphic

thickness of the package gradually decreases westward to the point where it is no more than 70 m thick in the area where it is truncated by the erosive scour (see Figure 2B).

The second sedimentary package, lying above the first one, shows contrasting geometries since its stratigraphic thickness reaches 60 m in the eastern area and decreases down to few meters in the central part before increasing up to about 70 m in the area where the lateral continuity of the beds is interrupted by a marked erosive scour (Figure 2B). This erosive surface marks the limit between the first and second sedimentary package in this area of the southwest face. The geological nature of this surface will be discussed later.

The third package lies conformably on top of the second one and is also characterized by a highly variable stratigraphic thickness: reaching maximum thickness in its central part (up to 170 m), the package pinches out both to the east and to the west.

3.3. Lithofacies Description and Spatial Occurrence

The bulk of the carbonate succession of the west block of Lime Peak is formed by five principal carbonate and non-carbonate lithofacies. Rarely, a few other lithofacies are also present, but since their spatial occurrence is very limited, they were not subject to in-depth investigation and are only briefly mentioned in the text. Reid [51] already provided a detailed description of the lithofacies occurring at Lime Peak. For this reason, in this work we will reuse her nomenclature (i.e., [51]) to refer to some of the limestone bodies (often representing different lithofacies) exposed at Lime Peak.

3.3.1. Lithofacies of the First Package

At Lime Peak, the lower part of the sedimentary sequence is characterized by the presence of volcaniclastic red-weathering mudrocks (VM; Figure 2C). This lithofacies is recessive in terms of competence and outcrops in patchy areas scattered in the vegetation. According to Reid [51], it represents background volcaniclastic sedimentation before the onset of carbonate production. VM is overlaid by very thick-bedded limestone (VTB; Figure 2C). The contact between the two lithofacies was not investigated in detail in this study. Reid [51] described it as transitional with volcaniclastic red-weathering mudrocks grading upward into very thick-bedded limestone (VTB). VTB by far makes up the largest portion of the first package (Figure 2C). This lithofacies has dark to light grey weathering and a fresh surface colour. In the eastern and central part of the sedimentary package, VTB beds are largely tabular in shape, with thickness ranging between 0.5 and 5 m. In the western part of the package, the beds belonging to this lithofacies, which can be easily followed visually, thin and pinch out toward the west into thin-to-medium-bedded impure limestone (TMB; Figures 2C and 3B). In this area, we observe vertical alternations between VTB (light grey, more competent) and TMB (dark grey, less competent).

These alternations seem to be arranged in repeated vertical cycles. VTB appears extremely fossiliferous at macroscopic scales: some levels, such as the coral layer (Figure 4B) of Reid [51], host abundant corals (*Retiophyllia* sp.) in life position (Figure 5D) along with clusters of *Spongiomorpha ramosa*, *Spongiomorpha gibbosa*, *Polytholosia ramosa* and *Polytholosia cylindrica*. Within the first package, VTB is found resting above both massive limestone having a tabular shape (TM) and limestone conglomerate or breccia (LB) (Figure 2C). In both cases, vertical contact with the underlying lithofacies is sharp. TM has a whitish to yellowish weathering colour and appears greyish at the fresh surface. This lithofacies does not show any clearly discernible stratification and presents abundant fractures. It is often very fossiliferous at the macroscale. LB, appearing recessive compared to both the TM and VTB, has a yellowish weathering colour and a variable colour (depending on the composition of the clasts) at the fresh surface. Its occurrence seems to be concentrated in a single stratigraphic horizon (Figure 2C), where occurs in the form of two slightly different variants: limestone conglomerate or limestone breccia. Limestone conglomerate occurs as big lenses (10 to 15 m thick) usually showing meter-scale bedding and grading.
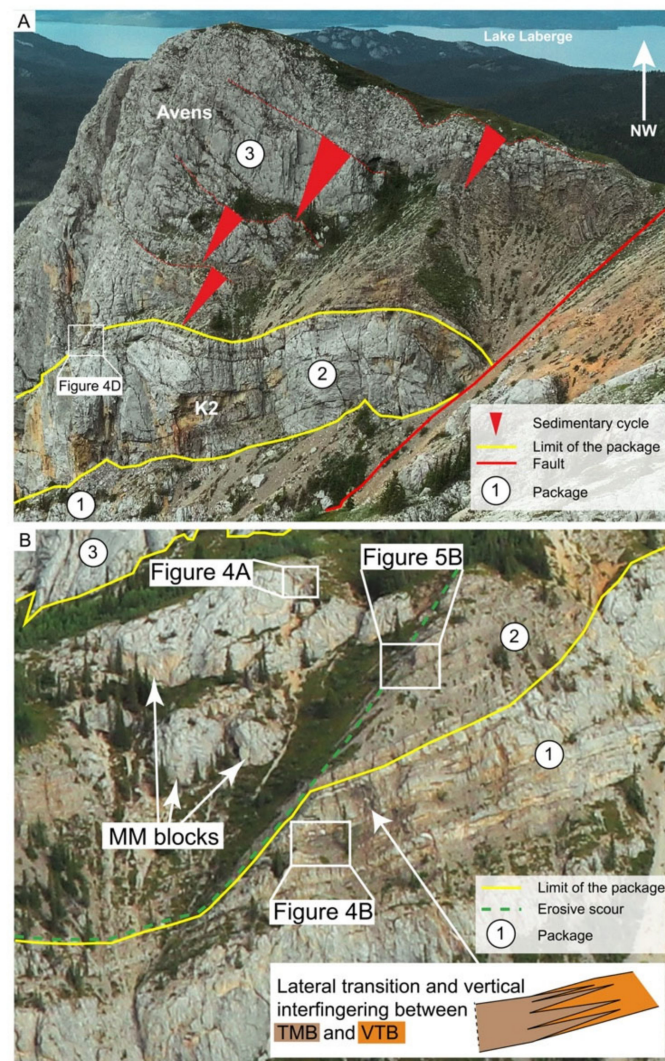
Figure 3. Particulars of the different lithofacies, Part 1. (**A**) View of Avens body (above the tabular mound limestone (TM) named K2) showing drag folds near a main fault affecting this area of Lime Peak: the continuity of the beds is interrupted by the fault. Sedimentary cycles (from thin-to-medium-bedded (TMB) impure limestone to very thick-bedded (VTB) limestone) are indicated by the red arrowheads; (**B**) Close-up of the central part of the southeast central face of Lime Peak showing the erosive scour and the first and second packages; (for a coloured version, the reader is referred to the web version of this article). 1, 2 and 3 are the studied packages.

These lenses flank or are on top of TM and minorly VTB. Their contact is sharp (erosive). The clasts within the conglomerate are rounded to sub-rounded in nature (Figure 4C). The space between the bigger clasts is filled with a sand-sized matrix or by a coarse, whitish, calcite cement (the microscopic composition of both the matrix and the clasts within the conglomerate is detailed in the microfacies section). On the other hand, limestone breccia develops as small and irregular pockets of a few meters. In this case, the contact between LB and TM is transitional. This breccia is composed of carbonate angular clasts surrounded by a yellowish dolomitic matrix. For a more detailed description of LB, the reader is directed towards Reid ([51], p. 142 onward). Several dacite dykes crosscut the sedimentary beds of the first package in different areas. Although the age of the dikes at Lime Peak has not yet been constrained, they might belong to either the Early Cretaceous Goddard suite (138–136 Ma) or to the Early Cretaceous Teslin and Whitehorse suites (116–106 Ma), which repeatedly intersect the Triassic and Jurassic stratigraphy in the Whitehorse region [82].
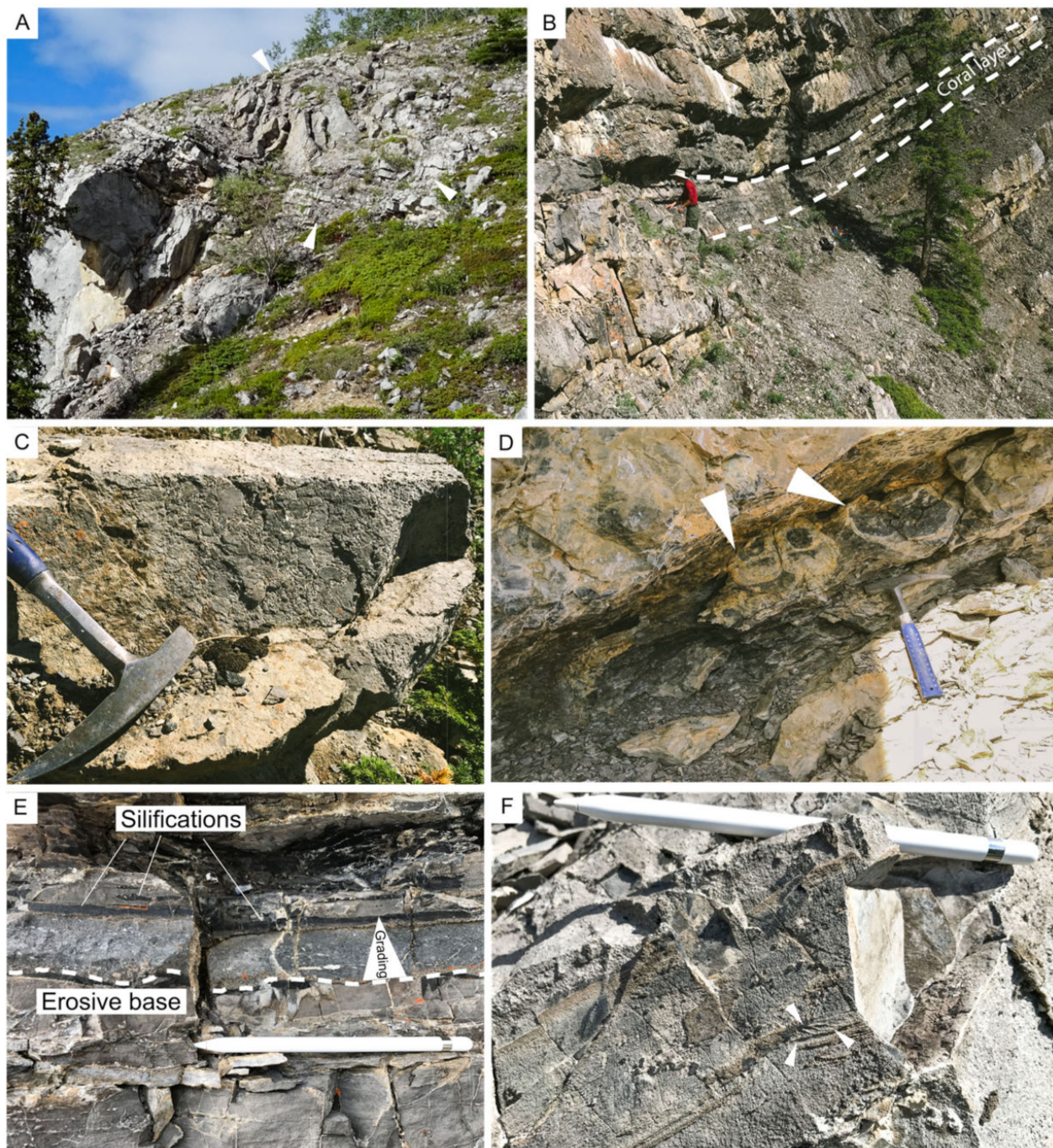
Figure 4. Particulars of the different lithofacies, Part 2. (**A**) Slump feature within medium- to thick-bedded impure (MTB) limestone beds in sharp contact with massive mound (MM) limestone gravitational block in the southeast face (white triangles); (**B**) Close-up of the coral layer within the very thick-bedded (VTB) limestone of the southeast face; (**C**) Particular of a breccia at the base of the southeast face—note the roundness of some clasts; (**D**) Big-sized gastropods (up to 50 cm in length; white triangles) within the MTB (MCF 2) beds of the southeast face; (**E**) Close-up of a graded bed within the TMB limestone—note the scoured, erosive base and the silicified portions; (**F**) Lamination and traction ripples within an MTB bed (white triangles); (for a coloured version, the reader is referred to the web version of this article).
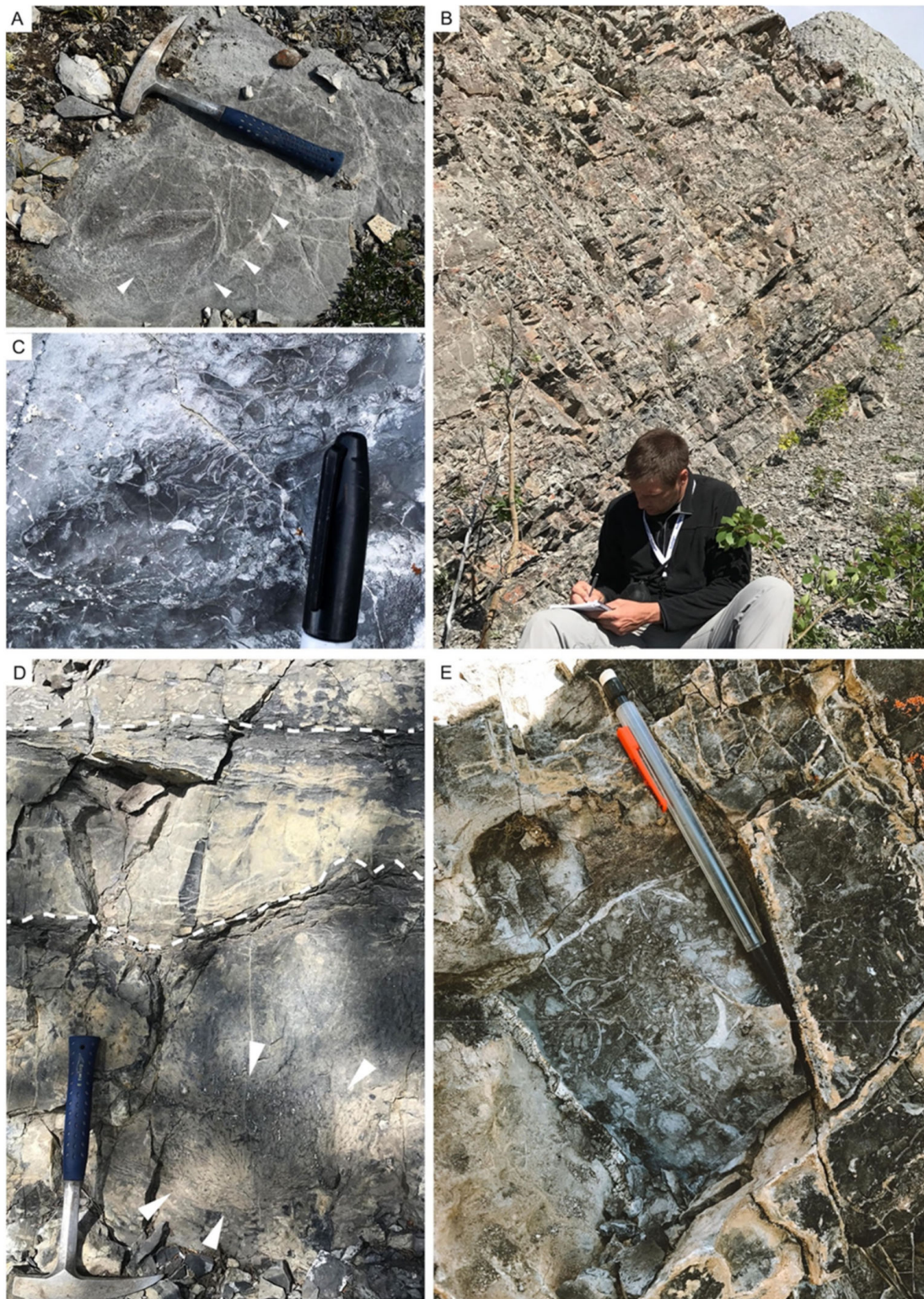
Figure 5. Particulars of the different lithofacies, Part 3. (**A**) Weathered surface showing a specimen of megalodontid bivalve on the western part of Avens (shell indicates by white triangles); (**B**) Particular of the thin to medium-bedded (TMB) impure limestone; (**C**) Particular of a patch with numerous small inozoan and sphinctozoan sponges (MCF 7); (**D**) Particular of the coral layer with alternation of beds rich in *Retiophyllia* sp. in living position (white triangles) and layers rich in *Spongiomorpha gibbosa*; (**E**) Close-up of a very fossiliferous level of TMB; (for a coloured version, the reader is referred to the web version of this article).

3.3.2. Lithofacies of the Second Package

The eastern part of the second sedimentary package is characterized by the presence of K2, a tabular mound (TM) body that is about 60 m thick and does not present any discernible stratification in its central part. In its upper part, K2 grades into medium- to thick-bedded impure limestone (MTB; Figure 2C). This lithofacies bears a dark blue weathering colour and a very dark colour at the fresh surface. Beds are generally 20 to 50 cm thick with a semi-nodular appearance, present abundant fractures and look strongly recessive compared to the other lithofacies. MTB beds contain big-sized gastropods reaching up to 50 cm in length (Figure 4D). The lateral contacts of K2 are transitional: to the east, K2 grades laterally into very thick-bedded limestone (VTB, Figures 2C and 3A), whereas to the west, it grades into thin- to medium-bedded impure limestone (TMB). This lithofacies is particularly well-exposed further to the west, where it makes up most of the second sedimentary package. TMB has a yellowish to brownish weathering colour and a darkish colour at the fresh surface. Beds within this lithofacies are extremely fossiliferous (Figure 5E), present abundant fractures and have thicknesses ranging from few cm to up to 30 cm (Figure 5B). Erosive bases, tabular and/or nodular silicifications, graded beds (Figure 4E) and ripple laminations (Figure 4F) are all characteristic features of this lithofacies. TMB is also a very common infill of the area associated with the erosive surface, along with massive mound limestone (MM). Slumping features (Figure 4A) are locally observed within TMB.

3.3.3. Lithofacies of the Third Package

The majority of the third package is formed by massive mound limestone (MM). This massive body, called Avens, is up to 200 m high, bears a whitish to pale yellow weathering colour and presents abundant fracturation. Avens appears very fossiliferous, even at the macroscale (Figure 5C). In particular, at the very western end of Avens there is an area where multiple large megalodontids (Figure 5A) and *Wallowaconcha* cf. *raylenea* can be seen on the weathered surface of the MM. Within Avens, stratification is rarely discernible except in the eastern part, where faint bedding can be observed. Here, a stratification starting from the MM and continuing into very thick-bedded limestone (VTB) can be recognized (Figures 2C and 3A). Eastward, at some distance from the MM–VTB transition, the VTB beds are associated laterally and vertically with thin- to medium-bedded impure limestone (TMB). In particular, the vertical alternations between VTB and TMB are arranged in at least four cycles.

4. Methods

In total, 426 samples were collected from the Lime Peak area. In order to study the microfacies content and their distribution within the massive limestone body of Avens, we systematically sampled it by abseiling down from its top. A total of 6 vertical transects were done, with samples taken each 3 metres (see Supplementary Materials: Figure S2). Some of these samples were too damaged (fractured) to be used, and others were disregarded due to pervasive recrystallization (see Supplementary Materials: Figure S2). At least one thin section (3.5 × 2.3 cm) per sample was prepared at the Department of Earth Sciences, University of Geneva. Sedimentological observations in the field were coupled with the study of microfacies assemblages, which were observed under a regular petrological microscope. To classify the different carbonate microfacies encountered during this study, we used the redesigned carbonate classification scheme by Lokier and Al Junaibi [86].

Cathodoluminescent imaging was obtained using a CITL 8200 Mk 5-1-optical cathodo-luminescence microscope with a cold cathode (Cambridge Image Technology Ltd.—United Kingdom) mounted on a Leitz petrological microscope (Leica Microsystems—Switzerland)at the Department of Earth Sciences, University of Geneva. Beam conditions were set at 15–18 kV and 100–210 nA.

In this work, the term microbialites is used following the definition of Burne and Moore [87], who described microbialites as "organosedimentary deposits that have accreted as a result of benthic microbial community trapping and binding detrital sediment and/or

forming the locus of mineral precipitation". We also follow Riding's [88] definition of the term reef, i.e., "all calcareous deposits created by essentially in place sessile organism". To be able to study the composition of reef/autochthonous microfacies along with their distribution and abundance in the Lime Peak area, we first had to define whether each sample had a reefal nature or not. To do so, microfacies criteria, including the importance of in-place reef builders (sponges, corals and microbialites, among others), the presence of reef cavities and the presence of microbialites along with the presence of other encrusting organisms, were taken into account. Overall, samples with reef affinity correspond to MCF 7 and MCF 6A and 6B (see below). Technically, MCF 11 could have also been included in the point-counting analysis due to its framestone nature. However, within MCF 11, *Retiophyllia* sp. formed small and well-spaced thickets rather than a structured reef; for this reason, this microfacies was excluded from the point-counting analysis. When using the term "reef" or "reefal" in this work, we strictly refer to MCF 7 and MCF 6A and 6B and not to the entire depositional environment where reef-related deposits are commonly found. For the latter, we use the term "platform margin".

To study the composition of reef microfacies at Lime Peak, a total of 52 thin sections were additionally scanned by means of a high-resolution film scanner (Nikon CoolScan 4000 ED; Zweigniederlassung - Switzerland). Of these, 42 came from the massive mounds (Avens) and 10 from the tabular mounds (K2 and other tabular bodies outcropping from the northwest side of Lime Peak; see Supplementary Materials: Figure S1). Since we had only a few samples from some of the vertically exposed bodies in the study area (e.g., the tabular limestone), we decided to also include reef samples belonging to equivalent limestone bodies exposed in other, gentler areas of Lime Peak (e.g., the tabular bodies exposed in the northwest side of Lime Peak; see Supplementary Materials: Figure S1). The samples were point-counted to assess the relative abundance of each reef component. Point-counting was performed using the image analysis software JMicrovision (User-friendly software for analyzing large images, version 1.3.3—Switzerland). According to the software's point-counting evolution plot, stabilization is achieved between 150 and 200 counted points. Hence, a total of 200 points by thin section were counted using a random grid. Point-counting classes were made following Peybernes et al. [22]: essentially, reef components were divided into two main classes—framework components and interstitial sediments (Figure 6). In our subdivision, the framework is given by those organisms that directly contribute to reef growth, such as sponges (inozoans, sphinctozoans, disjectoporids, chaetetids and Spongiomorpha spp.), corals, microbialites, tubular crusts and encrusters. Among the encrusters are solenoporacean algae, serpulids, calcified cyanobacteria, brachiopods, phylloid algae, sessile foraminifera such as *Planiinvoluta carinata* and *Tolypammina* sp., and sessile microproblematica such as *Radiomura cautica* and *Microtubus communis*. Unlike Peybernes et al. [22], in this work we did not differentiate between primary and secondary framebuilders: the reason for this choice lies in the importance of microbialites at Lime Peak, which act both as encruster and as framework constructor independently of metazoans (see MCF 6 below). In the interstitial sediment group are skeletal and non-skeletal grains, such as dwellers (e.g., foraminifera, molluscs, ostracods and brachiopods, among others), peloids and ooids, along with different forms of micrite (clotted and peloidal, interstitial and dense micrite) and cement (either cavity-filling or intergranular cements).

In order to be able to compare the reef associations of Lime Peak with those of other coeval reefs in Panthalassa and Tethys (see Section 8), we performed a similarity analysis for reef taxa (calcareous sponges, microproblematica and foraminifera). To do so, we used an updated version (see Supplementary Materials: Figures S6 and S7) of the database originally compiled by Peybernes et al. [22] that includes the occurrences of reef taxa in different Upper Triassic (Norian–Rhaetian) reef sites. In our updated version, we added the new taxa from Lime Peak (mostly reefal foraminifera) that were identified in this study. To be consistent with the work of Peybernes et al. [22], we made sure to add only the taxa coming from the reef microfacies (i.e., MCF 6A, 6B, 7) and the microfacies found closely associated with the latter (MCF 5). Foraminifera from other depositional environments

were not added to the database (e.g., lagoon and slope deposits). Moreover, we added some new entries (sponge taxa) from Slovenia [89] that were not included in the original database. Hierarchical cluster analysis (hCA) was obtained using PAST software (v. 4.04) with a UPGMA algorithm and Dice (=Sørensen) coefficient of taxonomic similarity. For details regarding this type of analysis, the reasons for its selection and the choice of included taxa, the reader is referred to Peybernes et al. [22].
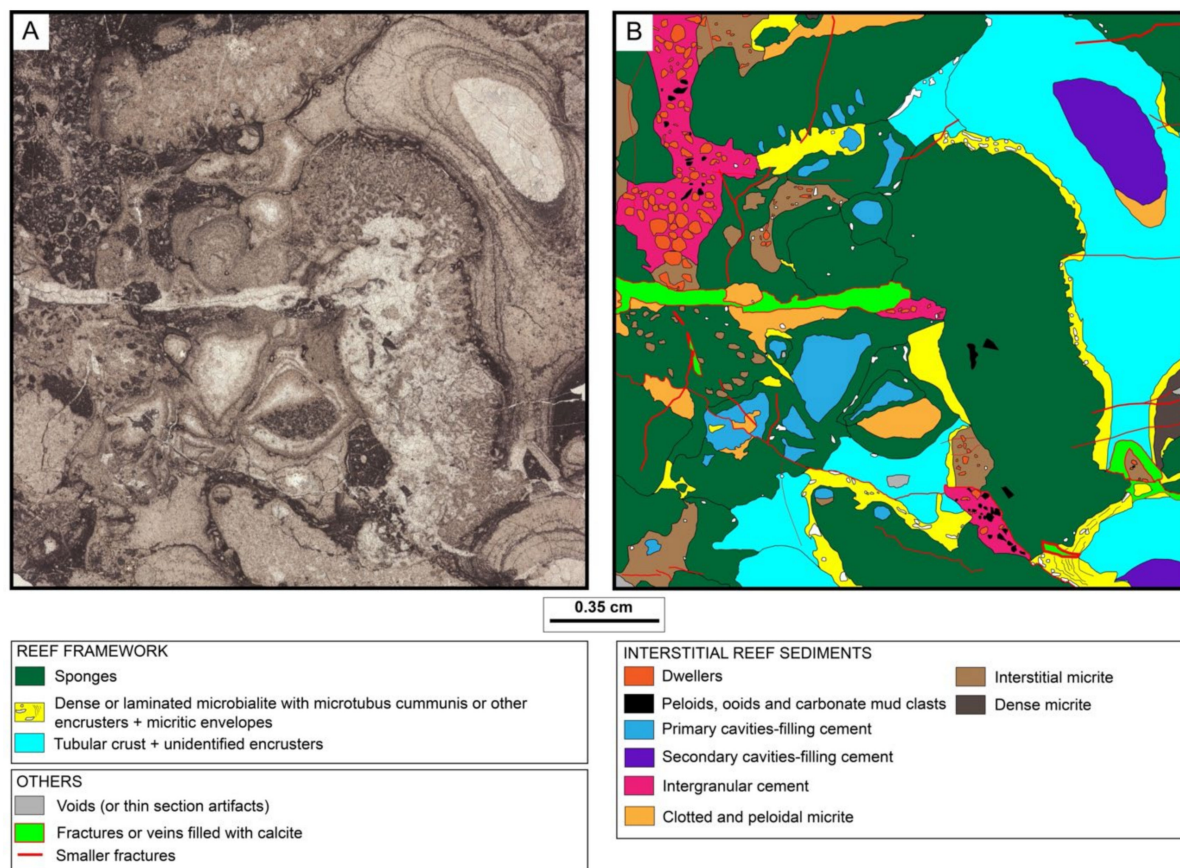

REEF FRAMEWORK
- Sponges
- Dense or laminated microbialite with microtubus cummunis or other encrusters + micritic envelopes
- Tubular crust + unidentified encrusters

OTHERS
- Voids (or thin section artifacts)
- Fractures or veins filled with calcite
- Smaller fractures

INTERSTITIAL REEF SEDIMENTS
- Dwellers
- Peloids, ooids and carbonate mud clasts
- Primary cavities-filling cement
- Secondary cavities-filling cement
- Intergranular cement
- Clotted and peloidal micrite
- Interstitial micrite
- Dense micrite

Figure 6. Interpretation of a typical reef facies. (**A**) Scan of a thin section; (**B**) Mapping of the different components making up the reef framestone. Cavity cements (e.g., the ones filling the internal cavities of sphinctozoans) and sediments were mapped only when a clear differentiation between the organism and the intragranular porosity (e.g., internal cavity in sponges) was possible (i.e., preservation of the rock allowed for clear recognition of the original intragranular porosity); (for a coloured version, the reader is referred to the web version of this article).

Ostracods (both calcitic and silicified) were extracted from bulk rocks using the technique described in [90]. When present in the residue, ostracods were hand-picked and mounted on rounded aluminium stubs. Pictures of the specimens were taken with a JEOL JSM7001F scanning electron microscope (SEM; JEOL Europe S.A.S.—France) at the Department of Earth Sciences, University of Geneva: conditions were 10 kV and 3.5 nA. In this work, ostracods were identified only at the genus level, and their assemblages are only briefly described; for a more detailed description, please refer to Forel et al. [47].

5. Age of the Deposits

Previous biostratigraphic investigations [91,92] carried out on the uppermost part of Lime Peak yielded a Late Norian age. For this work, two new samples (Figure 7A) were dissolved for conodonts using 10% acetic acid: the first one (CONO 6) was collected 50 m above the base of the carbonate complex, while the second one (CONO 8) comes from the upper part of Avens body (approximately 300 m above the base). Both samples yielded the

same conodont assemblage, consisting of *Mockina engladii*, *Mockina* aff. *engladii* and *Mockina bidentata* (see Supplementary Materials: Figure S5). This assemblage, which indicates a Late Norian age, suggests that the deposition of the Lime Peak carbonate complex occurred largely, if not exclusively, during the Late Norian.
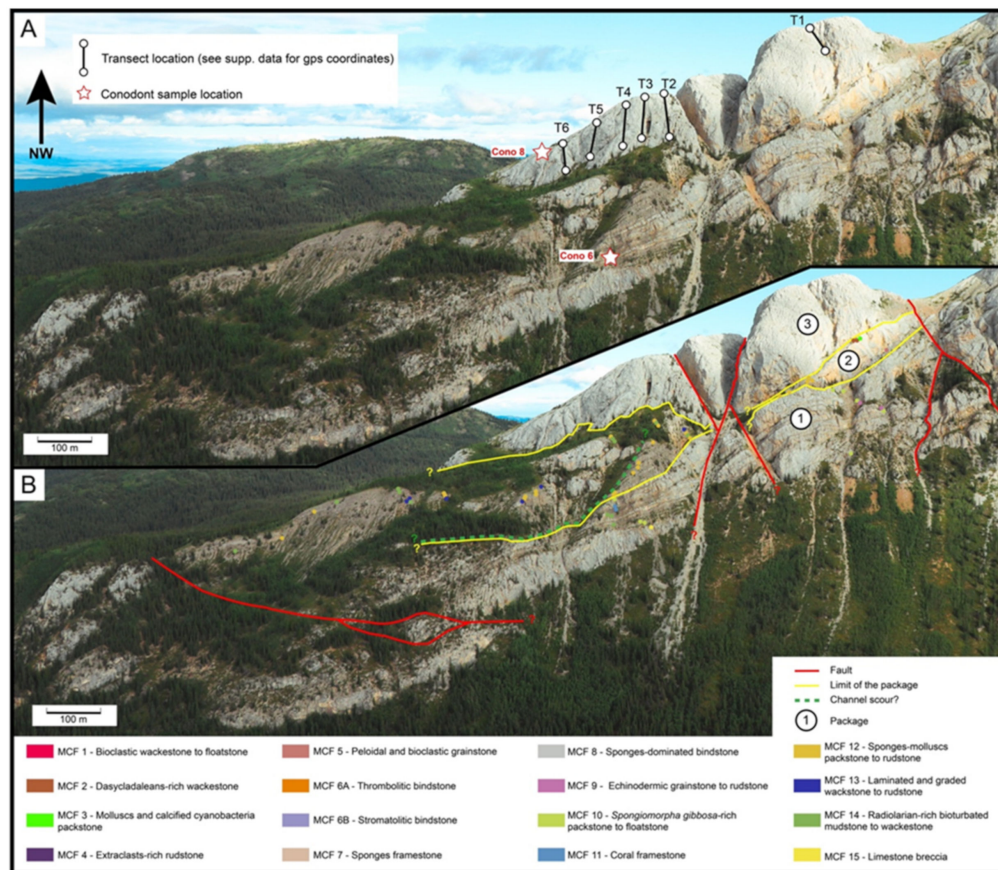

Figure 7. View of the southwest face of Lime Peak showing: (**A**) The location of the abseiling transects and the conodont samples; (**B**) The location of the studied samples inside the three packages. The small, coloured dots indicate the location of the samples studied, and the colour refers to the corresponding microfacies; (for a coloured version, the reader is referred to the web version of this article). 1, 2 and 3 are the studied packages. T1 to T6 are the 6 vertical transects done, with samples taken every 3 metres.

6. Results

6.1. Microfacies Description and Biotic Content

This section describes in detail the range of microfacies found within the study area at Lime Peak, along with their sedimentary structures and spatial distribution. These descriptions derive from both microscopic and macroscopic observations. In certain cases, to implement the description of a few microfacies and to better constrain their depositional relationships, we also studied some samples coming from isolated outcrops found in the northwest area of Lime Peak bearing the same microfacies (see Supplementary Materials: Figure S1 for outcrop and sample location). The spatial distribution of microfacies can be observed in Figures 7B and 8A,B (the reader is invited to look at Supplementary Materials: Figure S1 for a better-resolution image). Microfacies are illustrated in Figures 9 and 10, and selected components (i.e., sponges, foraminifera, ostracods) are additionally illustrated in Figures 11–16. For a list of all the foraminifera found at Lime Peak see Supplementary Materials: Figure S4. Characteristics of each microfacies are summarized in Table 1.
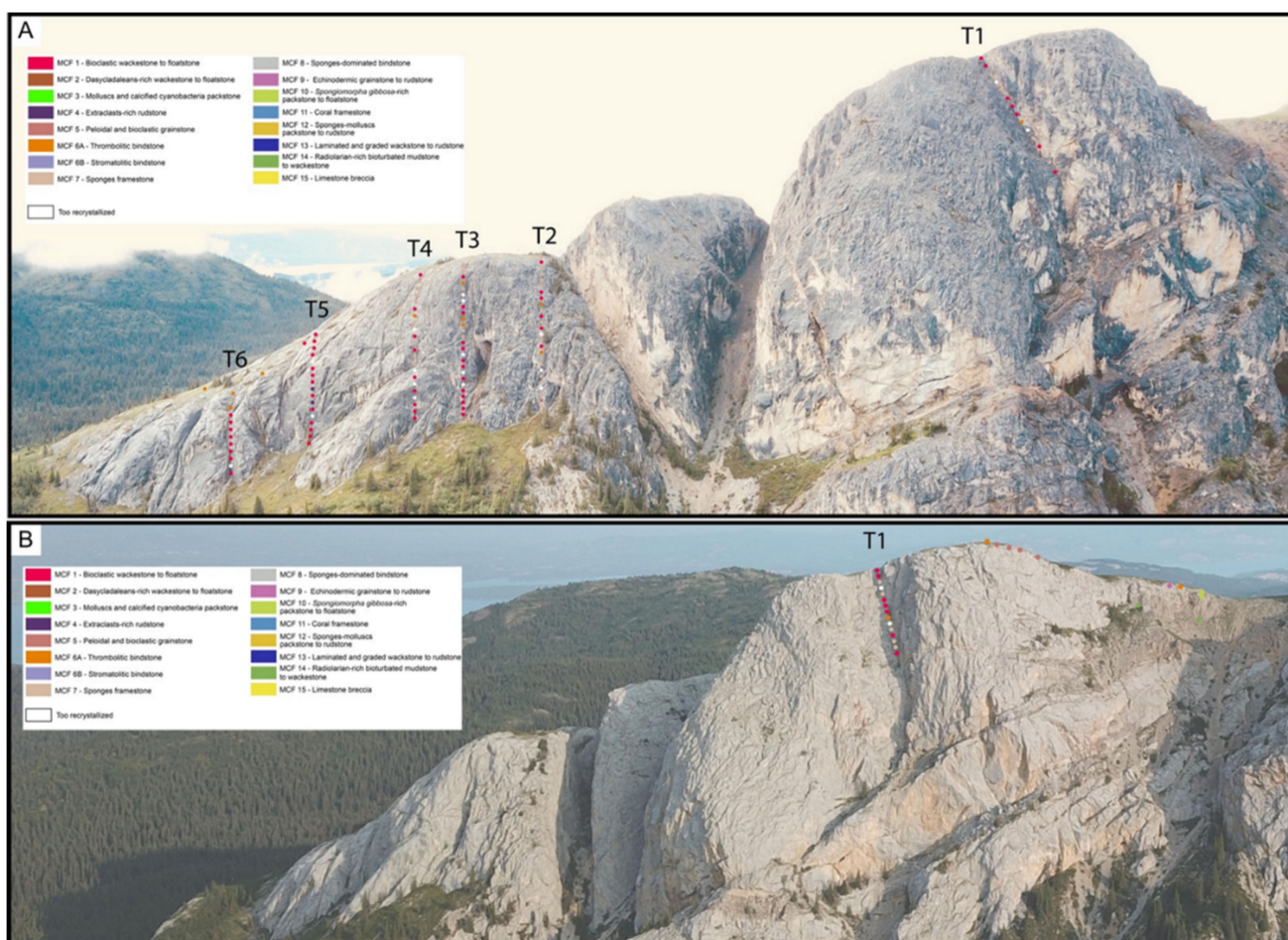
Figure 8. View of the massive limestone body Avens showing: (**A**) The sample locations and microfacies (colour-coded) with a focus on the westernmost part; (**B**) The sample location and microfacies (colour-coded) with a focus on the easternmost part of the limestone body; (for a coloured version, the reader is referred to the web version of this article). T1 to T6 are the 6 vertical transects done, with samples taken every 3 m.

MCF 1—Bioclastic wackestone to floatstone (Figure 9A). Abundant within Avens (frequently in association with MCF 7, and more rarely with MCF 4, 5, 6 and 9), it consists of a continuum from wackestone to rare floatstone. The bioclastic fraction, very unsorted in nature, is lightly to moderately fragmented; the matrix consists of dark micrite. Major bioclastic components are molluscs (both gastropods and bivalves), crinoids, dasycladales algae (frequent ?*Clypeina* sp.; Figure 11A), calcareous sponges, solenoporacean red algae and foraminifera. At times, reclining bivalves or brachiopods are found in closed articulated position showing geopetal infills (Figure 11G). Floatstone occurrences are given by a higher contribution of framebuilding organisms found as debris (mostly calcareous sponges and solenoporaceans red algae). On occasion, MCF 1 presents neptunian dykes and/or dissolution events that are often filled with clotted and peloidal micrite and/or very dark micrite (Figure 9A). Foraminiferal assemblages include very abundant *Taanella yukonensis* (Figure 14P), textulariids, common Duostominina (Figure 15G), Miliolidae, *Wernlina reidae* (Figure 14T), rare Nodosariidae and *Agathammina* sp. (Figure 14E). Ostracods extracted from a thin gravity layer within MCF 1 yielded an association dominated by the genera *Mirabairdia*, *Paracypris*, *Alatobairdia*, *Cornutobairdia*, *Bairdia*, *Bairdiacypris*, *Judahella* and *Leviella* (Figure 16).
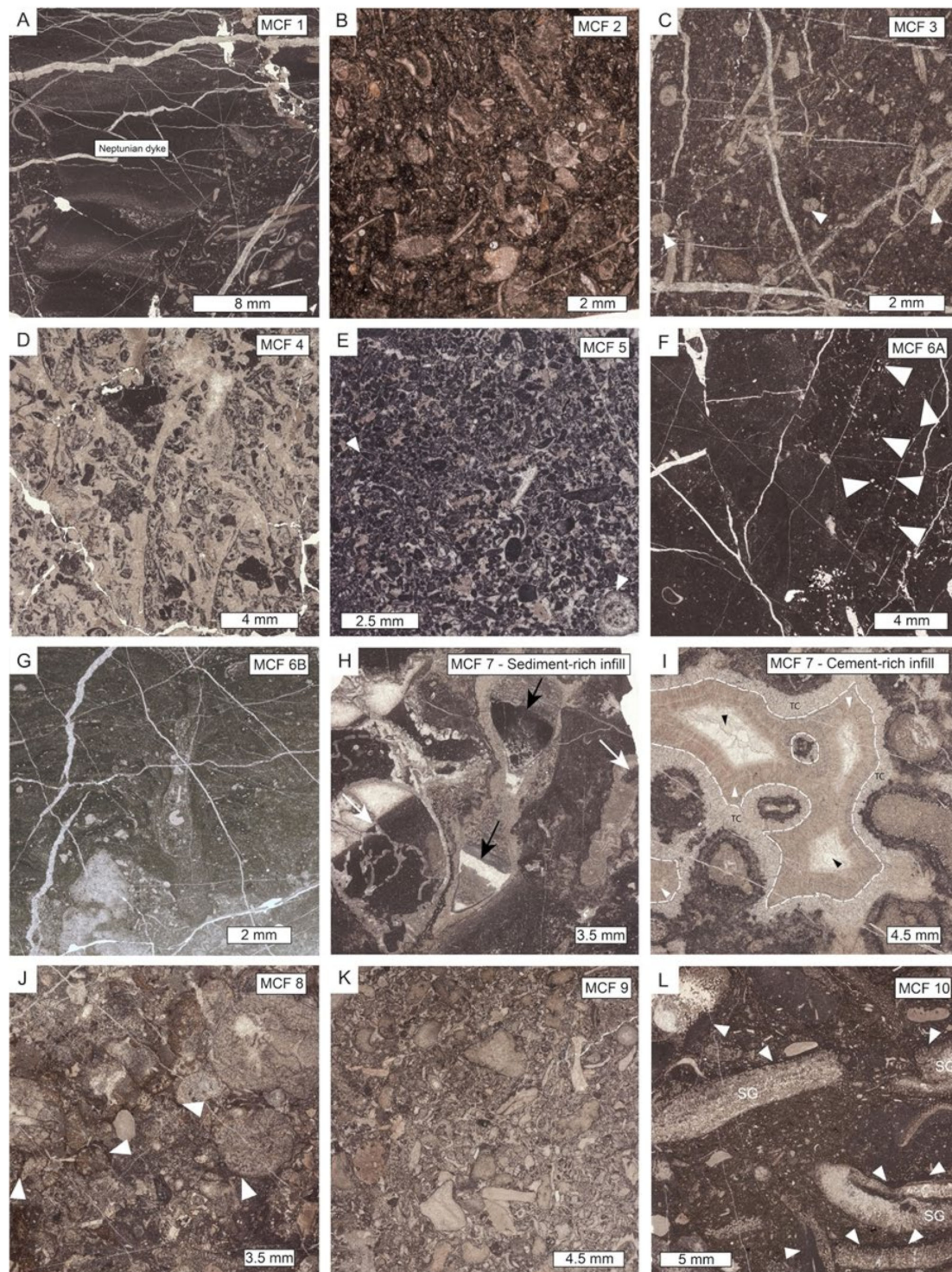
Figure 9. Microfacies of Lime Peak, Part 1. (**A**) MCF 1: Bioclastic wackestone to floatstone (sample WH 359). Note the dissolution feature at the center (neptunian dyke) filled with layered mudstone and peloidal micrite; (**B**) MCF 2: Dasycladales-rich packstone to floatstone (sample WH 227); (**C**) MCF 3: Peloidal and bioclastic packstone (sample WH 229 B). White triangles indicate possible fragments of phaceloid corals; (**D**) MCF 4: Bioclastic rudstone (sample WH 394); (**E**) MCF 5: Peloidal and bioclastic grainstone (sample WH 286). White triangles indicate dasycladales; (**F**) MCF 6A: Microbial bindstone, leiolitic to thrombolithic microfabric (sample WH 277). White triangles indicate the clusters of *Tolypammina* encrusting foraminifer; (**G**) MCF 6B: Microbial bindstone, stromatolitic macrofabric

(sample WH 406). Observe the space between the stromatolitic columns filled with a wackestone to packstone similar to MCF 1; (**H**) MCF 7: Metazoans framestone, sediment-rich end-member (sample WH 447). Note the double generation of geopetals with different orientation. White arrows correspond to synsedimentary infill in primary cavities and black arrows correspond to cement and sediment in secondary or dissolution cavities; (**I**) MCF 7: Metazoan framestone, cement-rich end-member (sample WH 404). The outer limit of the tubular crust (TC) is marked by the dotted lines, two types of cements (white and black triangles) infill the secondary cavity (decayed organism or dissolved shell on which the tubular crust grew); (**J**) MCF 8: Sponges bindstone (sample WH 164). Observe the thin layer of microbialite (white triangles) binding together the various debris; (**K**) MCF 9: Crinoidal rudstone (sample WH 148). Note the presence of microborers and microencrusters and microbial envelopes around grains; (**L**) MCF 10: *Spongiomorpha gibbosa* (SG) floatstone (sample WH 565). Note the microbial encrustation pointed by white triangles; (for a coloured version, the reader is referred to the web version of this article).
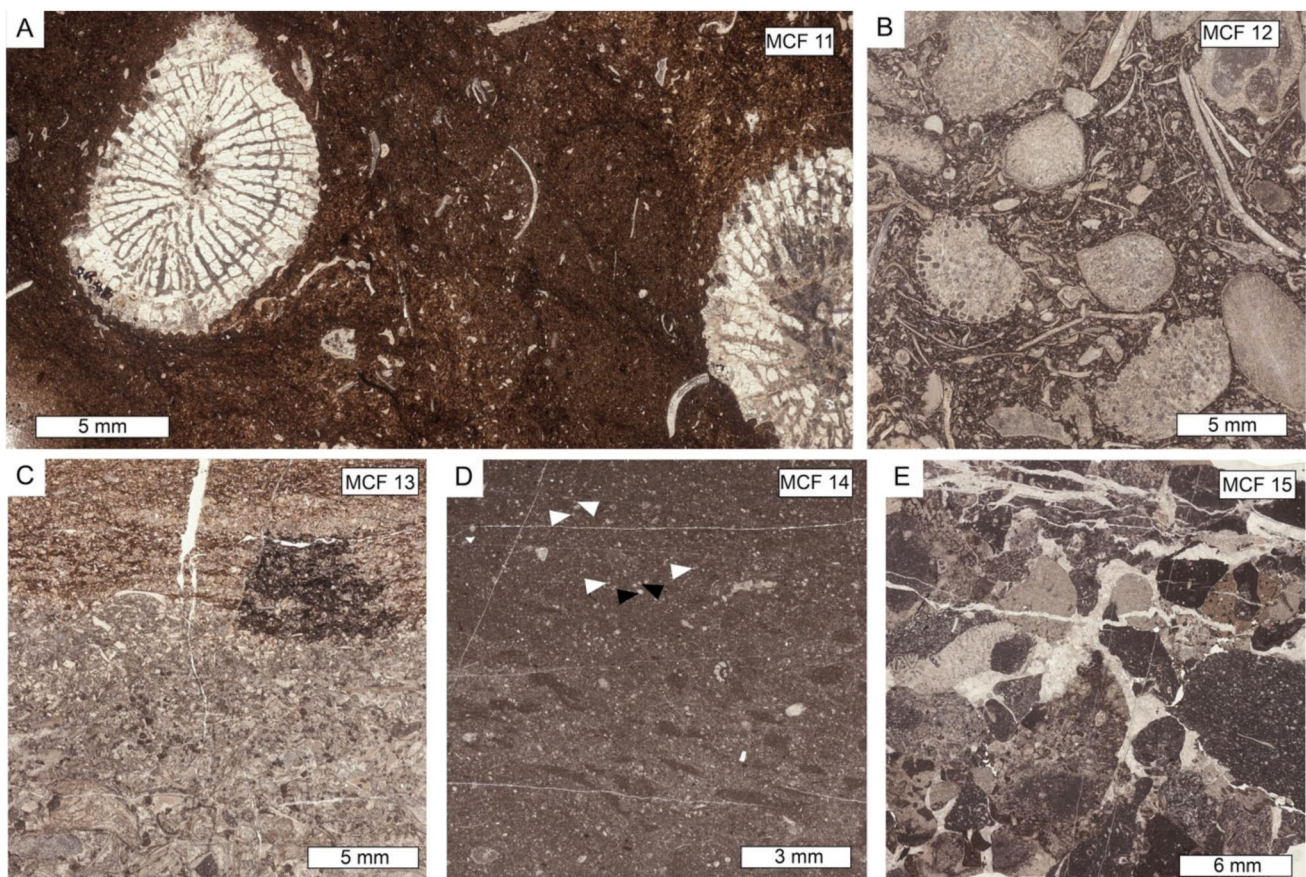

Figure 10. Microfacies of Lime Peak, Part 2. (**A**) MCF 11: *Retiophyllia* sp. framestone (sample WH 252, cross section). Note the fine, clayey bioclastic wackestone filling up the space between the corals; (**B**) MCF 12: Sponges—molluscs rudstone (sample WH 93); (**C**) MCF 13: Laminated and graded packestone to rudstone (sample WH 142); (**D**) MCF 14: Bioturbated wackestone (sample WH 125). Radiolarians (some are pointed by white triangles) and ostracods (some pointed by black triangles) abound; (**E**) MCF 15: Limestone conglomerate or breccia (sample WH 240); (for a coloured version, the reader is referred to the web version of this article).
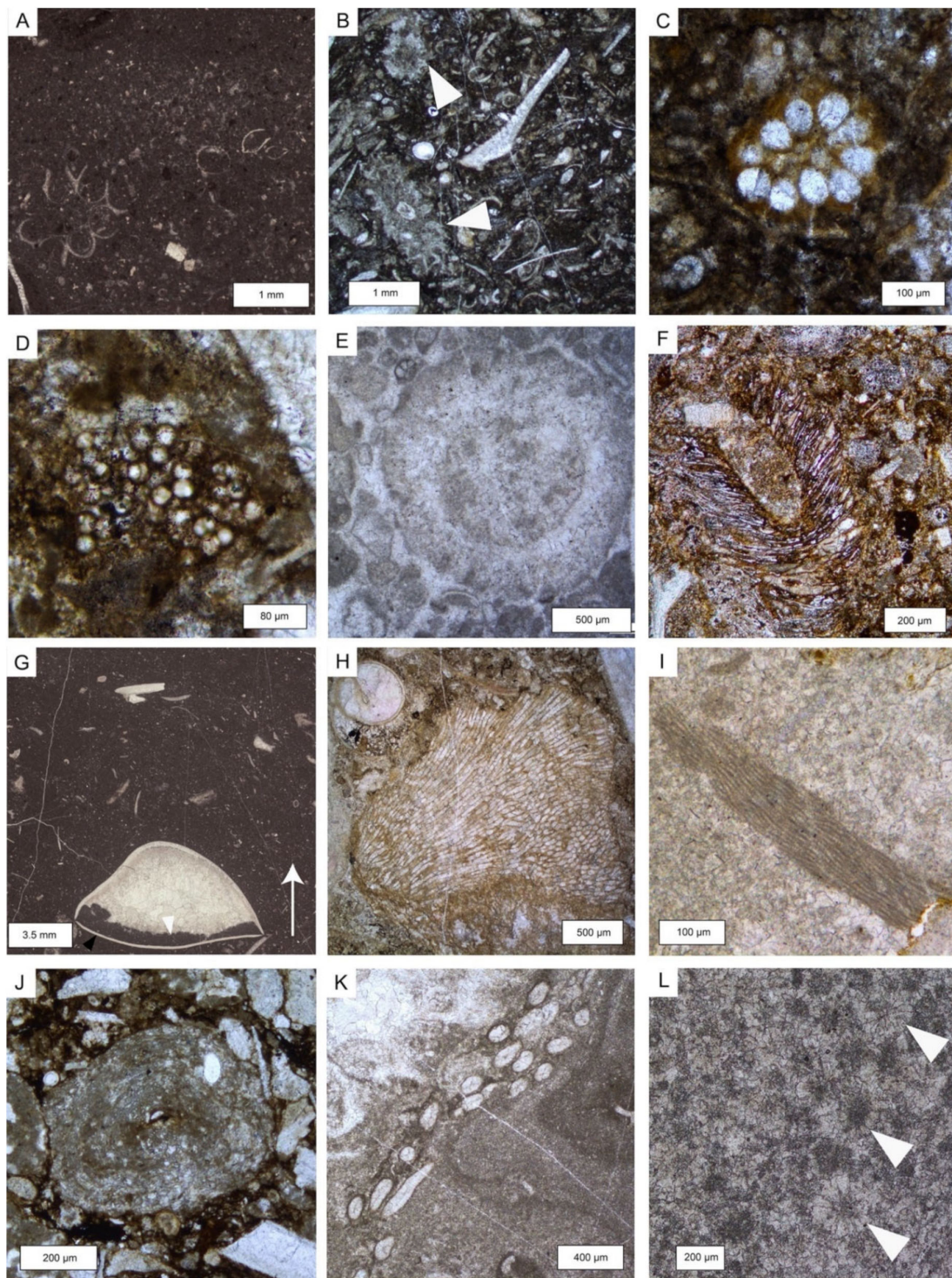
Figure 11. Selected biota and other features from Lime Peak, Part A. Dasycladales green algae (**A**–**F**): (**A**) ?*Clypeina* sp. (sample WH 153); (**B**) ?*Holosporella rossanae* (sample WH 234); (**C**) *Patruliuspora pacifica* (white triangles, sample WH 234); (**D**) ?*Patruliuspora oregonica* (sample WH 260 D); (**E**) ?*Kantia* sp. (sample WH 286); (**F**) ?*Teutoplorella* sp. (sample WH 91). (**G**) Reclining brachiopod in life position (up is indicated by the white arrow). Note the much less curved lower valve (black triangle) and the geopetal infill (white triangle) inside the organism (sample WH 267). Calcified cyanobacteria (**H**–**J**): (**H**) *Cayeuxia* sp. (sample WH 93); (**I**) *Girvanella* sp. (sample WH 236); (**J**) *Girvanella* sp. oncoid (sample WH 596). (**K**) *Microtubus communis* (sample WH 447); (**L**) White triangles indicate spar-rimmed peloids (sample WH); (for a coloured version, the reader is referred to the web version of this article).
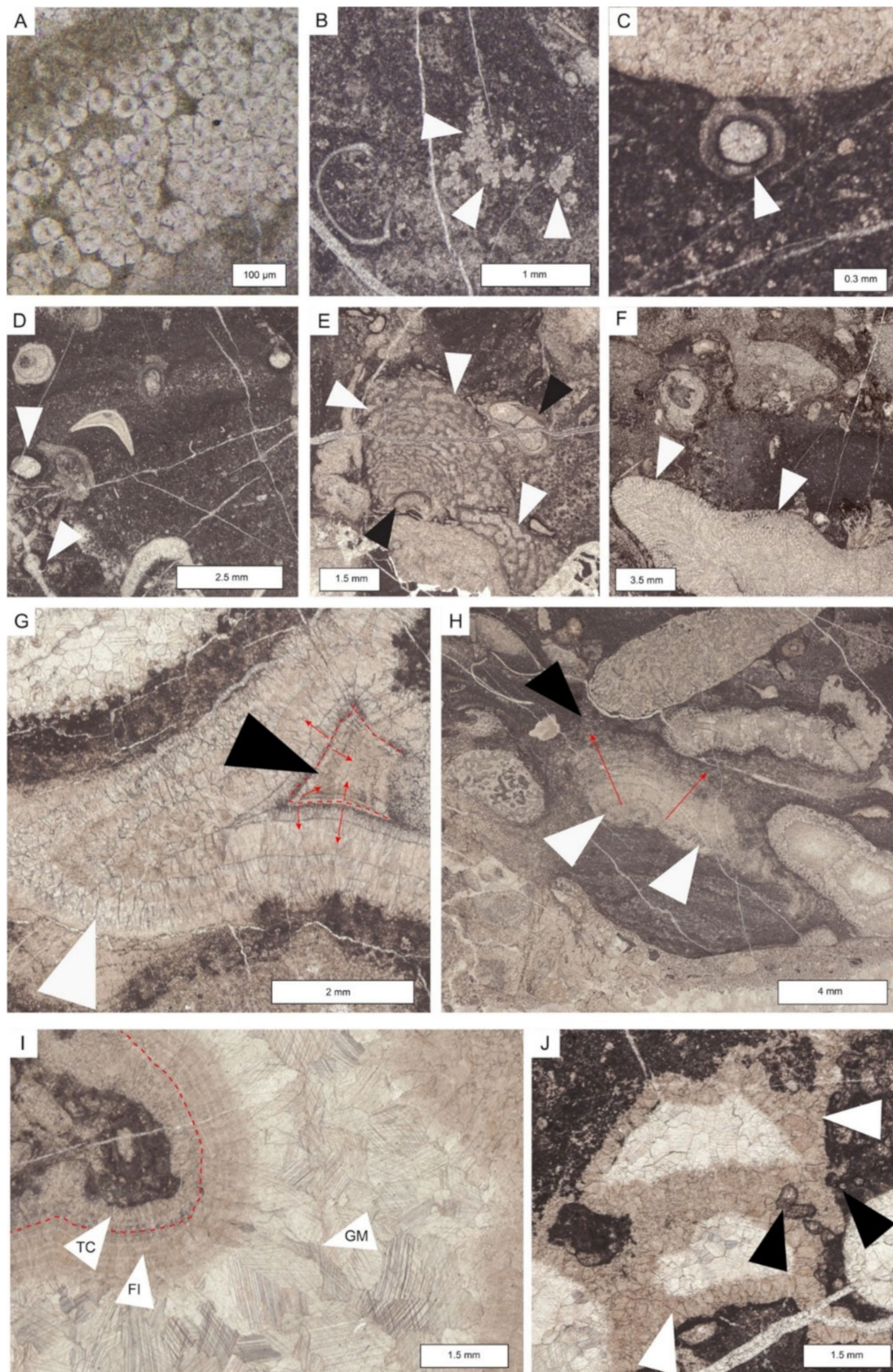
Figure 12. Selected biota and other features from Lime Peak, Part B. Microproblematica (**A**–**C**): (**A**) *Globochaete* sp. (sample WH 586); (**B**) *Baccanella floriformis* (white triangles; sample WH 588);

(**C**) *Radiomura cautica* (white triangle, sample WH 590). Worm tubes (**D,E**): (**D**) *Terebella* sp. (white triangles, sample WH 408); (**E**) Sample of MCF 7 showing the sphinctozoan sponge *Uvanella* sp. (white triangles) and serpulids (black triangles; sample WH 324). (**F**) Thamnasteroid coral (white triangles indicate the perifery; sample WH 231). Tubular crust and cements (**G–J**): (**G**) Tubular crust (white triangles) vs. cavity-filling cement (black triangles). Note the different growth direction, centrifugal vs. centripetal, respectively (arrows; sample WH 338). The dotted line represents the inferred limit of the dissolution cavity; (**H**) Particular of a tubular crust (white triangle; red arrows indicate the unique centripetal growth direction) grown upon a microbialite and evolving into a microbialite (black triangle; sample WH 116). (**I**) Different generations of cements filling up a secondary cavity delimited by a tubular crust. GM = granular mosaic cement, FI = fibrous isopachous cement, TC = tubular crust. The dotted line represents the inferred limit of the dissolution cavity (sample WH 338); (**J**) Unidentified encrusters (black triangles) within the tubular crust (white triangles; sample WH 233); (for a coloured version, the reader is referred to the web version of this article).
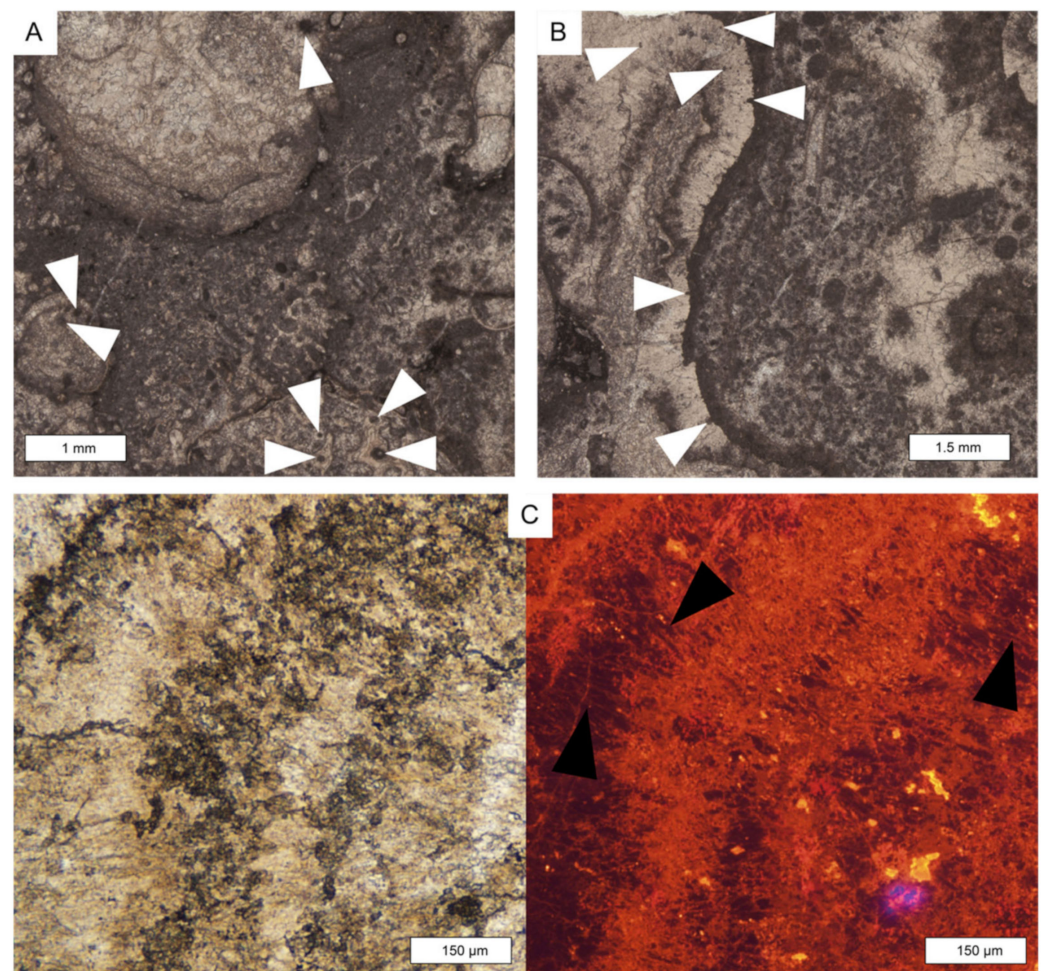
Figure 13. Selected biota and other features from Lime Peak, Part C. (**A**) Microborings (white triangles) in sponges of the tabular mound (TM) limestone (sample WH 181); (**B**) Microborings in the tubular crust (white triangles) in the TM (sample WH 181); (**C**) Particular of the tubular crust in normal (**left**) and cathodoluminescence (**right**) light. Black triangles point to areas where relicts of a tubular structure can be seen (sample WH 177); (for a coloured version, the reader is referred to the web version of this article).
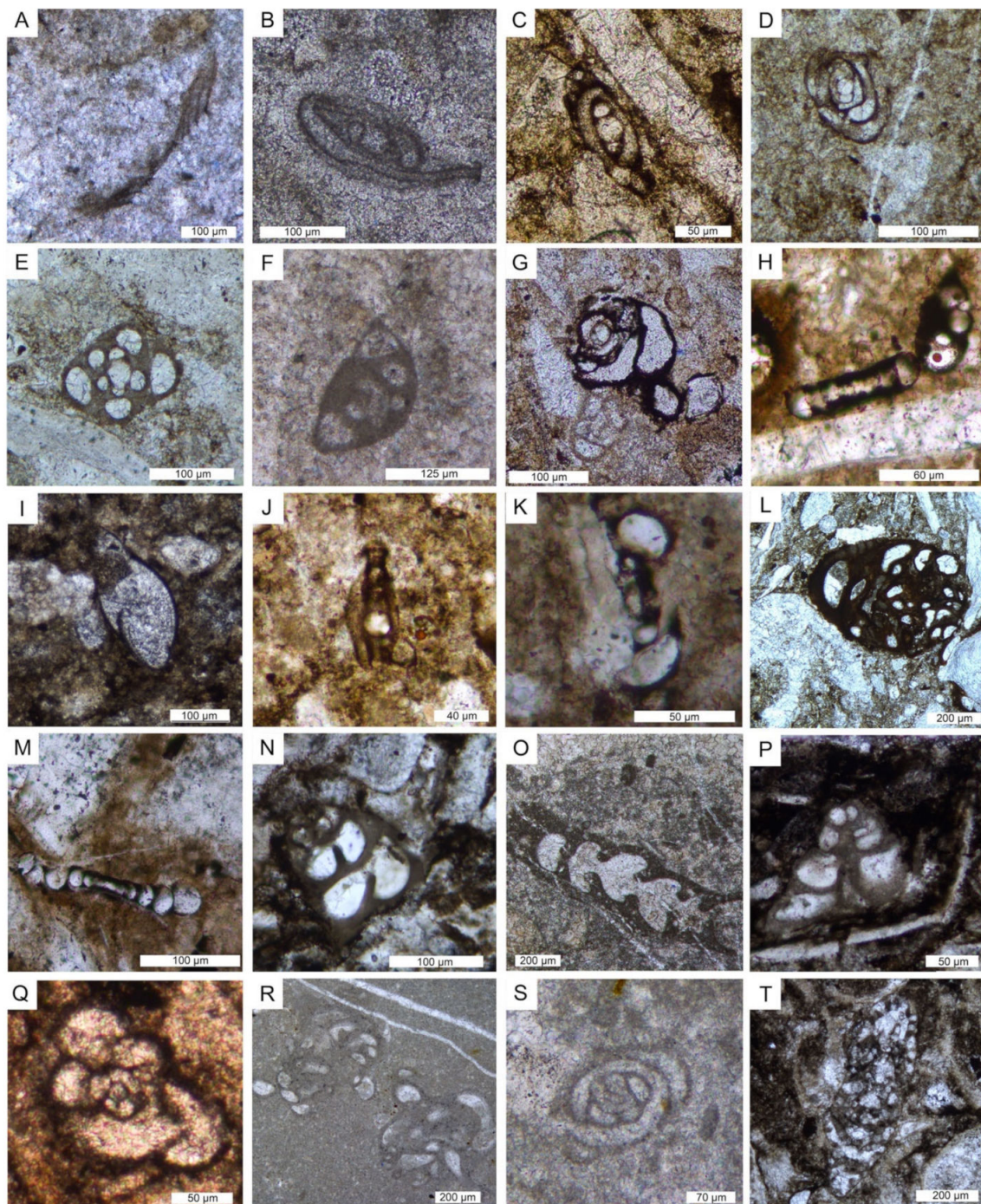
Figure 14. Porcelaneous, calcitic, microgranular and agglutinated foraminifera of Lime Peak. (**A**) *Hirsutospirella pilosa* (sample WH 231); (**B**) *Hydrania dulloi* (sample WH 192); (**C**) *Gsolbergella* sp. (sample WH 106); (**D**) *Hoyenella* sp. (sample WH 77); (**E**) ?*Agathammina* sp. (sample WH 76 A); (**F**) *Decapoalina schaeferae* (sample WH 560); (**G**) *Orthella* sp. (sample WH 188); (**H**) *Ophthalmidium* sp. (sample WH 226); (**I**) *Eoguttulina* sp. (sample WH 227 B); (**J**) *Paraopthalmidium* sp. (sample WH 79); (**K**) ?*Planinvoluta carinata* (sample WH 311); (**L**) *Alphinophragmium perforatum* (sample WH 135); (**M**) *Ammodiscus* sp. (sample WH 236 H); (**N**) ?*Duotaxis* sp. (sample WH 189 A); (**O**) ?fragment of the uncoiled part of ?*Endotebanella* sp. (sample WH 148); (**P**) *Taanella yukonensis* (sample WH 189 B); (**Q**) *Glutameandrata vallieri* (sample WH 233 A P); (**R**) ?*Tolypammina gregaria* (sample WH 277); (**S**) *Glomospira* sp. (sample WH 351); (**T**) *Wernlina reidae* (sample WH 227H); (for a coloured version, the reader is referred to the web version of this article).
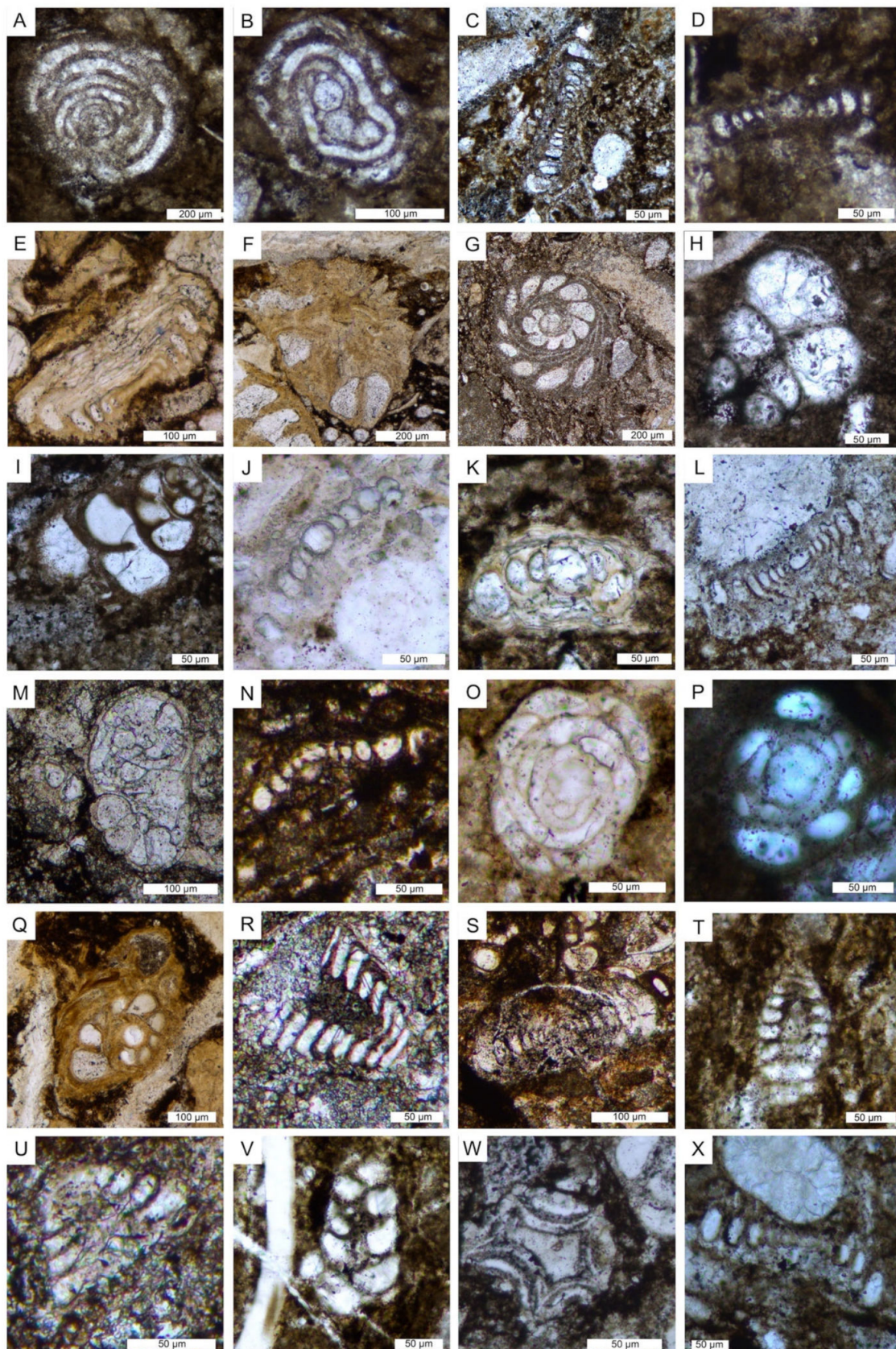
Figure 15. Aragonitic foraminifera of Lime Peak. (**A**,**B**) *Aulosina oberhauseri* (samples WH 259 L and WH 232 A, respectively); (**C**) *Aulotortus impressus* (sample WH 91); (**D**) *Aulotortus minutus* (sample WH 233 B); (**E**) *Coronipora* sp. (sample WH 305); (**F**) *Diplotremina subangulata* (sample WH 305);

(**G**) Duostominina (sample WH 80); (**H**) *Praegubkinella* sp. (sample WH 227F); (**I**) *Falsoreinholdella ohmi* (sample WH 259 I); (**J**) *Frentzenella frentzeni* (sample WH 263); (**K**) Juvenile Trocholinidae (sample WH 158 A); (**L**) *Licispirella iranica* (sample WH 91); (**M**) *Oberhauserella* sp. (sample WH 155); (**N**) *Papillaconus kristani* (sample WH 103); (**O**) *Parvalamella ashbaughi* (sample WH 79); (**P**) *Parvalamella sigmoidea* (sample WH 233 AP); (**Q**) *Praereinholdella* sp. (sample WH 305); (**R**) *Robertonella* sp. (sample WH 131); (**S**) *Semiinvoluta* sp. (sample WH 103); (**T**) "*Turrispirillina*" *carpatho-rumana* (sample WH 269); (**U**) *Trocholina* aff. *acuta* (sample WH 92); (**V**) *Trochosiphonia josephi* (sample WH 269); (**W**) *Tubulastella comans* (sample WH 259 H); (**X**) ?*Wallowaconus oregonensis* (sample WH 92); (for a coloured version, the reader is referred to the web version of this article).
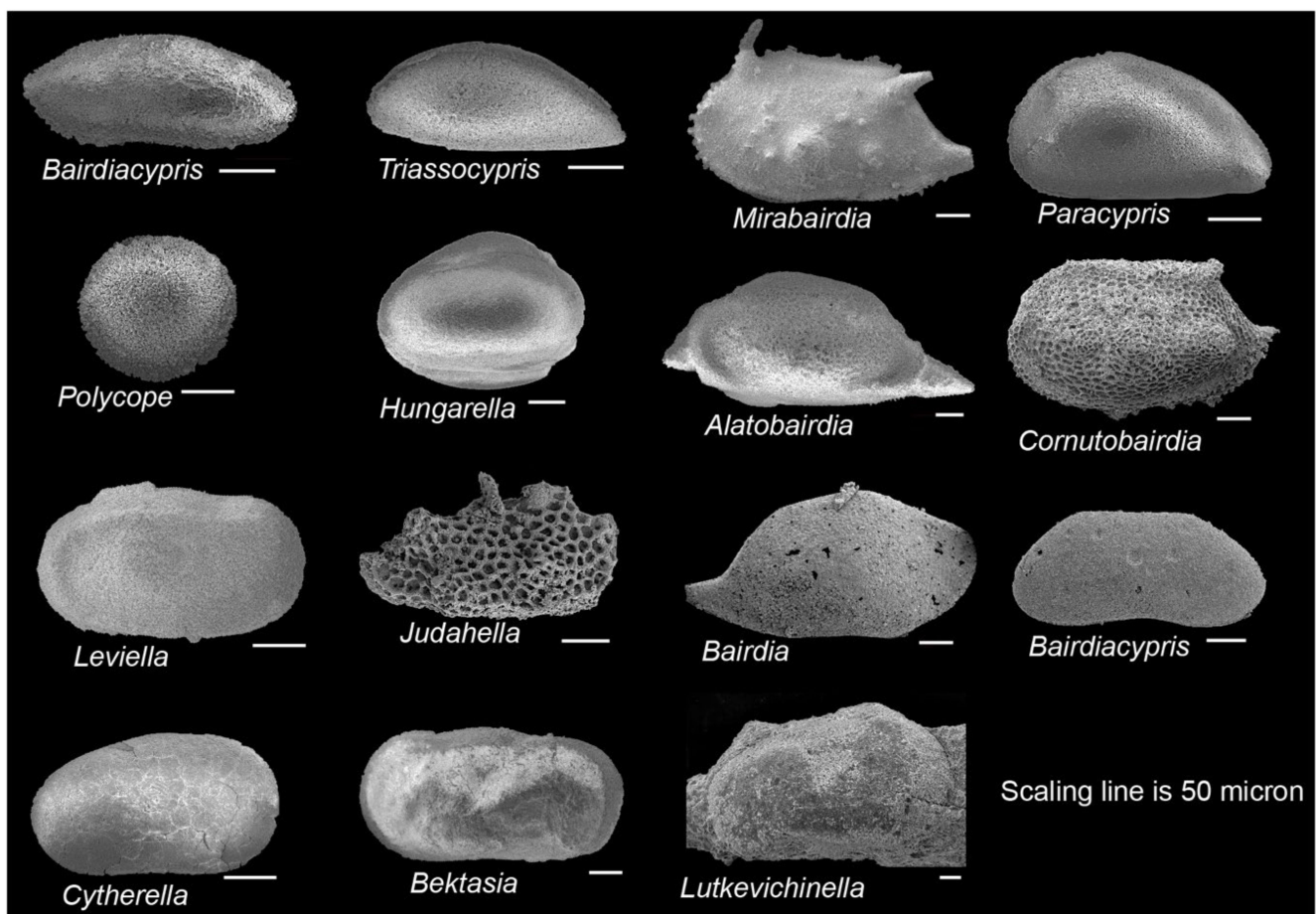
Figure 16. Selected ostracods from Lime Peak.

Table 1. Summary of the microfacies found at Lime Peak and their characteristics.

Microfacies	Lithofacies	Biotic Content and Foraminifers Assemblage	Other Components, Sedimentary Features and Other Remarks	Interpreted Depositional Environment
MCF 1—Bioclastic wackestone to floatstone	MM	Molluscs, crinoids+E12, dasycladaleans algae (frequent ? *Clypeina* sp.), calcareous sponges, solenoporacean algae, ostracods. Foraminifera assemblages include very abundant *Taanella yukonensis*, textulariidae, common Duostominina, Miliolidae, *Wernlina reidae*, rare nodosariidae and *Agathammina* sp.	Frequent neptunian dykes filled by clotted and peloidal micrite and/or very dark micrite	Inner platform (open)

Table 1. *Cont.*

Microfacies	Lithofacies	Biotic Content and Foraminifers Assemblage	Other Components, Sedimentary Features and Other Remarks	Interpreted Depositional Environment
MCF 2—Dasycladales-rich wackestone to floatstone	MTB	Dasycladalean green algae *Holosporella? rossanae, Patruliuspora oregonica* and *P. pacifica*, gastropods, bivalves, ostracods, spongiomorphs, echinoderms (echinoids and ophiurids), coral fragments, sponge fragments, megalodontid fragments, calcified cyanobacteria (*Girvanella* sp.), belemnites, *Baccanella floriformis*. Rich and diversified foraminifera assemblage dominated by very abundant *Aulosina oberhauseri, Parvalamella* spp., abundant *Wernlina reidae*, Taanella yukonensis, less common *Aulotortus* spp., *Frentzenella* spp., *Licispirella* sp., *Wallowaconus oregonensis, Falsoreinholdella* spp., *Praerheinoldella* spp., *Robertonella* spp., *Glutameandrata vallieri*, unidentified *Glutameandratidae*, and rare *Lamelliconus* sp., *Trocholina* spp., *Eoguttulina* sp., Ichtyolariidae, *Trochosiphonia* sp. Nodosariidae, Polymorphinidae, *Tubulastella comans*, Duostominina, *Diplotremina* sp., ?*Praegubkinella* sp., ?*Cycloforina* sp., *Agathammina, Hoyenella* sp., *Orthella* sp., *Opthalmipora* sp., Ammodiscidae, *Ammodiscus* spp., unidentified Miliolidae, Ammovertellinae, *Duotaxis* sp. and textulariidae	Beds containig this microfacies have a very dark color and have a fetid smell probably due to high organic matter and H2S content. Moreover, they bear large gastropods which are as long as 50 cm. Rest of oxidized ligneous fragments are common. Oncoids, microborings and micritic envelopes are very common. The matrix, often bioturbated and organic-rich, varies from being mud-dominated to very-fine bioclastic	Inner platform (restricted)
MCF 3—Peloidal and bioclastic packstone to rare grainstone	MTB and VTB west of K2	Molluscs (bivalves and gastropods), calcified cyanobacteria (mostly *Cayeuxia* sp.), dasycladalean green algae, serpulids, ostracods, rare brachiopods, echinoid spines, foraminifers, rare crinoids and fragments of reef-derived biota such as sponges, serpulids and red algae. At times, debris of organisms resembling very small phaceloid corals are abundant. Among the non-skeletal grains peloids and extraclasts of different shapes and sizes are abundant. Foraminifera assemblages are restricted to very abundant *Taanella yukonensis*, common Miliolidae, Duostiminina, *Glomospira* sp., unidentified glutameandratidae, rare *Decapoalina schaeferae* and Involutinina.	Beds containig this microfacies have a very dark in color. Micritic envelope and micritized grains are very abundant. The intergranular porosity is filled either by cement or by a matrix which is fine bioclastic to micritic in nature.	Inner platform (restricted)

Table 1. *Cont.*

Microfacies	Lithofacies	Biotic Content and Foraminifers Assemblage	Other Components, Sedimentary Features and Other Remarks	Interpreted Depositional Environment
MCF 4—Bioclastic rudstone	MM	Gastropods, bivalves, foraminifera, serpulids, corals, brachiopods, echinoderms, sponges. Foraminifera assemblages restricted to Duostominina	Angular extraclats (resembling MCF 4) and peloids. Aragonitic allochems (e.g., bivalves) have been dissolved. Rim of isopachous drusy cement and syntaxial overgrowths on some clasts; intergranular porosity is filled by a whitish to yellowish granular mosaic cement	Inner platform (open), tidal channel
MCF 5—Peloidal and bioclastic grainstone	TM and MM	Molluscs (bivalves and gastropods), dasycladalean green algae (?*Clypeina* sp. and possibly ?*Kantia* sp.), ostracods, crinoids and fragments of reef-derived biota. Foraminifera assemblages are constituted by very abundant *Glomospira* sp., common Duostominina, Miliolidae, Glutameandratidae and rare *Decapoalina schaeferae* and *Taanella yukonensis*	Peloids, extraclast. Micritization processes are widely diffused and led either the formation of a micritic envelope or to the complete micritization of the allochems	Margin area, sand banks
MCF 6A—Thrombolitic bindtsone	MM	Microbialite encrusted by *Planiinvoluta carinata* and other small sphinctozoan sponges. Areas of clotted and peloidal micrite show the presence of ostracods and foraminifera (textulariids, nodosariids and miliolids).	Microbialite acts as framebuilder. Microbial fabric has either a leiolitic to thrombolytic appearance	Outermost margin area
MCF 6B—Stromatolitic bindstone	MM	Microbialite encrusted by small ponges, Tolypammina sp. Microtubus communis, Terebella sp., serpulids and Radiomura cautica. The areas between the microbial fabric bear crinoids, molluscs and ostracods. Foraminifera assemblages are restricted to common textulariids and rare unidentified nodosariidae and miliolids.	Microbialite acts as framebuilder. Microbial fabric has either a stromatolitic appearance	Inner platform

Table 1. *Cont.*

Microfacies	Lithofacies	Biotic Content and Foraminifers Assemblage	Other Components, Sedimentary Features and Other Remarks	Interpreted Depositional Environment
MCF 7—Metazoans framestone	TM and MM	Inozoan sponges, sphinctozoan sponges, *Spongiomorpha ramosa* and *gibbosa*, disjectoporoids sponges, chaetetids sponges, corals, phylloid and solenoporaceans algae, serpulids, brachiopods, ostracods, calcified cyanobacteria, microproblematica. Foraminifers assemblages are dominated by sessile forms like *Planiinvoluta carinata*, *Tolypammina* sp., *Alphinophragmium* sp. and *Hirsutospirella pilosa* which are found encrusting the main framework. Within the sediment which infills the cavities we find *Textularia* sp., unidentified miliolids, *Agathammina* sp., *Gsolbergella* sp., *Hoyenella* sp., *Sigmoilina* sp., *Hydrania dulloi*, *Ophthalmidium* sp., *Paraophthalmidium* sp., unidentified textulariids, unidentified glutameadratidae, *Ammodiscus* sp., unidentified Ammodiscidae? *Endotebanella* sp., ?*Glomospira* sp., *Taanella yukonensis*, nodosariidae, duostominina	Microbialite is abundant and acts both as binder of pre-existing framework and as framebuilder. Numerous primary (framework) and secondary (dissolution and/or decaying) cavities which are filled either by cements, muddy extraclasts, peloidal micrite or very dark micrite	Margin area, reef
MCF 8—Sponges bindstone	TM	Sponges, solenoporacenas algae, calcified cyanobacteria, echinoderms and rare corals. Foraminifera assemblages are restricted to very abundant specimens of Duostominina, *Taanella yukonensis*, rare *Aulosina oberhauseri*, *Coronipora* sp? *Lamelliconus* sp., *Robertonella* sp., *Gsolbergella* sp., *Hoyenella* sp., *Wernlina reidae* and unidentified Ammodiscidae	Cavities are very rare. Microbialite acts as binder of a pre-existing substrate	Margin area, crest
MCF 9—Crinoidal grainstone to rudstone	TM and VTB	Crinoids, calcified cyanobacteria (*Cayeuxia* sp.), calcareous sponges (chaetetids the most significant), molluscs. Foraminifera assemblages restricted to abundant Duostominina and rare unidentified Miliolidae	Micritic enveloppes around grains are very frequent. Intergranular porosity filled by a whitish granular mosaic calcite and rarely by micrite	Upper slope
MCF 10—*Spongiomorpha gibbosa* packestone to floatstone	VTB	*Spongiomorpha gibbosa*, echinoderms, brachiopods, bivalves, ostracods, dasycladalean algae (*Clypeina* sp.). Foraminifera assemblage is mostly dominated by very abundant Duostominina, *Wernlina reidae* and *Taanella yukonensis*	Matrix is formed by dark micrite. Very frequent microbial encrustations	Slope

Table 1. *Cont.*

Microfacies	Lithofacies	Biotic Content and Foraminifers Assemblage	Other Components, Sedimentary Features and Other Remarks	Interpreted Depositional Environment
MCF 11—*Retiophyllia* sp. framestone to floastone	VTB	Presence of *Retiophyllia* sp. either in living position or as debris. The matrix between the coral branches is given by a wackestone rich in sponge spicules, molluscs (small gastropods and bivalves), echinoderms and ostracods. Foraminifera assemblages are restricted to very abundant Nodosaridae, and rare *Wallowaconus oregonensis*, *Ammodiscus spp.* and other unidentified Ammodiscidae	When found in living position, *Retiophyllia* sp. forms small 30–40 cm wide thickets. Its branches are often silicified and without biogenic encrustations or synsedimentary cement	Slope
MCF 12—Sponges-molluscs packstone to rudstone	TMB	Sponges (common chaetetids, *Spongiomorpha sp.* inozoans and sphinctozoans), calcified cyanobacteria (*Cayeuxia* sp.), coral fragments (*Retiophyllia* sp. and *Montlivaltia* sp.), echinoderms, brachiopods, gastropods, bivalves, brachiopods, ostracods, rare green algae (?*Kantia* sp.). The foraminifera assemblages are formed by abundant *Wernlina reidae*, *Taanella yukonensis*, Duostominina, common *Wallowaconus oregonensis*, *Coronipora* spp., Nodosaridae, *Agathammina* spp. and Miliolidae together with rare *Diplotremina* sp., ?*Oberhausella* sp., *Falsoreinholdella* spp., *Praereinholdella* spp., *Robertonella* spp., *Trochosiphonia josephi*, *Parvalamella* spp., *Aulosina oberhauseri*, *Aulotortus impressus*,?*Lamelliconus* sp., ?*Licispirella iranica*, ?*Turrispirillina* spp., *Frentzenella frentzeni*, *Papillaconus kristani*, *Trocholina* spp., *Semiinvoluta* spp.	Microbial encrustations are quite common	Slope
MCF 13—Laminated and graded wackestone to rudstone	TMB	Sponges (common chaetetids, Spongiomorpha sp. inozoans and sphinctozoans), calcified cyanobacteria, molluscs, brachiopods, ostracods, sponge spicules. Foraminifera assemblages restricted to Duostominina and nodosariids	Erosive base, strongly developed lamination and normal grading	Slope/Toe of the slope
MCF 14—Radiolarian-rich bioturbated mudstone to wackestone	TMB	Ostracods, recrystallized radiolarians, sponge spicules, gastropods, thin-shelled bivalves, terebratulid brachiopods. Foraminifera assemblages mainly contain nodosariidae and Duostominina	Matrix is muddy to very fine bioclastic	Toe of the slope
MCF 15—Grain-supported limestone breccia or conglomerate	LB	Fragments of corals and sponges	Rounded to sub-angular carbonate and volcaniclastic lithoclasts. Intergranular porosity filled by a whitish granular mosaic calcite cement	?

MCF 2—Dasycladales-rich wackestone to floatstone (Figure 9B). This microfacies is found exclusively in the medium- to thick-bedded impure limestone of the second package (Figure 2C). Outside the study area, we also recovered this microfacies from an isolated outcrop in the northwestern side of Lime Peak where it is found in association with MCF 3 and less frequently MCF 7 (see Supplementary Materials: Figure S1). Frequently, this microfacies presents a very darkish colour even at the fresh surface. This dark colour is the result of a higher organic matter content as indicated by organic "flakes" (most likely solid bitumen) sparse in the matrix and bitumen drops in fractures and pores. Rest of oxidized ligneous fragments are also commonly present within this microfacies. The bioclastic fraction of this, poorly sorted and heterogeneous wackestone to floatstone, is regularly unbroken to slightly broken. The biotic content, quite heterogeneous and variable in composition, is most of the times dominated by dasycladales [*Holosporella*? *rossanae* (Figure 11B), *Patruliuspora pacifica* (Figure 11C) and *Patruliuspora oregonica* (Figure 11D)], gastropods [which range in size from mm sized up to 40 cm long (Figure 4D)] and bivalves. The variation in the concentration of these bigger bioclasts determines the change from wackestone to floatstone. Common are also ostracods, foraminifera, echinoids and ophiuroids along with fragments of corals, sponges, *Spongiomorpha ramosa* and big fragments of bivalves (?megalodontids) and calcified cyanobacteria [mostly *Cayeuxia* sp. (Figure 11H) and *Girvanella* sp. (Figure 11I)]. Belemnites and *Baccanella floriformis* (Figure 12B) tend to be rarer. Borings and micritic envelopes are very common. The matrix, sometimes bioturbated, varies from being mud-dominated to very-fine bioclastic. At times, the bulk content of MCF 2 slightly differs and is dominated by ostracods, *Girvanella* sp., tinier bivalves (shell thickness between 50 and 300 microns) and gastropods. MCF 2 bears the richest and most diversified foraminiferal assemblage among all the microfacies. It is dominated by very abundant *Aulosina oberhauseri* (Figure 15A,B), *Parvalamella* spp. (Figure 15O,P), abundant *Wernlina reidae*, *Taanella yukonensis*, less common *Aulotortus* spp. (Figure 15C,D), *Frentzenella* spp. (Figure 15J), *Licispirella* sp. (Figure 15L), *Wallowaconus oregonensis* (Figure 15X), *Falsoreinholdella* spp. (Figure 15I), *Praereinholdella* spp. (Figure 15Q), *Robertonella* spp. (Figure 15R), unidentified miliolids, *Glutameandrata vallieri* (Figure 14Q), unidentified Glutameandratidae, rare *Lamelliconus* sp., *Trocholina* spp. (Figure 15U), *Eoguttulina* sp. (Figure 14I), Ichtyolariidae, *Trochosiphonia* sp. (Figure 15V), Nodosariidae, Polymorphinidae, *Tubulastella comans* (Figure 15W), Duostominina, *Diplotremina* sp. (Figure 15F), Oberhausellidae, ?*Praegubkinella* sp. (Figure 15H), *Agathammina* sp., *Hoyenella* sp. (Figure 14D), *Orthella* sp. (Figure 14G), *Ophthalmipora* sp., Ammodiscidae, *Ammodiscus* spp. (Figure 14M), Ammovertellinae, *Duotaxis* sp. (Figure 14N), *Trochammina* sp. and textulariids. This microfacies bears a rich and diversified ostracod assemblage in which the genera *Bairdia*, *Cytherella*, *Bektasia*, *Leviella*, *Hungarella* and *Lutkevichinella* (Figure 16) prevail.

MCF 3—Molluscs and calcified cyanobacteria packstone to rare grainstone (Figure 9C). This microfacies occurs only in the medium- to thick-bedded impure limestone of the second package in association with MCF 2. As for MCF 2, we also recovered this microfacies from the northwestern side of Lime Peak. According to Reid [51], this microfacies would also occur in the very thick-bedded limestone to the west of K2. Grains within this microfacies are poorly to moderately sorted. Identifiable bioclasts are molluscs (bivalves and gastropods), calcified cyanobacteria (mostly *Cayeuxia* sp.), dasycladales, ostracods, rare brachiopods, echinoid spines, foraminifera, rare crinoids and fragments of reef-derived biota such as sponges, serpulids and red algae. At times, debris of an organism resembling a very small, unidentified phaceloid coral are abundantly observed (see Figure 9C). Other grains are profuse peloids and extraclasts of different shapes and sizes. Micritic envelopes and micritized grains are very copious. The intergranular porosity is filled either by cement or by fine bioclastic to micritic matrix. Foraminiferal assemblages are restricted to rich *Taanella yukonensis*, common Miliolidae, Duostiminina, *Glomospira* sp., unidentified Glutameandratidae, and rare *Decapoalina schaeferae* and Involutinina.

MCF 4—Bioclastic rudstone (Figure 9D). This microfacies is only rarely found within Avens in association with MCF 1. It consists of moderately to heavily fragmented bio-

clasts (foraminifera, gastropods, bivalves, serpulids, corals, crinoids, sponges and other unidentified bioclasts) and angular extraclasts (strongly resembling MCF 1). Aragonitic bioclasts (e.g., molluscs) underwent dissolution. Some clasts present rims of isopachous drusy cement, while echinoderms display syntaxial overgrowths; intergranular porosity is filled with a whitish to yellowish granular mosaic cement. Foraminiferal assemblage is mostly dominated by Duostominina representatives.

MCF 5—Peloidal and bioclastic grainstone (Figure 9E). This microfacies is frequently encountered in the eastern part of Avens body (Supplementary Materials: Figure S1) in association with MCF 7 and 6A. It is also found in the second package inside K2 in association with MCF 7 and 8. Grains within this microfacies range from moderately to well-sorted. Identifiable bioclasts are foraminifera, molluscs (bivalves and gastropods), dasycladale green algae (?*Clypeina* sp. and possibly *Kantia* sp.; Figure 11E), ostracods, crinoids and fragments of reef-derived biota such sponges and serpulids. Other grains are peloids, some extraclasts and rare ooids. Overall, grains appear to have been strongly affected by micritization that led to either the formation of a micritic envelope or to the complete micritization of allochems. Foraminiferal assemblages are constituted of very abundant *Glomospira* sp. (Figure 14S), common Duostominina, Miliolidae, Glutameandratidae and rare *Decapoalina schaeferae* (Figure 14F) and *Taanella yukonensis*.

MCF 6A—Thrombolitic bindstone (Figure 9F). Unlike in the other framework microfacies (i.e., MCF 7), in MCF 6A, microbialites do not have only an accessory role but form most of the constructive rigid framework. MCF 6A is found in the eastern end of Avens body associated with MCF 7 and 5 and minorly within very thick-bedded limestone associated with MCF 9 and 10. In MCF 6A, the microbial fabric presents a leiolitic to thrombolytic fabric in which dark aphanitic areas alternate with areas where clotted and peloidal micrite prevail (Figure 9F). Intercalations of MCF 5 are often found within MCF 6A. In MCF 6A, the micritic areas are heavily encrusted by *Tolypammina* sp. (Figure 14R) and minorly by small sphinctozoan sponges. Clotted and peloidal micrite areas show the minor presence of ostracods and foraminifera (textulariids, nodosariids and miliolids).

MCF 6B—Stromatolitic bindstone (Figure 9G). MCF 6B was only found in one sample (WH 406) from the internal part of Avens (see Supplementary Materials: Figure S1) in association with MCF 1 and not far away from the area where megalodontids and *Wallowa-concha* cf. *raylenea* are exposed. MCF 6B displays a stromatolitic structure that consists of aggrading laminae of clotted and peloidal micrite alternating with denser micritic laminae (Figure 9G). The microbialites fabric is arranged in lateral micro-columns. Boring is very common in the microbialites fabric. Within the microbial fabric, there are encrusting organisms such as *Microtubus communis* (especially in the denser micritic laminae, Figure 11K), *Terebella* sp. (Figure 12D), serpulids (Figure 12E) and *Radiomura cautica* (Figure 12C). At times, the microbialites embody bivalves and/or brachiopods. The space between the micro-columns is filled with sediment that is very similar to MCF 1 and consists of molluscs, crinoids, ostracods, dasycladales and foraminifera. Peloids are also common. In MCF 6B, the foraminiferal assemblage is restricted to *Planiinvoluta carinata* (Figure 14K), common textulariids and rare, unidentified Nodosariidae.

MCF 7—Metazoans framestone (Figure 9H,I). This microfacies is mostly present within Avens (associated with MCF 1, 5, 6A) and inside K2 in the second package (associated with MCF 5 and 8). At the macroscale, within the massive and tabular mounds, this microfacies seems to be clustered in patches that are generally only few meters wide. MCF 7 is characterized by the presence of framework organisms that often show preferential upward growth direction and form a rigid framework. This framework creates two types of well-defined primary cavities: intra-organisms (i.e., inozoans chambers (abundant)) and/or inter-organisms (less common). Among the framework organisms, we find inozoan sponges, sphinctozoan sponges (for more information see [59]), *Spongiomorpha ramosa* and *S. gibbosa*, disjectoporoids sponges, chaetetids sponges and subordinate corals, either colonial (some of the coral species present at Lime Peak probably belongs to the genera *Retiophyllia* sp., *Chondrocoenia* sp., *Gablonzeria* sp., *Margarastraea* sp., *Distichomeandra* sp.,

Astraeomorpha sp., *Procyclolites* sp. and *Crassitella* sp., see [53]) or solitary (which, according to [53], might belong to one or more of the genera *Distichophyllia*, *Cuifa* and *Montlivaltia*). Tubular crust (Figure 12G,J) generally postdates sponges and corals and uses them as rigid substrate to grow on. However, in several cases, this crust does not behave entirely as a secondary encruster but also forms an active framework that is later used by other organisms as a hard substrate to grow on (e.g., see Figure 12H). This tubular crust is generally, in turn, overgrown by microbialites. At times, the two are found intergrowing (e.g., Figure 12H) and are encrusted (e.g., Figure 12G,J) and bored by other organisms. The differences between tubular crusts and microbialites primarily lie in their colour (yellowish vs. grey to black) and the fact that tubular crusts show an internal fibrous to tubular structure (better observed in cathodoluminescence: see Figure 13C), whereas microbialites do not show any peculiar internal microstructure (besides microlaminations that are given by different layers of microbialites (MB) overgrowing each other).

The organisms that build the primary framework, especially tubular crusts and sponges, locally present traces of boring activity. In particular, microborings appear to be common within the MCF 7 samples from the tabular mound limestone (Figure 13A,B). This rigid framework is further colonized by sessile organisms such as calcareous algae (phylloids and solenoporaceans), small encrusting sponges (such as *Radiomura cautica*), serpulids, brachiopods and worm tubes (*Terebella* sp.), bivalves, calcified cyanobacteria (*Cayeuxia* sp.), microproblematica (*Microtubus communis*, *Baccanella floriformis* and other unidentified encrusters) and various sessile foraminifera. Among the encrusting foraminifera, *Planiinvoluta carinata* and *Tolypammina* sp. are the most abundant, with rare occurrences of *Alphinophragmium* sp. (Figure 14L) and *Hirsutospirella pilosa* (Figure 14A). The cavities in this microfacies can be either primary or secondary. As mentioned above, primary cavities exist either as constructive cavities between different framebuilders or as intragranular cavities. Constructive cavities are almost exclusively filled with sediments. This infilling can be divided into three categories: (1) clotted and peloidal micrite, (2) wackestone to packstone rich in mollusc debris, crinoids, foraminifera (very similar to MFC 4, see below) and rare *Globochaete* sp. (Figure 12A) and more rarely (3) a grainstone rich in foraminifera, ostracods, peloids and spar-rimmed peloids (Figure 11L). Within these different infills, two different types of micrite occur: (1) clotted and peloidal micrites that are made up of very small peloids (on average 10 to 50 μm in diameter) and are usually clustered in groups and might present an outer spar rim [57]—this form of micrite is also known as internal micrite [93], peloidal cement [94], automicrite [95,96] or peloidal micrite [97]—and (2) interstitial micrite that is present in the wackestone to packstone infills. In terms of foraminiferal assemblages, there are major dissimilarities among the different infills: clotted and peloidal micrite bears poorly diversified assemblages restricted to *Textularia* sp. and some unidentified miliolids. On the other side, the wackestone to packstone and the grainstone infills bear different forms, including *Agathammina* sp., *Gsolbergella* sp. (Figure 14C), *Hoyenella* sp., *Decapoalina schaeferae*, *Hydrania dulloi* (Figure 14B), *Ophthalmidium* sp. (Figure 14H), *Paraophthalmidium* sp. (Figure 14J), *?Turrispirillina* spp. (Figure 15T), Nodosariidae, other unidentified Miliolidae, microgranular or agglutinated foraminifera such as unidentified Textulariidae and Glutameadratiidae, *Ammodiscus* sp. and other Ammodiscidae, ?*Endotebanella* sp. (Figure 14O) ?*Glomospira* sp., *Taanella yukonensis* and aragonitic foraminifera such as Duostominina. Primary cavities can also originate as intragranular cavities within the sponges (in the internal chambers of sphinctozoans, e.g., see Figure 9H). These cavities can be filled with either sediment (similar to the three types described above) or by a whitish, drusy to equigranular mosaic cement. In a few samples, abundant ostracods occur within the internal chambers of sponges. They were extracted, and the assemblages show dominance of the genera *Bairdiacypris*, *Bairdia*, *Paracypris* and *Polycope* (Figure 16). Secondary cavities represent an important fraction of the bulk of MCF 7: they are formed by the decay of some reef builders, or by their (early) dissolution. Secondary cavities can be recognized by the presence of microbial or, more commonly, tubular crusts that grow on them (Figure 12G,I) and delimit the outer surface of the cavities. This type of cavity is often

filled with different generations of cements that grow centripetally, a criterion allowing them to be distinguished from look-alike tubular crusts (their coloration is different, and cements are also commonly banded). At first, cavities are filled with multiple generations of light grey radiaxal fibrous isopachous and/or fibrous isopachous cements (Figure 12I) that are frequently intercalated with thin layers of microbialites. Occasionally, the innermost portion of the cavities is successively filled with a whitish, drusy or granular mosaic cement (Figure 12I). In only one sample (WH 312), the internal portion of a secondary cavity also showed the presence of a layer of dog-tooth cement. Dissolution cavities filled with sediments are rarer. When occurring, the infill is different from the one filling primary cavities and can also display a different orientation (e.g., Figure 9H). This infilling sediment can be divided into two categories: (1) a clotted and peloidal micrite with abundant mudclasts and (2) a very dark mudstone in which a very poor biotic content, restricted to few ostracods and molluscs, is found in a dense micritic matrix.

MCF 8—Sponges bindstone (Figure 9J). This microfacies is often located within K2 in the second package in association with MCF 5 and 7. In a few cases, MCF 7 and 8 coexist in the same thin section, pointing to their close connection. Almost the entirety of this microfacies is formed by reef biota (e.g., sponges, red algae, calcified cyanobacteria and rare corals) very similar to that of MCF 7. However, unlike in MCF 7, the reef biota in MCF 8 is not in life position. Organisms in MCF 8 are lightly to moderately fragmented and do not show any preferential growth direction. Rare extraclasts and crinoids are also abundant. The remaining fraction is made up of smaller allochems, including peloids, ostracods, foraminifera and molluscs, which are scattered between the bigger bioclastic fraction or in small cavities. The allochems in MCF 8 are frequently bound by a thin layer of microbialites. In MCF 8, the cavities appear to be depositional and not constructional. Intergranular porosity is either filled with micrite or whitish granular mosaic cements. Foraminiferal assemblages are restricted to very abundant specimens of Duostominina, *Taanella yukonensis*, rare *Aulosina oberhauseri*, *Coronipora* sp. (Figure 15E), juvenile Trocholinidae (Figure 15K), *Robertonella* sp., *Gsolbergella* sp., *Hoyenella* sp., *Wernlina reidae* and unidentified Ammodiscidae.

MCF 9—Crinoidal grainstone to rudstone (Figure 9K). This microfacies is mostly located in the very thick-bedded limestone of the first and third package in association with MCF 6A and 10. The bioclastic fraction of this strongly unsorted microfacies is habitually abraded and/or broken. Crinoids are the main constituents, along with calcified cyanobacteria (*Cayeuxia* sp.), red algae, calcareous sponges (chaetetids are very frequent), molluscs and foraminifera. Foraminiferal assemblages are dominated by very abundant Duostominina and rare Miliolidae and *Taanella yukonensis*. Micritic envelopes around grains are frequent. The intergranular spaces are filled with a whitish granular mosaic calcite and rarely by micrite. Although the general composition is very similar to that observed in MCF 8, MCF 9 lacks the important network of microbialites characterising MCF 8.

MCF 10—*Spongiomorpha gibbosa* packestone to floatstone (Figure 9L). This microfacies is almost exclusively identified in the very thick-bedded limestone of the first and third package in association with MCF 6A, 9, 11 and 14. The bioclastic fraction of this microfacies is generally very unsorted. The concentration of *Spongiomorpha gibbosa* varies from being slightly present (wackestone) to very abundant (floatstone), and specimens appear unbroken or only slightly fragmented. The abundance of stromatolitic microbialites within this microfacies varies from scarce to abundant. Often, the specimens of *Spongiomorpha gibbosa* present well-developed microbialites only on one side of the organism (Figure 9L). Besides *Spongiomorpha gibbosa*, the bioclastic fraction of this microfacies is rich in crinoids, corals, brachiopods, bivalves, thin-shelled bivalves (most likely belonging to one or more of the genera *Halobia*, *Eomonotis* or *Monotis*) and ostracods. Dasycladales algae (?*Clypeina* sp.) are also present within MCF 10, and their abundance varies from absent to common. Reid (1985) reported the presence of sphinctozoan sponges such as *Polytholosia ramosa* and *Polytholosia cylindrica* in upright position within MCF 10, along with poorly preserved solitary corals. The matrix is formed by dark micrite. Foraminiferal assemblage

is dominated by very abundant Duostominina, *Wernlina reidae*, *Taanella yukonensis* and rare *Paraophthalmidium* sp.

MCF 11—*Retiophyllia* framestone to floatstone (Figure 10A). This microfacies is found within the very thick-bedded limestone of the first package, where it is in vertical association with MCF 10 and 14. It is important to say that *Retiophyllia* sp. occurrences are also located within the massive mound limestone; however, those occurrences are counted as part of the reef patches (MCF 1). The framestone end-member of MCF 11 is associated with the in-living-position, fragile, branching coral *Retiophyllia* sp. (upward growing, Figure 5D). MCF 11 occurs in very thick-bedded limestone horizons, formed by slightly more impure limestone, in which these corals are particularly abundant (e.g., coral layer in Figures 4B and 5D). Within this framestone, *Retiophyllia* sp. is often silicified and without biogenic encrustations or synsedimentary cement. In the floatstone end-member of MCF 11, *Retiophyllia* sp. is not in living position but is only coarse debris in a finer matrix. This matrix, which is also equivalent to the one from the framestone end-member, is a wackestone rich in sponge spicules, molluscs (small gastropods and thin-shelled bivalves), crinoids and ostracods (very similar to MCF 14, see below). In the matrix of this microfacies, foraminifera are rare and limited to very abundant Nodosariidae and rare *Taanella yukonensis*, *Ammodiscus* spp. and other unidentified Ammodiscidae.

MCF 12—Sponges–molluscs packstone to rudstone (Figure 10B). This highly heterogeneous and unsorted microfacies is present principally in the thin- to medium-bedded impure limestone of the second package (Figure 7B) where, within thin- to medium-bedded impure limestone, it is associated with MCF 13 and 14. The coarser bioclastic fraction, which gives the floatstone to rudstone appearance, includes calcareous sponges (very common chaetetids, rare *Spongiomorpha* sp. and other sponges that also occur in MCF 7), calcified cyanobacteria (*Cayeuxia* sp.), *Girvanella*-oncoids (Figure 11J), solenoporacean red algae and minor coral debris. The matrix within the coarser bioclasts consists of a packstone with abundant crinoids, gastropods, foraminifera, brachiopods, bivalves, brachiopods, ostracods and rare green algae (?*Kantia* sp., *Patruliuspora* spp. and ?*Teutoplorella* sp.). Microbial encrustations are quite common. The foraminiferal assemblages are represented by abundant *Wernlina reidae*, *Taanella yukonensis*, Duostominina, common *Wallowaconus oregonensis*, *Coronipora* spp., Nodosariidae, *Agathammina* spp. and miliolids, together with rare *Endothyra* sp., *Diplotremina* sp., ?*Oberhauserella* sp. (Figure 15M), *Falsoreinholdella* spp., *Praereinholdella* spp., *Robertonella* spp., *Trochosiphonia josephi*, *Parvalamella* spp., *Aulosina oberhauseri*, *Aulotortus impressus* (Figure 15C), ?*Lamelliconus* sp., *Licispirella* sp., ?*Turrispirillina* spp., *Frentzenella frentzeni*, *Papillaconus kristani* (Figure 15N), *Trocholina* spp. and *Semiinvoluta* spp. (Figure 15S).

MCF 13—Laminated and graded wackestone to rudstone (Figure 10C). This microfacies is very common within the thin- to medium-bedded impure limestone of the second package, where it forms beds showing strongly erosive contacts (Figure 4E) with other microfacies such as MCF 12 and 14. The normal grading observed is given by sediments that range from very coarse sand to gravel found at the base, to mud at the top. In terms of carbonate classification, when complete, this microfacies displays a transition from very coarse rudstone to fine wackestone to mudstone. The coarser part of the deposits is formed by abundant shallow-water biota (mostly calcareous sponges, calcified cyanobacteria and molluscs, among others), while the strongly laminated finer part (in which traction ripples are rarely found; see Figure 4F) of the deposit is formed by ostracods, sponge spicules and small foraminifera within a very fine bioclastic matrix. Some thin laminae show a darker colour, which is most likely given by a higher content of organic matter. The foraminiferal assemblages only comprise Duostominina and nodosariids. The ostracod assemblages are dominated by the genera *Bairdia*, *Bektasia*, *Bairdiacypris*, *Paracypris*, *Triassocypris* and *Polycope* (Figure 16).

MCF 14—Radiolarian-rich bioturbated mudstone to wackestone (Figure 10D). This microfacies stands in the thin- to medium-bedded impure limestone. Within the first and third package, it is associated with MCF 10, 11, and 13, while in the second package, it is

associated with MCF 12 and 13. This microfacies is generally unsorted; its bioclastic content is dominated by ostracods, recrystallized radiolarians, sponge spicules, rare gastropods, thin-shelled bivalves and minor foraminifera. The matrix is very fine bioclastic in nature. The beds that contain this microfacies yield abundant terebratulid brachiopods. The foraminiferal assemblages are formed by very abundant Nodosariida and Duostominina.

MCF 15—Grain-supported limestone conglomerate or breccia (Figure 10E). This microfacies is present within the limestone conglomerate or breccia. Clasts, very unsorted and rounded to sub-angular in nature, consist mostly of carbonate lithoclasts, with only minor volcaniclastic ones. Only at times do clasts consist of fragments of single organisms such as corals and sponges. Carbonate clasts generally have microfacies ranging from framestone (MCF 7) to wackestone (MCF 14). The intergranular porosity is occupied by a whitish, granular, mosaic calcite cement.

6.2. Composition of the Reef Facies

The average results from the point-counting analysis (for the whole dataset see Supplementary Materials: Figure S3) are shown in Table 2 and Figure 17. At Lime Peak, the main framebuilders are by far sponges, microbialites and tubular crusts. Of the latter, sponges account for 25.22% and 35.05%, microbialites for 20.14% and 15.20%, and tubular crust for 10.61% and 15.00% of the massive and tabular mounds limestone, respectively. Corals (0.66% in the massive and 1.15% in the tabular limestone) and encrusters (2.67% in the massive mound limestone (MM) and 2.55% in the tabular mud limestone (TM)) are only of secondary importance. Within the MM, in the interstitial sediments fraction, we find abundant clotted and peloidal micrite (17.13%) followed by interstitial micrite (5.07%), peloids or ooids (4.51%), dwellers (3.52%), intergranular cement (3.32%) and dense micrite (3.13%). Primary and secondary cavity-filling cements account for 0.84% and 3.19%, respectively. Within the TM, the main constituent of the interstitial fraction is clotted and peloidal micrite (10.10%), followed by peloids or ooids (6.05%), interstitial micrite (5.00%), dwellers (3.15%), intergranular cements (2.55%) and dense micrite (1.70%). Primary and secondary cavity-filling cements account for 2.70% and 1.84%, respectively. In general terms, the most important difference between MM and TM limestone is seen in the proportion of framework vs. infill: whereas in MM, the gap between the two parts is reduced with framework making up 59.29% of the volume vs. 40.71% of the total infill; in TM, the framework (66.95%) clearly predominates over the infill (33.05%). This difference is principally driven by the higher abundance of sponges and tubular crusts within the TM. Another important dissimilarity is seen in the higher content of clotted and peloidal micrite in the MM.

Table 2. Relative abundance of reef components.

			Reef Framework			
	Sponges	**Corals**	**Microbialite**	**Other Framework Organisms (Encrusters)**	**Tubular Crust**	**Total Framework**
Massive mound N = 42	**25.22**	**0.66**	**20.14**	**2.67**	**10.61**	**59.29**
	(0–139)	(0–34)	(0–126)	(0–12)	(0–82)	
Tabular mound N = 10	**33.05**	**1.15**	**15.20**	**2.55**	**15.00**	**66.95**
	(46–83)	(0–22)	(12–54)	(1–14)	(0–67)	

Table 2. *Cont.*

				Interstitial Sediments					
	Dwellers	Peloids or Ooids	Dense Micrite	Clotted and Peloidal Micrite	Intergranular Cement	Primary Cavities Cement	Secondary Cavities Cement	Interstitial Micrite	Total Interstitial Filling
Massive mound N = 42	**3.52**	**4.51**	**3.13**	**17.13**	**3.32**	**0.84**	**3.19**	**5.07**	**40.71**
	(0–39)	(0–47)	(0–50)	(0–120)	(0–39)	(0–10)	(0–10)	(0–70)	
Tabular mound N =10	**3.15**	**6.05**	**1.70**	**10.10**	**2.55**	**2.70**	**1.80**	**5.00**	**33.05**
	(1–19)	(3–31)	(0–12)	(6–33)	(1–21)	(0–25)	(0–6)	(0–23)	

N = number of point–counted samples; mean % values are in bold; bracketed values refer to the range of values for each catergory within the lithology.
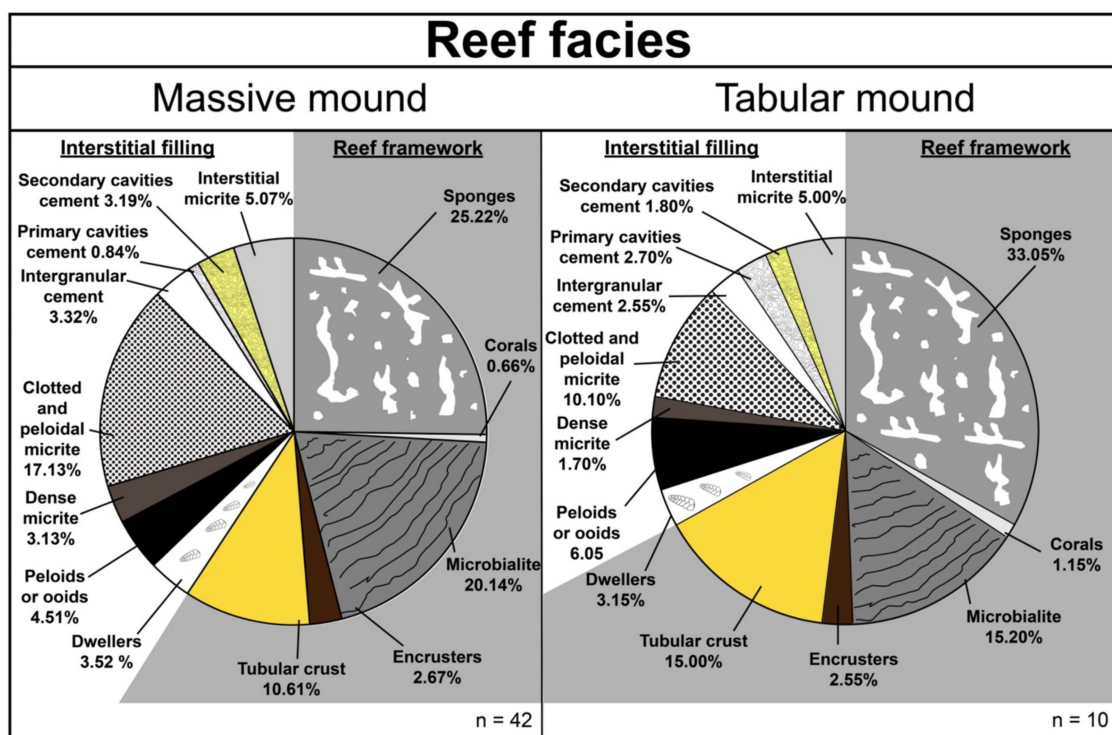

Figure 17. Composition of the reef facies after the point-counting analysis. Note that the framework of the tabular mound is denser: n, number of point-counted samples; (for a coloured version, the reader is referred to the web version of this article).

7. Interpretation of the Depositional Environments

One limitation to the study of the carbonate system at Lime Peak is related to faults that locally crosscut the area (e.g., see Figure 2B,C), hindering some of the original depositional relationships between the different limestone bodies: this makes any interpretation regarding the whole outcrop (east and west blocks) speculative. The model for the growth of the southeast side of the Lime Peak complex proposed in [51] did not take into account part of the faulting and, in particular, the major fault running through the southeast face between Avens and Campion bodies (see Figures 2B and 3A). Overall, the best approach to reconstruct the carbonate depositional environments appears to examine the system by tectonically isolated blocks and by sedimentary packages. Within these, the original relationships have been preserved, allowing us to study the depositional processes between the different litho/microfacies along with the pathways that contributed to their formation.

7.1. Depositional Environments during Sedimentation of the First and Third Packages

7.1.1. Toe of the Slope-to-Basin and Slope Environments

Our reconstruction of the depositional environments starts from the western part of the first package (Figure 18A). According to our sampling, in this area, the first package is formed by MCF 10, 11 and 14. These microfacies are found in repeated vertical alternations. The distribution of microfacies is paralleled by lithofacies, with MCF 14 occurring in thin-to medium-bedded impure limestone (TMB), while MCF 10 and 11 are contained in the westward pinching-out very thick-bedded limestone (VTB).
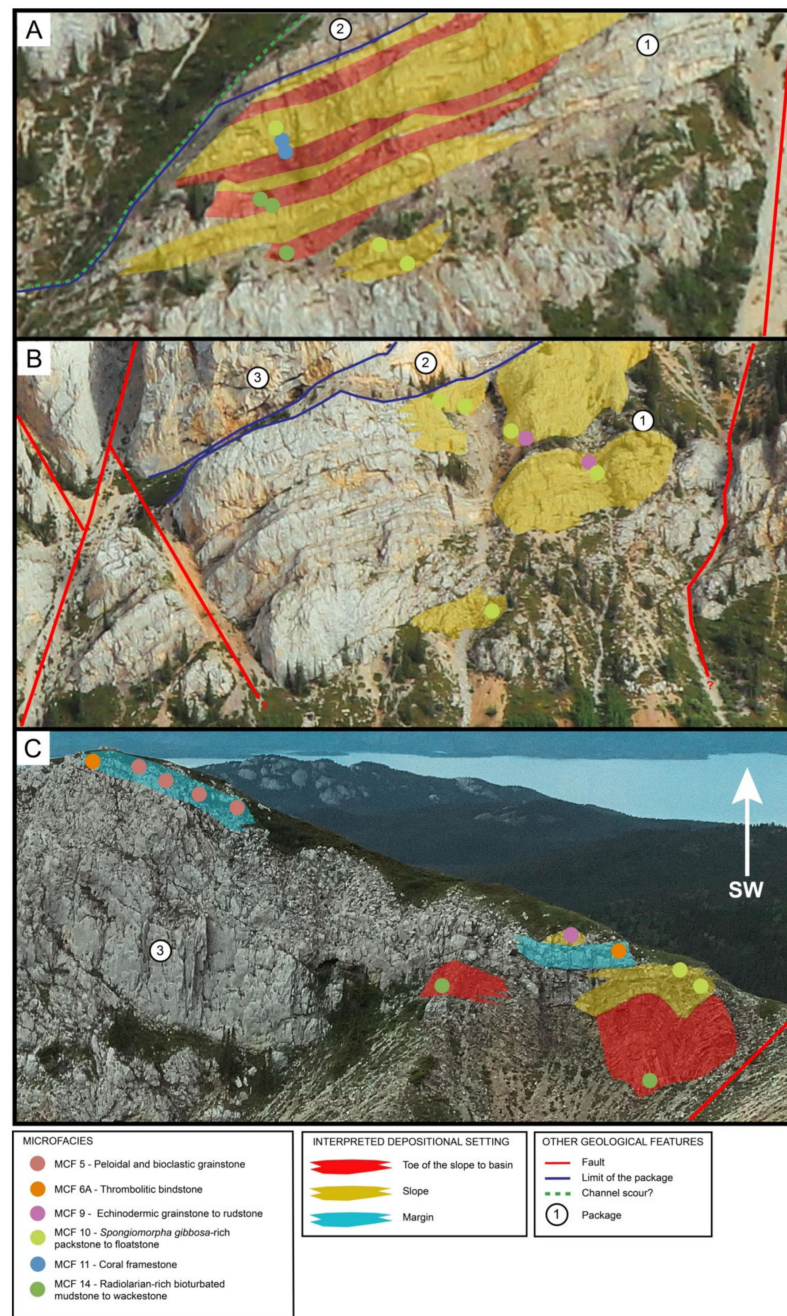

Figure 18. Interpretation of the depositional environments: (**A**) Western part of the first package; (**B**) Central part of the first package; (**C**) Eastern part of Avens (i.e., the third package). The lateral extension/mapping of depositional settings is extrapolated and only indicative. In this image, the mapping is restricted to the first and third packages; (for a coloured version, the reader is referred to the web version of this article). 1, 2 and 3 are the studied packages.

Therefore, microfacies and lithofacies alternations are matching. In this area of Lime Peak, vertical alternations can be identified thanks to the colour contrast between TMB (dark brown) and VTB (light grey; Figure 3B). Similar vertical alternations between TMB and VTB are also observed in the eastern side of Avens body (Figure 3A). MCF 14 strongly resembles the hemipelagic deposits described from other Upper Triassic localities of the North American Cordillera (e.g., see Vancouver Island in [45] or the Pardonet Hills in [98]). The paucity of phototrophic biota and the frequent bioturbation within these deposits indicate that the deposition chiefly occurred below the limit of the photic zone but above the ACD, as attested by the excellent preservation of aragonitic shells and tests (>depths of 150–200 m), and in a well-oxygenated environment, most likely in a base or toe of the slope setting of a relatively shallow basin.

The shallowing of the carbonate system is marked by the occurrence of MCF 11. Although the wackestone to packstone matrix of MCF 11 is quite similar to MCF 14, the widespread presence of the photosynthetic coral *Retiophyllia* sp. (this genus, along with other Triassic scleractinians, is thought to have hosted zooxanthellae (for details see [99–102])) points to shallower water depths (<150–200 m). While a depositional depth within the photic zone for MCF 11 is suggested by the presence of small *Retiophyllia* sp. thickets, the low diversity and absence of otherwise abundant indicators of shallow to very shallow (photic) conditions, such as dasycladales (these algae usually abound in very shallow waters—i.e., depth < 5–10 m—some forms are known in modern environments to live at depth of up to 100 m; see [103,104]) or diffused microbial encrustations around grains (i.e., micritic envelopes) indicate that the deposition most likely happened in the lower photic zone in a low-light, open-water environment. In such open-water settings (i.e., not a cryptic setting such as reef cavities, where microbialites are generally formed by microorganisms having different metabolisms, e.g., see [105]), light availability is known to play a key role in favouring microbial encrustations (e.g., see [106–108]) that dominate in the shallower facies MCF 6A and MCF 6B (see below). Unlike in MCF 11, both microbialites and dasycladales (?*Clypeina* sp.) are often found in MCF 10, the third facies present in these alternations. Although both of their concentrations vary from rare to common, their presence indicates shallower depositional depths of the upper half of the photic zone. MCF 10 is by far the more abundant microfacies within the VTB and probably occupied a large portion of the upper slope. The observed variance in presence and abundance of both microbialites and dasycladales is therefore thought to reflect repetitive plurimetric to pluridecametric differences in depositional depth or light availability along the slope.

Further to the east (Figure 18B), MCF 10 is found in vertical association with MCF 9. The biotic content of MCF 9, rich in crinoids, red algae, bivalves, foraminifera, calcified cyanobacteria and other reef-related organisms, indicates that its deposition occurred in the uppermost part of the slope environment. In MCF 9, the intergranular porosity is generally filled with cement and only rarely by sedimentary micrite. Whereas the strictly mud-dominated matrix of MCF 10 indicates that the deposition occurred below the fair-weather wave-base (FWWB), the fabric of MCF 9 is characteristic of a more energetic environment above the FWWB. According to their characteristics, the depositional limit between MCF 10 and 9 can be placed at the base of the FWWB (depth of about 5–12 m).

7.1.2. Platform Margin Environment

The vertical association between MCF 9 and 10 can also be observed in the very thick-bedded limestone (VTB) to the east of Avens, in the third sedimentary package (Figure 18C). There, vertically associated with these two microfacies, we also find MCF 6A. The latter, also present to the west inside Avens, shows the greatest contribution by microbialites in the whole range of microfacies at Lime Peak (together with MCF 6B). It is difficult to establish whether the micrite in MCF 6A (Figure 9F) is fully derived from in situ precipitation and/or trapping favoured by microbial activity. However, three main clues suggest that the deposition of micrite in this microfacies was entirely microbially influenced: (1) often the micrite presents borings suggesting early lithification (at least a firmground); (2) when

present, the little patches of grainstone infills (similar to MCF 5) that are frequently found within MCF 6A suggest moderate to high energetic conditions during deposition. In such conditions, allochthonous micrite could not be deposited without the action of a trapping and/or binding agent; (3) the copious presence of the encrusting foraminifera *Tolypammina* sp. in the micritic fabric also suggests early lithification (e.g., see [109]). Albeit not known at present, platform margins dominated by microbial facies were quite common in the past, and many examples have been reported from the Triassic (e.g., the Sella Platform in [95,110], the Latemar platform in [10] and the Cassian dolomite in [111]) and other geological periods (e.g., the Permian Capitan Reef, USA in [112] and the Carboniferous Tengiz Platform in [113]). Hence, MCF 6A is interpreted to have been formed in the outer platform margin. MCF 6A is commonly found in lateral association with MCF 5 in the eastern part of Avens, whereas it is found in vertical association with MCF 7 in the vertical transects. MCF 7 is interpreted as a typical reef microfacies that generally abounds in the marginal area of Triassic carbonate platforms (e.g., see [9,10]). MCF 5, found in association with MCF 7, is also interpreted as having formed in a platform margin environment. The bulk of the sedimentation in this microfacies is a mix of components living/formed in situ all around the MCF 7 clusters, with minor contributions due to detritus coming from the bioherms. The lack of mud in this microfacies indicates at least moderate energy. We interpret MCF 5 as a sand shoal microfacies. Despite the lack of deposited mud, micritization was an active process in MCF 5. Micritization in marine environments is a well-known early diagenetic phenomenon that is caused either by abiotic [114] or biotic [115–117] processes. Part of these processes (e.g., biotically driven micritization by microboring by cyanobacteria) are particularly effective in case of low sedimentation rates (longer times at the sediment–water interface and thus longer exposure to light). The abundant micritization observed within MCF 5 therefore suggests low sedimentation rates.

7.1.3. Inner Platform

Further west, inside Avens (Figure 20), the microfacies interpreted to have formed at the platform margin are found in vertical association with MCF 1. The characteristics of this microfacies, including the abundance of gastropods, bivalves, dasycladales and carbonate mud, suggest deposition in a calm, shallow, inner-platform environment. Similar microfacies, described from elsewhere in the Panthalassa, have been interpreted to have formed in equivalent environments (see MF8 in [18] and F2 in [17]). Rarely associated with MCF 1 are MCF 4 and 6B. MCF 4 is a detrital microfacies that reworks both reef-derived material and inner platform microfacies (MCF 1) as large, angular pre-lithified (or at least partially lithified) clasts. The lack of carbonate mud and the coarse size of sedimentary grains and clasts in MCF 4 indicate moderate to high energy during deposition. Its close association with a low-energy microfacies (MCF 1) points to very contrasting energetic regimes within a relatively small spatial scale. In inner platform settings, such strongly contrasting energetic conditions are found between a tidal channel and the background lagoonal sedimentation. In particular, carbonate tidal-channel lag deposits have characteristics very similar to the ones observed in MCF 4 (e.g., see [118,119]). Finally, the micro-stromatolitic MCF 6B formed in small areas of the inner platform in close association with patches of megalodontid bivalves and *Wallowaconcha* cf. *raylenea*. Similar association between microbially dominated facies (although having different fabrics) and megalodontids in inner platform have already been reported in other Upper Triassic systems of the Panthalassa [17]. The area to the north of the zone where this association was observed is covered by vegetation, and no microfacies indicating intertidal or supratidal environments were found Figure 19.
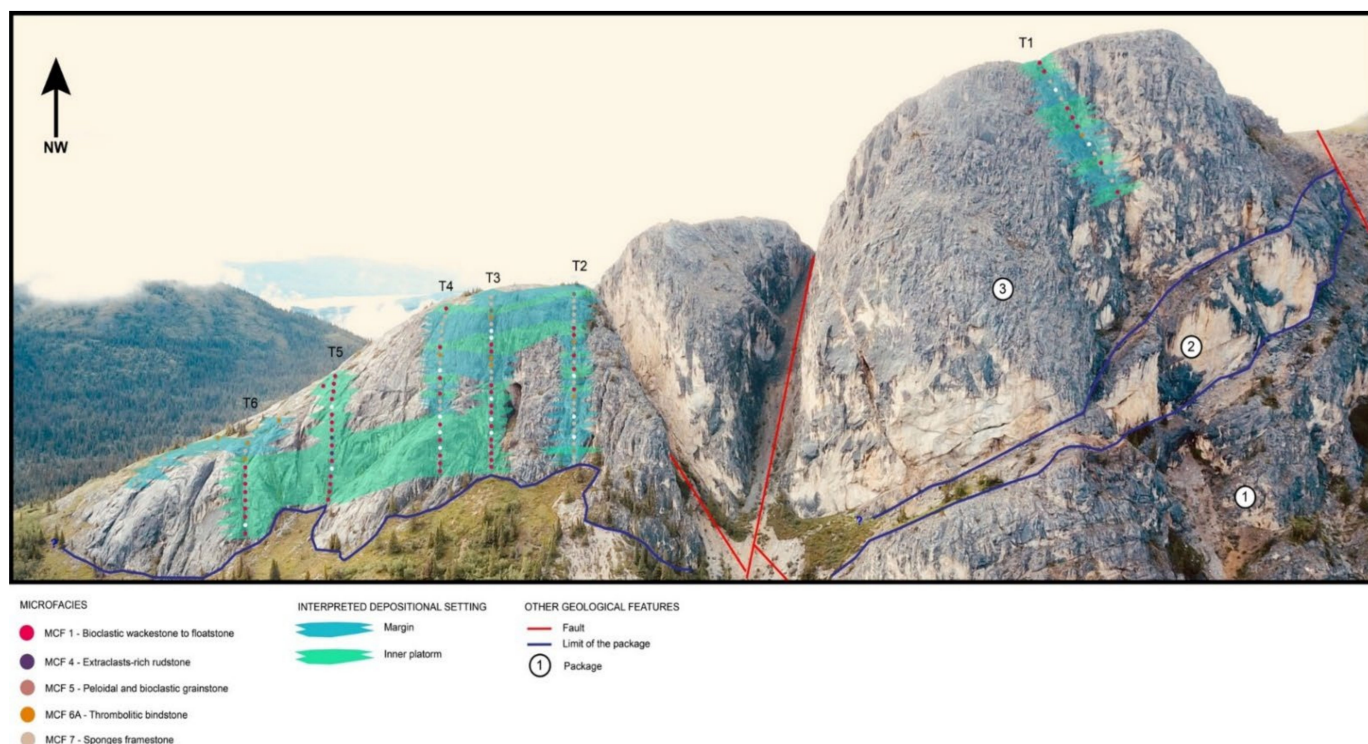
MICROFACIES

● MCF 1 - Bioclastic wackestone to floatstone
● MCF 4 - Extraclasts-rich rudstone
● MCF 5 - Peloidal and bioclastic grainstone
● MCF 6A - Thrombolitic bindstone
● MCF 7 - Sponges framestone

INTERPRETED DEPOSITIONAL SETTING

▬ Margin
▬ Inner platform

OTHER GEOLOGICAL FEATURES

▬ Fault
▬ Limit of the package
① Package

Figure 19. Interpretation of the depositional environments in the central and eastern part of Avens. The lateral extension/mapping of depositional settings is extrapolated and only indicative. In this image, the mapping is restricted to the first and third packages; (for a coloured version, the reader is referred to the web version of this article). 1, 2 and 3 are the studied packages. T1 to T6 are the 6 vertical transects done, with samples taken every 3 metres.

7.1.4. Depositional Model for the First and Third Packages

After Figure 20, the interpretation of the depositional environments in which the microfacies characteristic of the first and third packages were formed allows us to propose a depositional model that summarizes the depositional setting at Lime Peak (Figure 21).

Lime Peak formed in the marginal area of a carbonate platform. MCF 14 characterizes the toe of the slope-to-basin environments. The slope saw the deposition of MCF 11, 10 and 9 from deepest to shallowest, respectively. It is important to notice that there is a paucity of gravity deposits associated with the alternation of MCF 10, 11 and 14, suggesting that the slope was largely near or at the angle of repose during the deposition of these microfacies. Under such conditions, the deposition was dominated by in situ autochthonous carbonate deposition.

The marginal area of the carbonate system was characterized by the deposition of MCF 5, 6A and 7. We interpret MCF 6A as having occupied the outermost part of the margin since it is the microfacies that is more commonly associated with upper slope deposits (MCF 9). The other two microfacies, MCF 5 and 7, formed the core of the platform margin. The latter was shaped by a consortium of sand shoals (MCF 5) and bioconstructed patches (MCF 7), somewhat similar to what is observed in modern reef tracts where sandy areas are closely associated with coral framestones (e.g., see [120]). Contributions to MCF 7 were given by primarily by sphinctozoan sponges and minorly by inozoans, *Spongiomorpha ramosa* and *Retiophyllia* sp. colonies. These organisms have skeletons that are relatively small and very rarely taller than 30–40 cm (the tallest organisms are sphinctozoan sponges such as *Polytholosia cylindrica cylindrica, Cryptocoelia zitteli* (see [59]), *Spongiomorpha ramosa* and *Retiophyllia* sp. colonies). Therefore, it is assumed that reef patches did not form much topographic relief. Within the platform margin, indicators of high-energy conditions such as reef crest breccias are lacking. However, the energetic conditions at the platform margin should have been enough to prevent the deposition of micrite in the shoaly areas

(MCF 5). For this reason, the margin was likely affected by moderate- to relatively low-energy conditions. The presence of dasycladales in both MCF 5 and MCF 7 suggests very shallow bathymetric condition (upper photic zone). Moderate- to low-energy conditions in a very shallow bathymetric position suggest that Lime Peak formed in a protected area of the Lewes River arc, such as the leeward side of a volcanic island or an isolated carbonate platform.
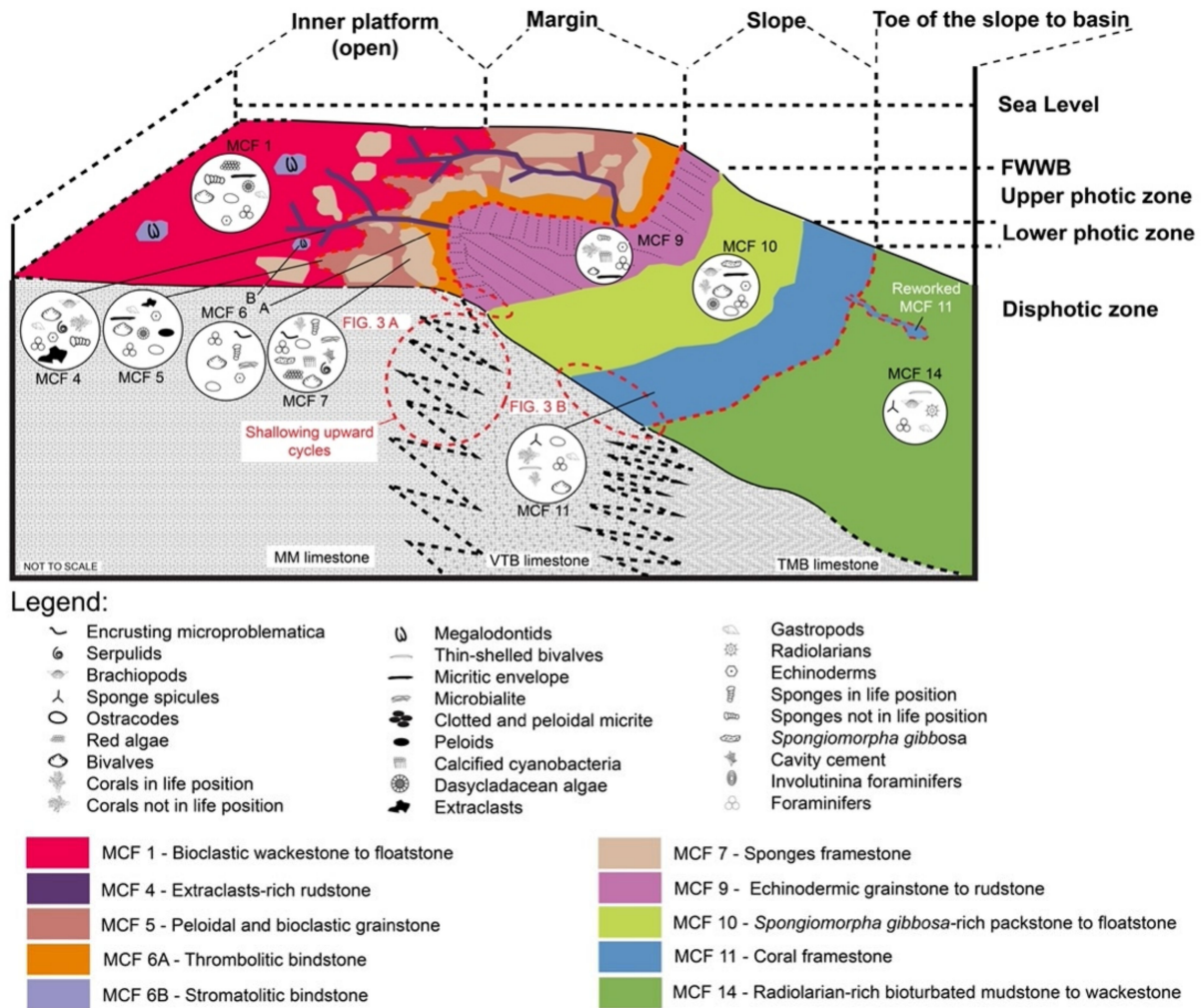

Figure 20. Depositional model for the sedimentation of the first and third packages; (for a coloured version, the reader is referred to the web version of this article).

The inner platform was dominated by MCF 1, with the minor occurrence of MCF 6B and MCF 4. In MCF 1, the common presence of stenohaline organisms such as crinoids (crinoids seem to occur as long as conditions are not restricted; e.g., see [121]) advocates for well-established water circulation in the inner platform.

7.2. Depositional Environments during Deposition of the Second Package

7.2.1. Slope and Toe of the Slope-to-Basin Environments

The western part of the second package is defined by a thick set of thin- to medium-bedded impure limestone (TMB) that is largely formed of alternations of MCF 12, 13 and 14 (Figure 21). As previously mentioned, MCF 14 is interpreted to represent the background hemipelagic sedimentation in a toe of the slope setting. MCF 13 resulted from gravity flow deposits. The strong basal erosional surface (eroding both MCF 14 and 12) along with the normal grading (Figure 4E), in which basal very coarse sand to gravel are overlain by Bouma T_{c-e} or T_{d-e} type sequences, suggest deposition via concentrated density flows

(e.g., see [122] and references therein). Of the three microfacies, the most frequently found is MCF 12. It is located in beds that are very rarely more than 30 cm thick and show little or no erosive bases. The paucity of erosive bases along with sediment fabric (poor sorting and mud-rich matrix; see Figure 5E) points toward deposition via debris flows. Even though debris flows can achieve considerable velocities [123], they often lack erosive bases due to a process called hydroplaning [124,125]. During hydroplaning, a thin layer of water, pinched between the flow and the sea floor, reduces the resistance between them, inhibiting the erosive process [126]. Apart from the difference in mud content, both MCF 12 and 13 have a biotic content very similar to that of MCF 7 and 8. The material for both gravitational deposits was likely sourced from the platform margin. The difference in the types of gravity flows seen in MCF 12 and 13 can be explained in two different ways: (1) the divergent nature of the flow may be due to slightly different source areas with diverse sediment characteristics (with the more mud-supported MCF 12 being sourced from a slightly deeper area than MCF 13) or (2) MCF 12 and 13 could represent the physical evolution of a single flow. Debris flows are known to transform into concentrated density flows along their course [127,128]. However, during our field campaign, we did not observe any lateral transition (within the same bed) from MCF 12 to MCF 13. Each bed containing MCF 12 and 13 resulted from a short-lived, probably single event. Such events were probably very small in size, since medium- to thick-bedded impure limestone (MTB) forms at most 5 to 10 cm thick beds.
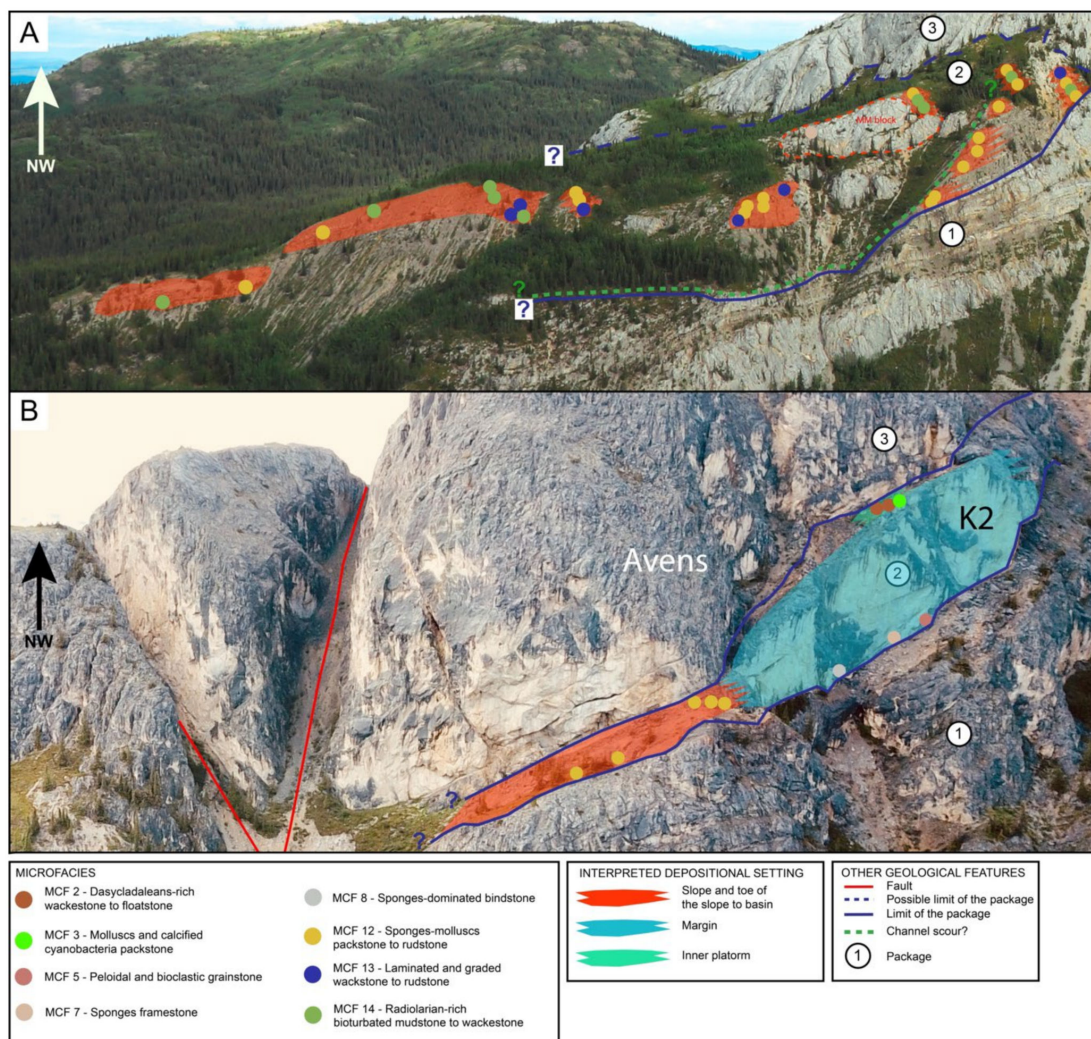

Figure 21. Interpretation of the depositional environments in the second sedimentary package. (**A**) Western part of the package; (**B**) Eastern part of the package. The lateral extension/mapping

of depositional settings is extrapolated and only indicative; (for a coloured version, the reader is referred to the web version of this article). 1, 2 and 3 are the studied packages. K2 is the tabular mound limestone (TM) of the second package. The "?" indicate that the fault could not be followed in the field beyond the red line.

The large, marked erosive scour observed in this area of Lime Peak is filled with a mixture of TMB and MM (Figure 2C). In the southeast face, just to the west of the second package (Figure 3E), some beds (which also show signs of slumping; Figure 4A) containing MCF 12 and 14 are found to be in direct lateral contact with irregular massive mound limestone (MM) and very thick-bedded limestone (VTB) blocks. Reid [51] tried to unveil the nature of these massive blocks through the study of their geopetal features. However, the study was inconclusive since, according to the author, different blocks have different geopetal "signatures". In fact, two blocks have geopetal bedding showing apparent concordance with adjacent strata, two blocks are discordant, and one block shows many different geopetal orientations within it. We determined these blocks are gravitational and are derived from the platform margin or the upper slope. The main clue is given by the presence of shallow-water phototrophic biota (corals, calcified cyanobacteria and green algae; MCF 7) within MM laterally associated with strictly aphotic microfacies such as MCF 14. We agree with Reid [51], and we interpret this erosive surface as a submarine paleo-channel scour that is obliquely crosscut, and this deposit (with individual MM blocks) as an olistostrome.

The central area of the southeast face that runs between the second package and K2 is not ideally exposed due to tectonic complications (Figure 2B) impeding lateral following of the TMB beds. However, MCF 12 is the only microfacies found in the TMB beds just to the west of K2, and it is therefore assumed to have occupied a large part of the upper slope environments during the formation of the second package.

7.2.2. Platform Margin

Moving eastward, the tabular mound limestone (TM) named K2 (Figure 21B) by Reid [51] crops out. MCF 7 is frequently found within this body, and, as for the other two packages, it is interpreted to have formed at the platform margin. The major difference between MCF 7 in this package versus what has been previously reported for the same microfacies in the other two packages is given by the type of bioconstructors. Unlike massive mound limestone (MM), where framework organisms can be relatively tall and wide (up to 30–40 cm, see above), tabular mound limestone (TM) is dominated by much smaller organisms (see also the observations in [55]). In the TM, the larger contribution to the framework of MCF 7 is given by smaller sphinctozoan sponges (e.g., *Paradeningeria* sp. and *Cryptocoelia* sp.), *Spongiomorpha* sp. and nodular and encrusting chaetetids. These organisms, which are rarely more than few cm high, are frequently intergrown. When present, bigger organisms tend to have an encrusting/massive growth form (e.g., Thamnasteroid corals). Different framebuilding organisms presumably led to different reef architectures (e.g., average number of cavities, average cavity size, cavity connection and surface available for epibionts). The above-mentioned intergrowth between organisms is responsible for a more complex framework structure and a higher amount of framework in MCF 7. This in turn influenced the sedimentation within the reef framework, as shown by the different average content of the sediment infill (Figure 17).

K2 is marked by the widespread presence of MCF 8. In this sponge-rich bindstone, the reef biota (sponges, red algae and corals) are not found in living position but as rubbles. In MCF 8, the intergranular porosity is filled with either cement or micrite. This suggests that this microfacies had a distribution that neared the fair-weather wave base. In MCF 8, the main binding agent appears to be microbialites, and marine cement is only subordinate. In modern day, rubble stabilization is achieved by a combination of organic encrusters (i.e., coralline algae, worms and bryozoans) and diagenetic cementation [129]. Holocene binding

of reef rubbles by microbialites has rarely been reported [130,131]. Nowadays, the highest rate of rubble binding is achieved in fore-reef areas. Rigid binding of rubble appears to be very rare in deep fore-reef environments, whereas no reports of rubble binding in the reef crest have been recorded [129]. Following these points, MCF 8 microfacies is interpreted as having formed in the external part of the platform margin.

The rest of the bulk of the margin is given by the sand shoal microfacies MCF 5. Within MCF 5, there are no major compositional differences observed between TM and MM. Again, the lack of high-energy indicators (e.g., reef crest breccias; for a comparison see the reef crest facies in [9]) confirms that the platform margin was affected by relatively low to moderate energy even during deposition of the second package.

7.2.3. Inner Platform

K2 (tabular mound limestone (TM)) splits out to form multiple, very thick-bedded limestone (VTB) beds. One of our samples (WH 598) collected in the uppermost of these beds (the one capping K2) yielded MCF 3. Reid [51] reported the presence of MCF 3-equivalent microfacies (conspicuous presence of "branched filamentous blue-green algae", now formally called calcified cyanobacteria) inside the VTB east of K2 (Figure 2C). MCF 3 shows elements typical of both inner platform (e.g., calcified cyanobacteria, dasycladales and Involutinida type foraminifera) and platform margin (serpulids, crinoids and red algae) environments, indicating deposition in a transitory environment linking the margin to the inner platform.

MCF 3 is vertically associated with MCF 2. This microfacies appears to be very similar to the lagoonal microfacies described at other localities in the Whitehorse region (e.g., see the black limestone unit in [85]). In the occurrences studied by Morrison [85], a 5–10% "carbonaceous matter content" was reported from MCF 2-equivalent facies. Among its biotic content, organisms characteristic of Upper Triassic lagoonal environments such as Involutinida and Robertinida foraminifera along with dasycladales are very profuse (e.g., see [17,26,36,37,132]). Although the fabric of MCF 2 is quite variable, the abundance of the mud-supported, organic-rich end-members supports a generally low- to very-low-energy lagoonal environment.

7.2.4. Deposition of the Second Package: A Different Tale?

The interpretation of the depositional environments allows us to propose a depositional model for the second package (Figure 22). As previously mentioned, the second sedimentary package shows very contrasting geometries compared to what is seen in the first and third packages (see Figure 7B). Reid [51] linked the deposition of K2 with a period of low-stand or still-stand. The hypothesis of the author was based on the fact that, contrary to other massive limestone bodies in the area (e.g., Avens and Campion), K2 shows a very elongated shape. According to the author, the dominance of progradation over aggradation indicates a lack of accommodation space during the deposition of this body. The second package is characterized by a thick set of slope-to-toe of the slope sediments (Figure 22). The thickness of the latter is greater than the equivalent sediments deposited on the platform top. The eye-catching feature of these slope sediments is the rarity of purely autochthonous microfacies equivalent to MCF 10 and 11, which are abundantly observed in the same environment during deposition of the two other packages. This rarity can be due to very short timespans between single gravitational flow events, with continuous reworking of slope sediments diluting the deposition of autochthonous slope deposits. In this context, autochthonous microfacies would have only been able to form in the more distal toe of the slope-to-basin environments; this is probably the reason why MCF 14 dominates over other allochthonous microfacies. Distal areas were indeed only occasionally disturbed by gravity flows, permitting the continuous deposition of deep allochthonous deposits over long periods. During the deposition of the second package, unlike during the deposition of the first and third packages, the slope environment was a site of active reworking of shallower, water-derived material. The accumulation of a thick set of allochthonous sediments in the

slope-to-toe of the slope is a known phenomenon during low-stand periods (low-stand wedge, see [133]). This discussion brings further evidence to support Reid's idea that the deposition of K2 (and of the second package in general) was linked to a period of low sea level characterized by low accommodation space at the platform top.
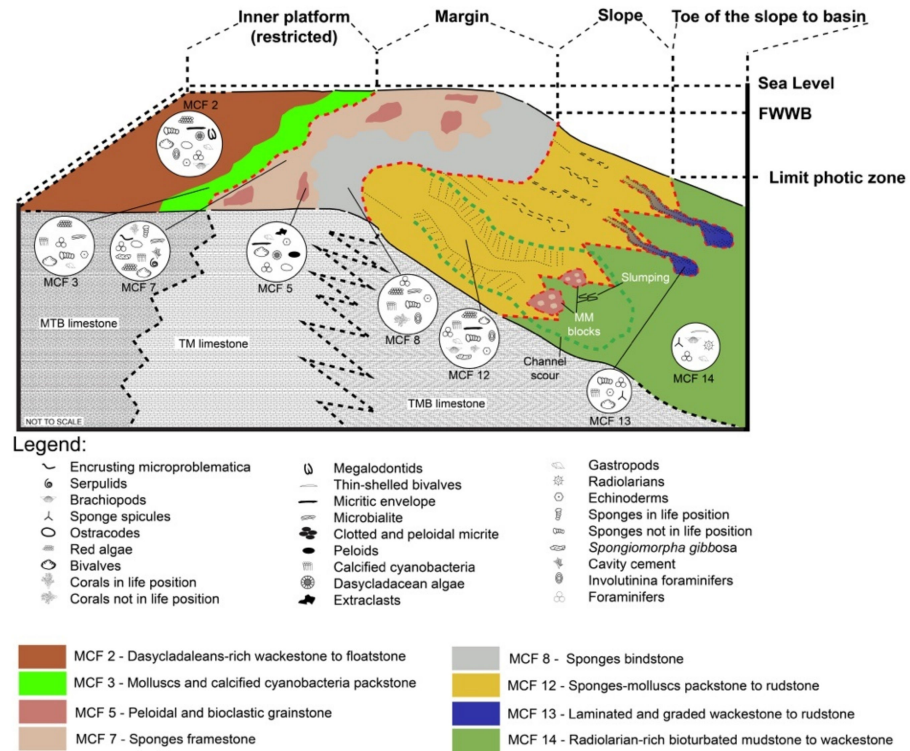

Figure 22. Depositional model for the sedimentation of the second package; (for a coloured version, the reader is referred to the web version of this article).

During the deposition of the second package, low accommodation space at the platform top was also responsible for a major change in the physical conditions in the inner platform environments. In MCF2, the inner platform microfacies, a dearth of stenohaline biota (crinoids are completely lacking and sponges and corals are only present as reef-derived fragments) is observed, indicating that the platform was not characterized by normal marine conditions. Supporting this hypothesis is the composition of MCF 2, which at times is enriched with calcified cyanobacteria *Girvanella* sp. (e.g., samples WH 188 and WH 236). According to [134], this form of calcified cyanobacteria appears to be particularly adapted to environments characterized by fluctuating salinities. Hence, we hypothesize that during the deposition of the second package the platform was characterized by restricted conditions. Such a configuration was likely caused by limited connection to the open ocean, which impeded the water exchange between inner and outer environments.

In the following discussion, we refer to the setting under which the first and the third packages were formed using the term HSL (high sea level or high accommodation space), whereas we use the term LSL (low sea level or low accommodation space) to refer to the settings under which the second package was deposited. These two terms have no quantitative mean and are proposed only in order to differentiate the two settings.

8. Discussion

8.1. What Is Lime Peak? New Insights Regarding Its Nature and Spatial Relationship with Other Upper Triassic Carbonates in the Whitehorse Region

The depositional model proposed by [85], which was later slightly modified by Hart [61], depicts the carbonate rocks of the Lewes River Group as having been formed in a wide and rather continuous carbonate system lying to the east (Figure 23A) of the

Lewes River volcanic arc (forearc). According to both authors, Lime Peak, located in the central facies belt, corresponds to a barrier reef complex that grew at some distance from the emerged lands, at the bank margin [61,85]. On the other hand, Ref. [51,55] interpreted Lime Peak as one of Hart's/Morrison's patch reefs. According to this last interpretation, the massive mound (MM) and tabular mound (TM) limestone would represent patch reefs, whereas the very thick-bedded (VTB) and thin- to medium-bedded (TMB) impure limestone would be deposited in the inter-reef areas.
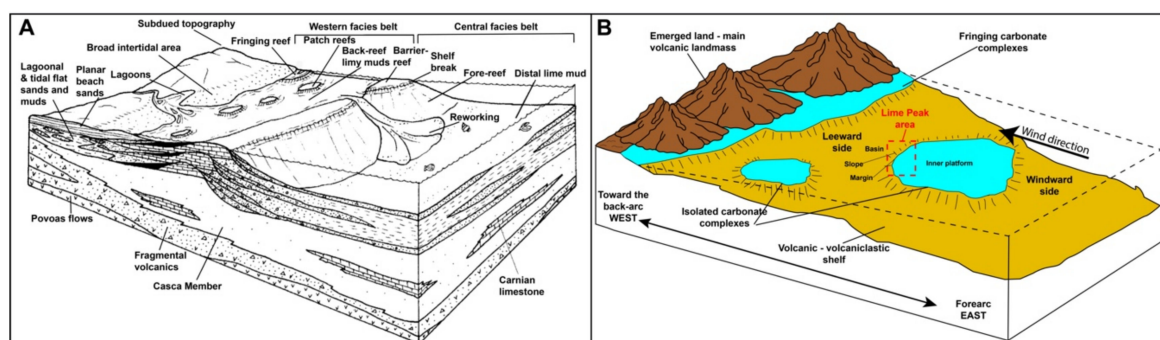

Figure 23. Reconstructions of the depositional setting of the Upper Triassic carbonates of Stikinia. (**A**) Model proposed by [85] and reworked by [61]; (**B**) Schematic reconstruction proposed in this work.

The recent mapping work [78,82,84] that focused on the area to the east of Lake Laberge (also part of the central facies belt) gave valuable new insights regarding the stratigraphy of the Lewes River Group in the central facies belt area. According to the authors (i.e., [82]), massive carbonates of the central facies belt formed on the volcanic shelf at some distance from the main volcanic landmass (see the reconstruction in [82]). In detail, the carbonate deposition in the area seems to have been more varied and irregular compared to what was imagined in the depositional models mentioned above. Massive carbonate occurrences are not laterally continuous at the basin scale [82]. Instead, they appear to have been derived from a multiplicity of irregular, distinct and possibly diachronous carbonate complexes [82]. Fine-grained, thin-bedded, argillaceous units of the Aksala Formation present in the area are coeval with the carbonate platforms and were presumably deposited in shallow to deep basins around these massive carbonates [82].

According to [82], the deposition of these massive mound limestone was strongly influenced by the inherited topography driven by volcanism and tectonics. Fossil examples of topographic-highs-triggered carbonate sedimentation in a volcanic arc setting have also been reported from Palaeozoic carbonates from the eastern Klamath terrane [135–138] and from Cainozoic carbonates of Fiji [139]. One of the most striking modern examples of how topographic highs can prompt shallow-water carbonate sedimentation is the Kepulauan Seribu complex in the Java Sea, Indonesia [140]. Kepulauan Seribu is a 40 km long archipelago that is formed of carbonate complexes that range from a few meters across to lengths up to 7 km. The archipelago sits on a NNE–SSW structural high that favoured shallow water carbonate production during the Holocene sea level rise [140].

The ranges of depositional environments found within the Lime Peak platform span from restricted shallow lagoonal environments to aphotic (sea bottom) basinal facies rich in radiolarians. The presence of the latter indicates open-water conditions around the area where the build-up developed [141]. The discovery of lagoonal facies at Lime Peak (i.e., MCF 1 and 2) is relevant because, until now, lagoonal facies within the Aksala Formation were thought to be limited to the western facies belt (e.g., see page 217 in [51]). Following this discussion, we regard Lime Peak as having formed in the marginal area of an isolated carbonate platform (Figure 23B).

8.2. Tectonic Influence on the Sedimentation at Lime Peak

Several samples of MCF 7 show multiple generations of geopetal infills inside the cavities. The different depositional planes shown by the geopetals are indicative of significant tectonic tilting of the Lime Peak carbonate system. The difference in geopetal orientation is observed between the infill of primary vs. secondary cavities. As previously pointed out, secondary cavities were formed by the dissolution or the decay of pre-existing organisms. The timing of such dissolution and cavity-forming events (hence, presumably the age of its infill as well) is currently unknown. It is therefore unclear whether the difference in orientation (angle of tilting) observed between synsedimentary (e.g., Figure 9H, white arrows) and secondary infills (e.g., Figure 9H, black arrows) was achieved in a short timespan (during the Norian), which would indicate important synsedimentary tilting, or in a longer timespan (e.g., the tilting could be Rhaetian, Jurassic or younger). In situ U–Pb dating of the calcite cements in the secondary cavities could give new insights regarding the timing of their formation and the evolution of the Lime Peak complex.

The microfacies and lithological cyclicities that can be observed in the eastern end of Avens body (Figure 3A) were driven by processes that induced rapid relative sea level changes. In the eastern part of Avens, these cyclicities are made up of four main shallowing-upward cycles in which each cycle is formed by the coupling of thin- to medium-bedded impure limestone (TMB) and very thick-bedded limestone (VTB, Figure 3A). Such cycles are cyclic but nonperiodic since only shallowing-upward sequences are observed. If the relative sea level changes responsible for these cycles were caused by steady eustatic fluctuations, one would expect to also find the deepening trend of such sequences. Yet within these cycles, deepening-upward sequences seem completely absent, suggesting that the increase in accommodation space was too rapid to be registered in the sedimentary record. Volcanic arcs are tectonically active areas in which the local tectonic activity is known to have a strong influence on the sedimentation [142,143]. In these settings, sharp lateral and vertical facies changes, caused by rapid and large-scale crustal movements, are notorious [142]. For instance, the Nias–Simeulue earthquake (M_W 8.6) of March 2005, with its epicenter located in the Sumatra forearc (Indonesia), caused an abrupt uplift/downlift in some areas. During the event, the northern coast of the Island of Nias was affected by an instantaneous uplift that exceeded 2.5 m (see [142] and references therein). Such events can, in a very short time, completely modify the depositional settings within the carbonate system and modify, among other things, relative water depth, the locus of the shallow-water sedimentation, sediment fluxes and restriction in the internal environments of the carbonate system. In such a context, basic sedimentation rules such as the Walther's law can be easily contradicted [144,145]. In light of these considerations, the above-mentioned cyclicities were most probably derived from abrupt subsidence events that were induced by local tectonic factors.

8.3. Evinosponges at Lime Peak

The alternation of light grey, radiaxal fibrous isopachous cement and thin layers of microbialites at Lime Peak (Figure 24) reminds us of diagenetic features that are widely present in the Middle Triassic of Europe. There, the margins of some platforms (e.g., the Esino Limestone, Southern Alps [146], the Marmolada Platform, Dolomites [147] and the Latemar Platform, Dolomites [148]) contain cavity-filling features of centimetre to metre size, which were misleadingly named evinosponges. Stoppani [149] was the first to describe these features and introduced the term evinosponges. He believed that they represent sessile encrusting organisms for which he created the genus "*Evinospongia*". The same features were reported later on in the Wettersteinkalk of Tirol under the name of Grossooliths [150,151]. Like the features observed at Lime Peak, European evinosponges consist of multiple generations of alternating thick, light grey and thin, dark grey bands [146]. Although [146] stated an early marine origin for these features, their precise nature, along with their original mineralogy (high-Mg calcite vs. aragonite precursor) is still under debate, with some authors arguing for an inorganic nature [151–153] and others for a biologically mediated

origin [147,154]. Lately, their high content in Sr (at times over 10,000 ppm) led [147] to claim an aragonitic carbonate precursor for these features. Since these structures have an agreed early marine origin [146,147], the dissolution phenomena that created the secondary cavities in which the evinosponges are found must have occurred very early in the diagenetic history of the rock. The discovery of similar features at Lime Peak is important because thus far they have been believed to be a phenomenon characteristic of a relatively short geological time period and with a narrow paleogeographical distribution [147]. Interestingly, in both cases, these features occur in cavities created or enlarged by the effect of (? meteoric) dissolution [146]. Such similarities imply a common mechanism for their formation. Further investigation of these fabrics, such as in situ high-precision stable isotope and trace element (e.g., see [21]) analyses, might give new insights regarding their nature.
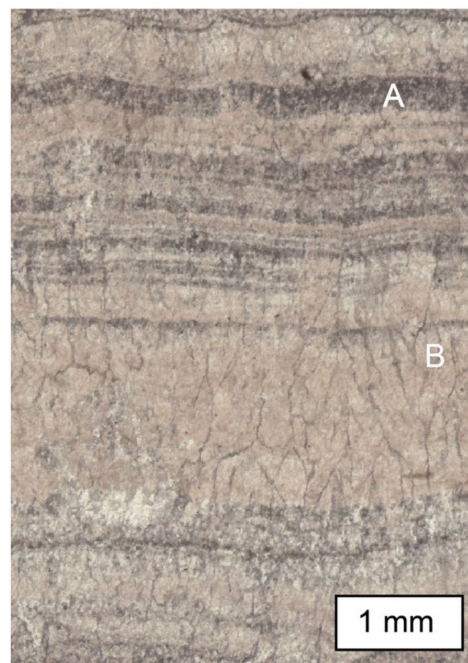

Figure 24. Example of "Evinosponges" from Lime Peak (sample WH 404). (**A**): micritic layer, (**B**): radiaxal fibrous calcite.

8.4. Carbonate Factory at Lime Peak

The carbonate factory at Lime Peak is indicative of warm, tropical conditions. This is supported primarily by the abundance of dasycladales green algae. At times, dasycladales are so abundant that they constitute rock-forming bioclasts (e.g., *Holosporella*? *rossanae* and *Patrulispora pacifica* in MCF 2). According to [104], dasycladales are mostly present in tropical waters, with a few species also found in warm, temperate seas. According to [155], the abundance of reef-dwelling porcelaneous foraminifera can be also taken as indicative of tropical conditions. Another clue is the presence of thick early marine cements (or evinosponges). Among the factors that promote the precipitation of early marine cements, water temperature and carbonate saturation state indeed play major roles [156]. For instance, coral reefs of the eastern tropical Pacific are very poorly cemented compared to Bahamian reefs. Manzello et al. [157] linked this peculiar characteristic of eastern tropical Pacific reefs to the low carbonate saturation state of the waters they grow in. Therefore, the abundance of thick marine "cements" suggests that the Lime Peak complex grew in waters characterized by high temperature and high carbonate saturation states. The presence of giant gastropods (Figure 4D) points toward the same interpretation, since nowadays, marine gastropods of similar sizes dwell only in tropical to subtropical waters [158,159]. Finally, according to [160,161], the giant alatoform bivalve *Wallowaconcha* cf. *raylenea* can also be considered a good indicator of warm, tropical waters.

The presence of organic matter (OM)-rich levels (MCF 2) during LSL at Lime Peak suggests high primary productivity within platform environments. Since primary productivity is, in turn, directly controlled by availability of nutrients [162], the area was probably characterized by moderate to high availability of nutrients, at least during LSL. Nutrient concentration has been shown to have a strong impact on coral reefs and carbonate systems in general [163–166]. Carbonate-producing biota have different preferences for nutrient levels. For instance, corals are organisms adapted to highly nutrient-deficient environments [163]. When nutrient levels are higher (e.g., mesotrophic conditions and above), the growth of plankton is stimulated. In such conditions, water transparency is increasingly reduced, and the development of corals is limited [163]. The turbidity of the water controls the depth of the limit between photic and disphotic zones. The presence of a rather shallow transition from the photic to the disphotic zone, caused by the turbidity of the water, might be the reason why disphotic facies (found within thin- to medium-bedded impure limestone) are found so close to the reef during certain shallowing-upward sequences (e.g., see Figure 3A).

Under mesotrophic conditions, suspension feeder organisms such as sponges are favoured over corals [166]. Unlike corals, calcareous green algae are known to be well-adapted to mesotrophic conditions, under which they become very competitive for benthic substrate [161]. Microbialites are also known to benefit from high nutrient availability. For instance, Camoin et al. [131,167] linked the widespread formation of thick microbialites in quaternary reef cavities in Tahiti with periods of higher nutrient availability.

As previously discussed, Lime Peak was probably formed on the shelf of a volcanic island arc that, during the Norian, was located in the middle of the Panthalassa at some (? considerable) distance from the North American craton. In such a scenario, nutrient enrichment could have been caused by river runoff, terrestrial groundwater discharge or upwelling of nutrient-rich waters. It is important to remember that upwelling does not necessarily mean very cold waters. Nowadays, there are many examples of areas in which physical oceanographic mechanisms periodically force uppermost nutricline waters onto shallower areas. There, uppermost nutricline waters are only a degree or two cooler than surface waters, enough to largely promote aragonite precipitation by photosynthetic organisms [166].

8.5. Organisms' Distribution within the Lime Peak Carbonate System

As mentioned in the introduction, Upper Triassic carbonate systems formed in the Panthalassa often underwent strong post-depositional deformation. In the worst cases, carbonate systems were completely dismantled during accretionary processes, and what remains are isolated carbonate clasts within accretionary complexes or limestone blocks in megabreccias (e.g., see the mode of occurrence of Upper Triassic carbonate in Japan in [17,18]). Therefore, very often the reconstruction of carbonate systems is principally based on the interpretation of scattered microfacies data, not taking into account considerations of lateral or vertical facies transition (e.g., see the work approach in [17]). So far, these microfacies-based reconstructions have relied mostly on observations from better-studied and better-preserved Tethyan systems [3,12,138]. Nonetheless, Tethyan systems were formed in completely different settings ([16] and references therein) and occurred at very different scales; for these reasons, they are probably not the best analogues to reconstruct Panthalassan systems. In this context, the reconstruction of an inner platform-to-basin model supported by depositional geometries at Lime Peak gives us the opportunity to display the distribution of organisms at the platform scale. Norian ostracods from Lime Peak were recently the subject of a publication [47] that examined their taxonomy and their paleoenvironmental distribution. The reader is referred to that publication for details. The distribution of other organisms within the Lime Peak platform is summarized in Figure 25A,B.
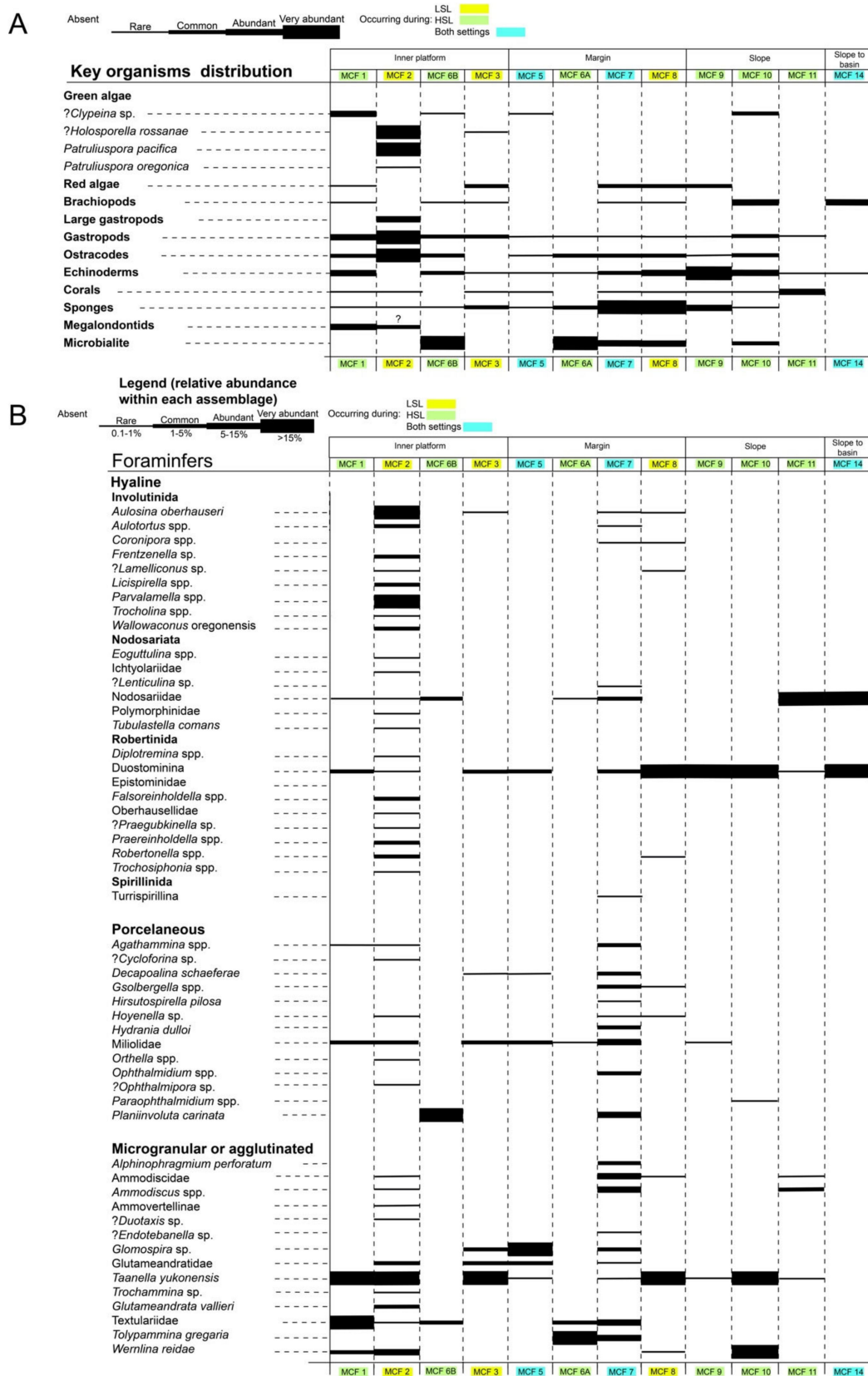
Figure 25. Relative abundance of selected biota (**A**) and foraminifera (**B**) at Lime Peak. The microfacies taken into account here are only the ones that are proven to bear in situ assemblage (obviously reworked sedimentary facies were excluded). Note that MCF 2 (inner lagoon) and MCF 7 (reef core) are the most diversified microfacies.

At Lime Peak, apart from the rare presence of the phylloid codiacean *Ivanovia triassica* Torres in MCF 7, all observed green algae are dasycladales. The most important factors controlling the distribution of modern dasycladales are water energy, salinity, temperature, light availability and substrate [104,168]. Fossil dasycladales are presumed to have been subjected to the same influences. In the Upper Triassic, dasycladales occurred in a wide variety of platform environments ([16] and references therein). Detailed studies on their spatial distribution at the platform scale are rare but indicate marked paleoenvironmental zonation [169–172]. At Lime Peak, dasycladales are widespread, and their distribution spans from the inner platform to the upper slope. Besides the genera *Kantia* and *Teutoplorella*, which are too rare (only found in few samples) to confidently interpret their paleoenvironment, the distribution of ?*Clypeina*, ?*Holosporella rossanae*, *Patruliuspora pacifica* and *Patruliuspora oregonica* is strongly microfacies-controlled. The genus *Clypeina* has been associated with low-energy settings in both Triassic [169–171] and Jurassic [173] deposits. At Lime Peak, this genus occurred widely during the deposition of the first and third packages, peaking in abundance in the internal platform (MCF 1). Its common presence in outer platform environments might be explained by the particularly low-energy setting in which Lime Peak grew up, making shallow outer environs suitable also for *Clypeina* (i.e., presumably the very shallow FWWB allowed the overlap of low energy and sufficient light availability). On the other hand, *Holosporella*? *rossanae*, *Patruliuspora pacifica* and *Patruliuspora oregonica* occur in situ (a few occurrences are also recorded from gravity layers on the outer platform) in the internal platform during LSL (MCF 2). Within MCF 2, their abundance is such that dasycladales are at times the main rock-forming organism of a microfacies recognized to have been deposited in a restricted and calm lagoon. Such a high concentration of green algae is very rare in the Upper Triassic of North America. Similar accumulations are probably only found in some facies of the Black Marble and Mission Creek quarries in Oregon and Idaho (Wallowa terrane), respectively [48,174]. Modern representatives of the family Polyphysaceae (to which both *Patruliuspora pacifica* and *Patruliuspora oregonica* belong) such as the genera *Halicoryne* and *Acetabularia* are euryhaline and appear to be well-adapted to high-salinity conditions [104]. In his works, Zorn [175,176] stressed that some Triassic dasycladales flourished in hypersaline lagoons. The prevalence of *Holosporella*? *rossanae*, *Patruliuspora pacifica* and *Patruliuspora oregonica* might be related to their tolerance to changing salinities and/or higher nutrient availability, as observed during LSL.

Gastropods are also widely distributed within the platform spanning from the slope to the inner platform, where they peak in abundance (MCF 2). The peak in abundance of the group is concomitant with the occurrence of very large specimens up to 45–50 cm in length. To our knowledge, such large gastropods have not been reported anywhere else in the Triassic. Payne [177] proposed that gastropod size might be increased by local ecological factors, of which the most important is nutrient availability. Recently, Ketwetsuriya et al. [178] concluded that high primary productivity was responsible for the presence of large gastropods (20–60 mm high) in the lower Permian of Thailand. At Lime Peak, large gastropods are found in MCF 2 beds that are very rich in green algae, foraminifera and organic content. Therefore, it is very likely that their presence at Lime Peak (in MCF 2) was driven by high food availability.

Corals are generally rare at Lime Peak and are only abundant within the deep photic microfacies MCF 11. *Retiophyllia* sp., the most common coral, is principally found during HSL, when its distribution spans from the reef microfacies in the margin (MCF 7) to the slope (MCF 11). This is not the first time that *Retiophyllia* sp. has been reported from a wide range of depositional environments. Stanton and Flügel [179] noted a wide bathymetric range for this genus from the Upper Triassic Steinplatte complex of Austria. These observations suggest that *Retiophyllia* sp. occurrences are not necessarily indicative of very shallow water. The depositional depth of each finding must be evaluated using other co-available data (e.g., microfacies and biotic association). During LSL, *Retiophyllia* sp. is very rare and was only found (as fragments) in MCF 3. During this period, the corals' contribution within the

reef is given by solitary corals or colonial forms that have an encrusting or massive growth form (e.g., *Astraeomorpha* sp.).

Sponges are very abundant at Lime Peak. Inozoans, sphinctozoans, disjectoporoids, *Spongiomorpha ramosa* and chaetetids peak in number within the reef microfacies. As already put forward by Reid [51], there is a major change in the sponge community within the reef between HSL vs. LSL. In particular, relatively tall sphinctozoan (e.g., *Polytholosia cylindrica cylindrica* and *Cryptocoelia* sp.) and inozoans leave the space to smaller sphinctozoan sponges (e.g., *Paradeningeria* sp. and smaller *Cryptocoelia* sp.), *Spongiomorpha* sp. and nodular and encrusting chaetetids during LSL. This drastic change in average size was interpreted by Reid [51] as related to the different physical processes that affected the platform margin during LSL, especially the reduction of accommodation space. Chaetetids in particular appear to be much more abundant in the reef during LSL than during HSL. An abundance of chaetetid sponges in very shallow waters does not seem to be uncommon: Connolly et al. [180], studying the paleoecology of the Carboniferous genus *Chaetetes*, remarked that this genus was particularly adapted to very shallow waters approaching intertidal depths. Outside reef microfacies, the most abundant sponge taxa at Lime Peak is *Spongiomorpha gibbosa*. The species appears to be very abundant in slope settings, where most of these platy sponges are found lying parallel to the bedding surface. The concentration of microbialites on their upper surface indicates that these specimens are found in living-position and likely lived within the photic zone under low sedimentation rate conditions. These sponges most likely lived free-lying on the muddy surface of the middle–upper slope.

Microbialites are ubiquitous in the photic zone at Lime Peak. They are characterized by different fabrics and morphologies depending on the depositional environment. Columnar stromatolitic microbialites are present within MCF 10 (e.g., Figure 9L) encrusting the upper part of *Spongiomorpha gibbosa*, and within MCF 6B (e.g., Figure 9G) encrusting the upper part of sponges. In both cases, columnar stromatolitic microbialites grew in very low-energy and well-oxygenated environments. These occurrences are very similar to the microbial encrustations described from the Upper Jurassic of Spain in Reolid et al. [106]. Their concentration on the upper surface of encrusted biota indicates both upward growth and a photophilic character [106,107]. Tosti et al. [111] reported abundant biomarkers of cyanobacteria in similar microbialites from the Ladinian–Carnian of the Dolomites. Within the metazoan-rich reef microfacies (MCF 7), microbialites postdate the main framebuilders (e.g., sponges and corals), occurring either as dense or laminated crusts on the framebuilders (Figure 6A) or as cavity-filling leiolitic to thrombolytic clotted and peloidal micrites (Figure 6A). Microbialites, developing as a crust on top of metazoans (mostly corals), are widespread in quaternary post-glacial reefs [131,167,181]. The formation of such crusts has been linked with the activity of sulfate-reducing bacteria that degrade organic matter in anoxic micro-environments within the reef cavities. Tosti et al. [111] reported abundant biomarkers of sulfate-reducing bacteria in clotted and peloidal micrite-rich reef cavities of the Upper Triassic of the Dolomites. Hence, it can be speculated that the formation of both types of microbialites in the reef-cavities at Lime Peak arose in semi-enclosed environments associated with low-oxygen conditions. Unlike in MCF 7, microbialites in MCF 8 occur as thin crusts that bind reef rubbles and were most likely formed at the seafloor in an open environment (Figure 9J). Beltrán et al. [130] analysed similar modern-day lithifying biofilms and showed that such types of binding crusts are composed of a highly variegate consortium of bacteria that differ from the ones found in surrounding reef environments. The last type of microbialites occurring at Lime Peak is found in MCF 6A. It represents the main constituent of the microfacies and acts as the builder of a hard framework later colonized by encrusters (*Tolypammina* sp. among others). This hard framework, which has a leiolitic to thrombolytic microfabric, is interpreted as having formed at the platform margin in an open, normally oxygenated environment with well-circulating water.

Another common reef constituent is the tubular crust (Figure 12G–J). These peculiar tubular crusts are mainly found as secondary framebuilders and rarely as primary frame-

builders (providing hard substrate for the colonization of other organisms such as sponges). Due to their diagenetic aspect, they can be easily confused with marine cement and might have been observed (but misidentified) at Lime Peak. Nonetheless, their centripetal growth, branching, fan-shaped aspect (branches are made of hollow tubules), the presence of borings within them, the fact that they are commonly superficially micritized, and their association with microbialites and/or encrusters all point to a biological origin. Their manner of occurrence and growth form somehow resemble the encrusting sponge genus *Murania* reported from other Triassic localities [28,182]. Monty [183] and later Granier [184] described very similar-looking crusts from the Devonian of Belgium and from the Jurassic of Spain, respectively, and referred to them as "Endostromatolites". According to Monty [183], in the Devonian of Belgium, the growth of such crusts is restrained to cavities, implying that the microbial communities at their origin were not photosynthesizers but rather heterotrophs. At Lime Peak, the internal structure of these organic crusts is generally poorly preserved, impeding precise taxonomic identification. Their growth was not confined to dark cavities but occurred primarily in areas that were exposed to the light during deposition (at the top and on the sides of reef-builders). They commonly grade into microbialites and are themselves micritized. Hence, we cannot exclude the contribution of photosynthesizers to their formation. The dimensions of the internal tubules, ranging from 5 to 10 µm, fit well with the dimensions of filamentous cyanobacteria [185], suggesting that this group of organisms might have also played a role in the formation of these pervasive crusts. Independent of their true nature, these unknown crusts provided important synsedimentary stabilization to the reef framework and thus had a major structural role in the growth of the reef patches.

The distribution of foraminifera at Lime Peak is summarized in Figure 26. By looking at this figure, the eye-catching facts are that: (1) hyaline and porcelaneous foraminifera occupy different ecological niches, and (2) microgranular and agglutinated foraminifera are more equally distributed, with some forms being ubiquitous while others are strongly facies-related. The foraminiferal distribution at Lime Peak seems to confirm the outcomes of previous studies, according to which the spatial distribution of some groups of Upper Triassic foraminifera are facies-related [13,26,132,186]. The deepest-water deposits of MCF 12 are dominated by ubiquitous Duostominina and nodosariids both during LSL and HSL. During HSL, the slope microfacies (MCF 10 and 11) were characterized by a consortium of nodosariids, Duostominina, Ammodiscidae, *Wernlina reidae* and *Taanella yukonensis*. The latter is a new form that was recently described from Lime Peak [46]; *Taanella yukonensis* is exclusively but widely found at Lime Peak, where it is ubiquitous in the photic zone of the carbonate platform. It reaches its maximal abundance in the inner platform environments of both HSL and LSL. As discussed above, under LSL settings, the slope environments were dominated by the redeposition of platform-margin-derived material. Most of the Involutinida found within MCF 12 and 13 are interpreted as having been reworked from the inner platform where they are abundant (see below). However, the genera *Coronipora*, *Semi-involuta* and also partially *Trocholina* (only one specimen was found in the lagoonal deposit of MCF 2) were only found within gravitational microfacies. Therefore, we hypothesize that such genera were originally dwelling on the outer platform before being incorporated into gravitational flows. This finding seems to support the preliminary observations by Piller [132], according to whom these Involutinida genera, unlike most of the forms within the same group, occur in outer platform environments. However, it is not in accordance with findings by [30] in Panthalassa (now Oregon), who found an abundance of similar forms in restricted lagoonal settings identical (but maybe deeper?) to, although older than, the restricted depositional environments identified at Lime Peak. In both LSL and HSL, the platform margin area is dominated by the maximum abundance of porcelaneous and encrusting foraminifera. According to [26], these taxa have very limited ecological tolerance and prefer stable environmental conditions typical at the platform margin. Encrusting forms such as *Tolypammina*, *Planiinvoluta* and *Hirsutospirella* are almost exclusively found in the framestone facies (MCF 7). *Tolypammina* is also present in great abundance encrusting the microbial framework in MCF 6A. The presence of *Hirsutopirella* [187,188] is significant

since it is the first confirmed occurrence outside Tethys (only one possible occurrence reported by [26]). There is a remarkable difference between the foraminiferal assemblages found in the lime sands (MCF 5) and the assemblages of the synsedimentary sediment infill in the primary cavities of MCF 7. In contrast to the first, which hosts low-diversity assemblages where duostominids, variostominids and glutameandratids prevail, the cavity infill is characterized by a much more diversified assemblage, in which reef-dwellers of the genera *Agathammina*, *Gsolbergella*, *Hydrania*, *Hoyenella*, *Decapoalina schaeferae* and *Ophthalmidium* abound. This difference is inferred to be due to the fact that the framework within the framestone facies (MCF 7) creates a multitude of sub-environments constituting different ecological niches ideal for the life of foraminifera with different physiological requirements [26]. Unlike other Upper Triassic reef localities of Tethys, Gondwana or Eastern Laurasia (see [26] for a compilation of the distribution of Upper Triassic foraminifera), typical reef forms such as *Galeanella*, *Miliolipora* (only one dubious specimen of *Miliolipora cuvillieri* was reported by [51]), *Bispiranella* and *Cucurbita* are virtually absent at Lime Peak.

Among the different depositional environments of the Lime Peak carbonate system, the inner platform is where the greatest variability in term of foraminiferal assemblages between LSL and HSL is observed. HSL assemblages are rather poorly diversified and see the presence of Duostomina, miliolids, nodosariids, *Taanella yukonensis* and textulariids. The presence of such stenohaline taxa [189] agrees with the interpretation of a lagoon with almost normal marine conditions during this time. On the contrary, the assemblages observed during LSL are particularly rich in terms of total specimens and diversity. In MCF 2, hyaline aragonitic forms make up the larger fraction of the assemblage. Genera such as *Aulosina*, *Parvalamella*, *Robertonella*, *Falsoreinholdella*, *Praereinholdella*, *Wallowaconus* and *Trochosiphonia* reach their peak abundance. The most eye-catching difference between the lagoonal facies at Lime Peak and other coeval lagoonal deposits [26,34,132,190] is the marked underrepresentation of the genus *Aulotortus*. Assemblages from Lime Peak are extremely similar to the ones described from the Norian lagoonal deposits of the Black Marble Quarry in Oregon [30,31,35–40,174] except for the lower amount of Trocholinidae. In particular, among the numerous taxa shared by the two sites, we can cite the genus *Falsoreinholdella* and species such as *Trochosiphonia stanleyi*, *Praereinholdella galei*, *Parvalamella ashbaughi*, *Tubulastella comans* or *Parvalamella nolfi*. Yet again, these assemblages occur in organic-matter-rich horizons in both sites. The reasons for their high concentration within this type of facies are currently unclear but might be linked to high food availability, particular substrate or other physicochemical factors. According to Forel et al. [47], some intervals within MCF 2 show the presence of *Lutkevichinella*, an ostracod genus that has been commonly associated with brackish conditions by several authors (see the references in [47]). Such intervals are dominated by agglutinated or microgranular genera such as *Wernlina*, *Glutameandrata*, *Taanella yukonensis* and *Ammodiscus* at the expense of hyaline taxa. Such behaviour can be explained by the high tolerance of agglutinated taxa to instable salinity conditions: in fact, according to Jones [191], agglutinated forms are generally more tolerant than calcareous ones to hyposalinity. In this regard, the co-occurrence of *Orthella* and *Hoyenella* within these punctuated episodes is relevant since it may indicate that these two forms, unlike other Triassic porcelaneous forms, may better tolerate salinity variations.

8.6. Reef Paleoecology and the Paleogeography of Stikinia

The distribution and characteristics of Upper Triassic reefs in eastern Panthalassa were recently reviewed and discussed by [192]. In this work, the authors recognized three major types of reefs in eastern Panthalassa: microbial, sponges–microbial and coral-dominated. The differences in reef types (principal bioconstructors, composition and reef morphology) observed among Panthalassan reefs was interpreted as the direct consequence of the diverse latitudinal settings under which the distinct reefs formed. This strong paleo-latitudinal trend was supposedly driven by eastern boundary currents that believably created cool-water environments in the north and warm-water environments in the south. Nutrient levels, associated with the upwelling of cool waters, are also thought to have possibly

played an important role [192]. On this point, available conodont $\delta^{18}O_{PO4}$ thermometry data, which are unfortunately restricted to the early Norian, seem to support the existence of a possible N–S thermal gradient in the Panthalassa during the Carnian–Norian [193]. According to Martindale's hypothesis, the formation of microbial patch reefs would be favoured at the northernmost sites (e.g., Pardonet Hill, BC, Canada; [194]) and coral-dominated reefs at the lowest paleolatitudes (e.g., Mina, NV, USA; Martindale et al., [195]). This interpretation is principally built on the characteristics of reef sites with strong cratonal affinity, such as Mina [196] and the Pardonet Hills [194,197]. These were affected by little or no post-depositional displacement, and therefore their paleogeographical relationship during deposition is thought to have been very similar to the one observed today. In their work, Martindale et al. [192] suggested that sponges–microbial reefs, such as Lime Peak, could have formed in transitional conditions between the high and low latitude reefs.

Our work demonstrates that Lime Peak formed in warm tropical waters. Such a hypothesis agrees with recent paleogeographic and geodynamic reconstructions that propose an intertropical location for Stikinia during the Upper Norian (Figure 27; see [196]), roughly at the same paleolatitude as Nevada (note, however, that Norian seas were warmer than in the present day; see [198,199]). This study contrasts with the outcomes of another recent paleogeographic work that, by analysing the similarity index of the conodont assemblages of Nevada, Stikinia, Quesnellia and high-latitude British Columbia, proposed a high-latitude location for Stikinia [70]. At Lime Peak, the reef microfacies during both HSL and LSL are mainly formed by small- to medium-sized hypercalcified sponges and other organic crusts (microbialites and tubular crust). Generally, corals appear to have provided only an accessory contribution to reef construction. However, we cannot exclude that the abundance of corals at Lime Peak could be slightly underestimated. Some of the secondary cavities present in MCF 7 were indeed formed by the dissolution of corals (which originally had a metastable, aragonitic composition), as attested by the shape of some moulds that preserved the coral's outline, particularly their septa. In terms of main framebuilders, the reef associations found at Lime Peak strongly resemble the reef communities from Japan discussed in [22]. The results of hierarchical cluster analysis on the reef biota (Table 3 shows the references for the cluster analysis), which display some small differences compared to the outcomes of Peybernes et al. [22], exhibit that the reef microfacies from Lime Peak (Yukon) bear the strongest similarity with the Japan–Oman–Slovenia cluster. From a paleobiogeographical point of view, the clustering of Slovenia with Oman, Japan and Yukon is difficult to explain, and more research is needed to assess which factors are responsible for this clustering. At the same time, the very low similarity between Lime Peak and Summit Point (Oregon, USA) is also very surprising. According to the reconstruction by Vérard [198], the two localities should have been very close paleogeographically. In this context, it is important to note that the reef biota from Summit Point has a very low similarity with any of the other reef sites analysed in this study and by [22]. Martindale et al. already noted the particularity of Summit Point reefs and stated that their composition resembles more than one Middle Triassic reef from the Tethys. As reminded by reefs are extremely sensitive environments that are subjected to many factors besides water temperature during their development (e.g., marine currents, nutrient supply, turbidity and sediment input). For instance, reefs from Lime Peak were most likely influenced by moderate to high nutrient levels during their development. In this context, it is also very likely that the particular reef assemblages from Summit Point reflect some very local environmental conditions during their development. Further investigations on this site are needed in order to assess the environmental conditions under which Summit Point reefs grew.
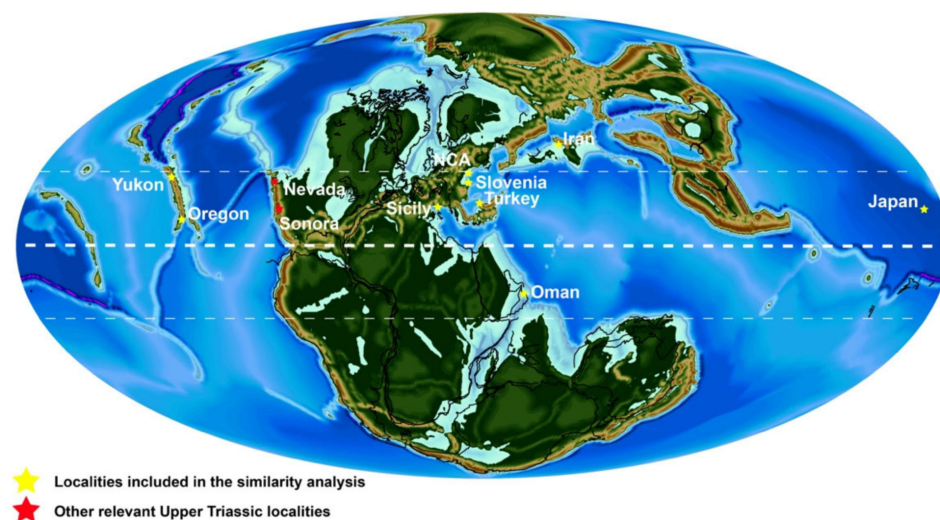
Figure 26. Global paleogeographic reconstruction for the Norian (220 Ma) after the PANALESIS model with the permission of the author Dr Christian Verard [198]. The reader is referred to Vérard et al. [198] for a more detailed explanation of the principles of the model, and to Bucur et al. [48] for the key points of the reconstruction at 220 Ma.

Table 3. References for the reef fauna of the Tethys and Panthalassa used in the similarity analysis (modified from [22]).

Areas	Time Interval	References
Slovenia	Norian–Rhaetian	[89,200–202]
Northern Calcareous Alps	Norian–Rhaetian	[9,12,203]
Iran	Norian	[14,204–211]
Sicily	Norian	[212–218]
Turkey	Norian	[204,219–225]
Oman	Norian	[12]
Japan (Reef type 2)	Norian	[18,25]
Oregon (Summit Point, USA)	Norian	[214,224]
Yukon (Canada)	Norian	[51,52,59,60] and this study

8.7. Comparison with Other Upper Triassic Carbonate Systems Studied during the REEFCaDe Project

As mentioned in the introductory parts, among the Upper Triassic localities of Panthalassa, Lime Peak is by far the one where depositional geometries are best preserved. This allowed us to construct more-robust depositional and facies models. These models can now be used to compare, test and implement other facies models that were previously proposed for other Upper Triassic Panthalassan carbonate systems in the framework of the REEFCaDe project.

Recently, Ref. [33] proposed a depositional model for the slope deposits of the Upper Carnian Hosselkus limestone of Northern California. Within these slope deposits, the authors described several breccia levels. These breccia levels, deposited during the waning stage of the carbonate platform (drowning), contain several limestone clasts of reworked shallow-water material. Since these clasts are the only preserved shallow-water material within the Hosselkus limestone, they provide the only window into the shallow-water sedimentation. The absence of proper shallow-water strata prevented [33] from reconstructing the shallow-water geometries. Nonetheless, the authors favoured the hy-

pothesis of a flat-topped platform due to the abundance of low-energy indicators in the shallow-water clasts.
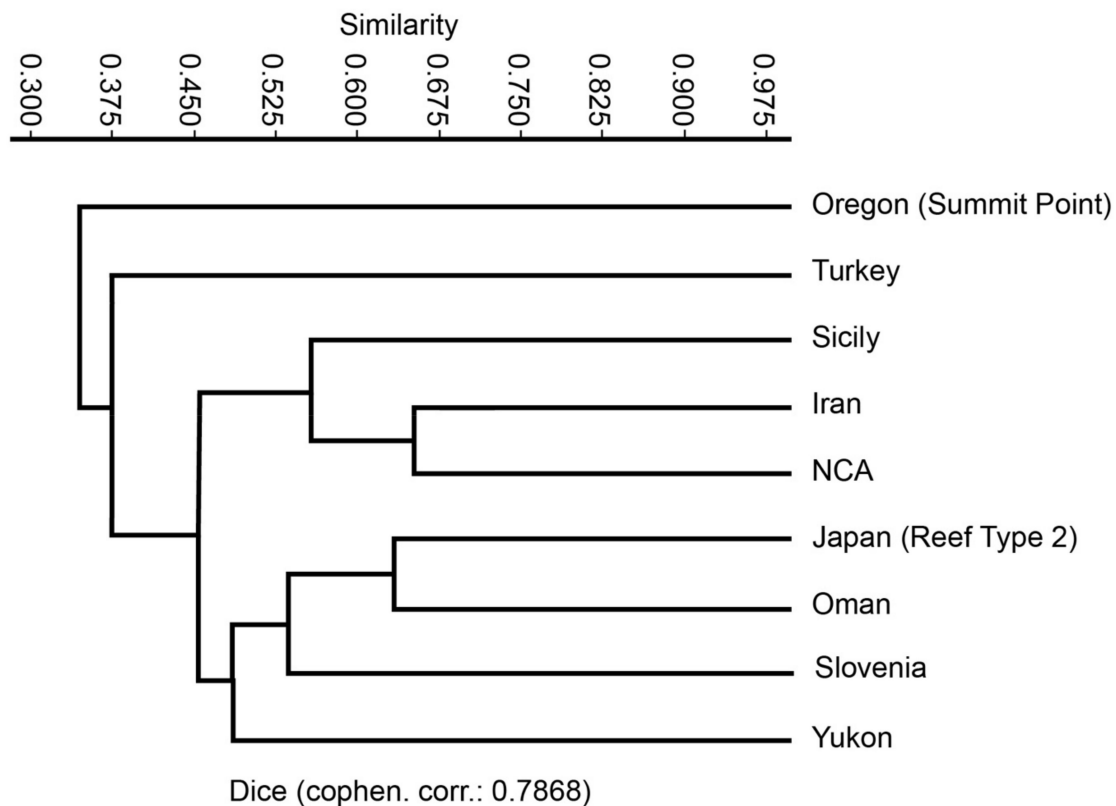

Figure 27. Dendrogram showing the results of hierarchical cluster analysis (UPGMA, Dice coefficient of similarity) between the selected Upper Triassic reef localities in Panthalassa and Tethys.

Some of the microfacies described from these clasts are very similar to the upper slope-platform margin facies during HSL at Lime Peak. In particular, their MCF 6b (see [33]) can be taken as equivalent to our MCF 6A, their MCF 6c to our MCF 7 and their MCF 6a to our MCF 10 (see Figure 9E in [33]). Similar upper slope-platform margins suggest that the Hosselkus limestone carbonate system could have had similar platform-margin geometries to Lime Peak.

More difficult seems to be comparing the facies models proposed for the mixed carbonate–siliciclastic Upper Triassic Antimonio and Vizcaíno terranes of Mexico proposed in [44] and [43], respectively. The Upper Triassic strata in these two terranes are interpreted to have been deposited in a continentally influenced ramp setting where the moderate to high siliciclastic input might have played a fundamental role in influencing the carbonate sedimentation. Hence, the depositional setting was very different from what is observed at Lime Peak.

Upper Triassic carbonates from the Russian Far East and Japan were presumably deposited in an atoll-type depositional setting [17,18,25,27,29]. Unlike the tectonically active setting under which Lime Peak was shaped, atoll-type carbonate forms in a setting that is mostly ruled by steady and constant thermal subsidence [226]. However, some of the facies described from Lime Peak were also recognized in these atoll settings. In particular, the peculiar Involutinidae-rich inner platform facies (LSL) were also described from many of these carbonates (MF 10 in [25], MF 7 in [18] and MF 2 in [17]). The interpreted physical conditions associated with the development of such facies, however, diverge. The authors of [18,25] linked the occurrence of this facies with prevailing open-marine conditions, while Lime Peak, the Black Marble Quarry of Oregon [174] and the Russian Far East [17] point toward more restricted conditions. It is important to note that, whereas the Involutinid

fauna in [18,25] is aulotortid-dominated, the genus *Parvalamella* dominated in [17], and the genera *Aulosina* and *Parvalamella* prevail in this study and in Oregon [174]. Accordingly, although the dominance of Involutinid-rich deposits in inner platform facies is widely recognized for the Upper Triassic, the specific Involutinidae fauna seems to drastically change from locality to locality, possibly reflecting the different level of water restriction present in the inner platform environments of the different carbonate systems. In terms of facies abundance, the more eye-catching difference between the atoll-type carbonates of the Japanese–Russian side and Lime Peak is the rarity of ooids in the latter. Given the many indicators of warm-water conditions and high saturation state, one might expect to also have widespread ooidal production at Lime Peak. Yet ooids tend to be rare and are only an accessory component of MCF 5. Nonetheless, the dearth of ooids does not have to be surprising, because many modern shallow and warm-water carbonate systems are characterized by the paucity of ooids (e.g., many carbonate producing areas of the Pacific; see the "oolite problem" of [227,228]. Rankey and Reeder [229], studying the occurrence of ooids in the Aitutaki Atoll (South Pacific), stated that ooid formation is facilitated by the convergence of hydrodynamic and chemical factors, including pH, alkalinity, carbonate supersaturation, wave-driven currents and a type of flow that permit their transport without flushing them out of the system. In areas where all of these criteria are not met, ooids do not form or are very rare. Hence, given the belief that Lime Peak was in a repaired position (leeward or within a protected basin) of the Lews River arc, the absence of ooids might be attributed to the lack of sufficient energy for their high production.

8.8. Brief Comparison with Upper Triassic Systems from the Tethys

The most striking difference between the Lime Peak carbonate systems and the ones known from the Tethys is their very different scales. The Norian Dolomia Principale/Hauptodolomite of the Southern Alps ([230] and references therein) and the Dachstein Limestone of the Northern Alps ([231] and references therein) formed platforms that were tens of kilometres wide and possessed widely extended platform interiors. In contrast, Lime Peak was a relatively small system that probably extended for only several hundred meters.

Eustatism is believed to have had major control on the sea level variations in the Tethys. This is shown by the broad correlations of third-order sea levels curves for Tethyan and extra-Tethyan regions ([16] and references therein). In contrast, at Lime Peak, the eustatic signal was very likely overprinted by the local tectonic control, which, overall, produced sharp vertical facies variations.

Unlike carbonate platforms in the Tethys, which are thought to have formed in an oligotrophic sea ([192] and references therein), Lime Peak formed under higher nutrient availability (mesotrophic?). In this context, reef-building filter-feeders prevailed over the photozoans (sponges dominated over corals).

9. Conclusions

Upper Triassic limestone of the Lime Peak area was extensively sampled to study sedimentology and biotic and microfacies content. Our results suggest that Lime Peak formed as a low-energy carbonate platform surrounded by an aphotic basin with openocean waters. Overall, the abundance of calcified green algae (dasycladales), the thick early marine "cements" (or evinosponges) and the presence of big gastropods and the giant alatoform bivalve *Wallowaconcha* cf. *raylenea* indicate that Lime Peak formed under tropical conditions with warm waters and high carbonate saturation state. These results agree with recent paleogeographic modelling that located Stikinia in an intertropical position during the Norian.

The carbonate system and its sedimentation were influenced by local tectonics, which controlled the available accommodation space for carbonate sedimentation. The carbonates of the area were mainly deposited under two different settings: HSL (high accommodation space) and LSL (low accommodation space). In terms of sedimentology, remarkable differences between the two settings are seen in all the depositional environments of the

carbonate platform. The water level above the platform margin controlled the physical conditions in the inner platform environments: the latter were characterized by well-established open-water circulation during HSL and restricted conditions during LSL. Such contrasting conditions are reflected by a notable turnover of biotic and sedimentary facies. In particular, during LSL, the inner platform environments were characterized by the deposition of organic-matter-rich microfacies. Their occurrence suggests anomalously high productivity and abundant nutrient levels, which may be of interest for petroleum research. Nutrient availability is thought to have had an important influence on the type of carbonate factory at Lime Peak. Very similar shallow-water organic matter-rich accumulations have been reported in the past from the Upper Triassic of Oregon and the Russian Far East. The processes that led to the formation of these particular deposits are worth being investigated further.

Finally, this study includes the most complete analysis of biotic distribution at the platform-scale in Panthalassa. Some of the microfacies described from Lime Peak have strong affinities with the ones described from other Upper Triassic carbonate systems of the Panthalassa. We hope that these new data will become a solid source of information for other workers to reconstruct more dismantled Upper Triassic Panthalassan carbonate systems formed in similar settings.

Supplementary Materials: The following are available online at https://www.mdpi.com/article/10.3390/geosciences12080292/s1, Figure S1: Location of the studied samples; Figure S2. Samples from the transects; Figure S3. Studied samples for the point-counting analysis; Figure S4. Authors of the identified foraminifera; Figure S5. Conodonts from Lime Peak; Figure S6. Selected taxa for the cluster analysis, part 1; Figure S7. Selected taxa for the cluster analysis, part 2.

Author Contributions: Conceptualization, N.D.P., S.R. and R.M.; methodology, N.D.P., S.R., R.M. and C.P.; formal analysis, N.D.P. and R.M.; investigation, N.D.P., S.R., R.M., N.F., M.-B.F. and C.P.; resources, R.M.; data curation, R.M.; writing—original draft preparation, N.D.P.; writing—review and editing, N.D.P., S.R., R.M., C.P., M.-B.F. and N.F.; visualization, N.D.P.; supervision, S.R. and R.M.; project administration, R.M.; funding acquisition, R.M. All authors have read and agreed to the published version of the manuscript.

Data Availability Statement: The samples used in this study can be obtained upon request from the authors.

Conflicts of Interest: The authors declare no conflict of interest.

References

1. Knowlton, N.; Brainard, R.E.; Fisher, R.; Moews, M.; Plaisance, L.; Caley, M.J. Coral Reef Biodiversity. In *Life in the World's Oceans: Diversity, Distribution, and Abundance*; McIntyre, A.D., Ed.; Blackwell Publishing Ltd.: Hoboken, NJ, USA, 2010; pp. 65–77, ISBN 9781405192972.
2. Flügel, E. Evolution of Triassic Reefs: Current Concepts and Problems. *Facies* **1982**, *6*, 297–327. [CrossRef]
3. Stanton, R.J.; Flügel, E. An Accretionary Distally Steepened Ramp at an Intrashelf Basin Margin: An Alternative Explanation for the Upper Triassic Steinplatte "Reef" (Northern Calcareous Alps, Austria). *Sediment. Geol.* **1995**, *95*, 269–286. [CrossRef]

4. Chiocchini, M.; Farinacci, A.; Mancinelli, A.; Molinari, V.; Potetti, M. Biostratigrafia a foraminiferi, dasicladali e calpionelle delle successioni carbonatiche mesozoiche dell'Appennino centrale (Italia). In *Biostratigrafia dell'Italia Centrale*; Mancinelli, A., Ed.; Studi Geologici Camerti, n. speciale; Università di Camerino: Camerino, Italy, 1994; pp. 9–129. [CrossRef]

5. Galli, M.T.; Jadoul, F.; Bernasconi, S.M.; Cirilli, S.; Weissert, H. Stratigraphy and palaeoenvironmental analysis of the Triassic–Jurassic transition in the western Southern Alps (Northern Italy). *Palaeogeogr. Palaeoclimatol. Palaeoecol.* **2007**, *244*, 52–70. [CrossRef]

6. Romano, R.; Masetti, D.; Carras, N.; Barattolo, F.; Roghi, G. The Triassic/Jurassic boundary in a peritidal carbonate platform of the Pelagonian Domain: The Mount Messapion section (Chalkida, Greece). *Riv. Ital. Paleontol. Stratigr.* **2008**, *114*, 431–452. [CrossRef]

7. Tunaboylu, B.; Altiner, D.; Isintek, I.; Demirci, D. Foraminiferal biostratigraphy and sequence stratigraphy of peritidal carbonates at the Triassic-Jurassic boundary (Karaburun Peninsula, Western Turkey). *J. Asian Earth Sci.* **2014**, *90*, 61–76. [CrossRef]

8. Todaro, S.; Di Stefano, P.; Zarcone, G.; Randazzo, V. Facies stacking and extinctions across the Triassic–Jurassic boundary in a peritidal succession from western Sicily. *Facies* **2017**, *63*, 20. [CrossRef]

9. Martindale, R.C.; Krystyn, L.; Bottjer, D.J.; Corsetti, F.A.; Senowbari-Daryan, B.; Martini, R. Depth Transect of an Upper Triassic (Rhaetian) Reef from Gosau, Austria: Microfacies and Community Ecology. *Palaeogeogr. Palaeoclimatol. Palaeoecol.* **2013**, *376*, 1–21. [CrossRef]

10. Marangon, A.; Gattolin, G.; Della Porta, G.; Preto, N. The Latemar: A Flat-Topped, Steep Fronted Platform Dominated by Microbialites and Synsedimentary Cements. *Sediment. Geol.* **2011**, *240*, 97–114. [CrossRef]

11. Jin, X.; Shi, Z.; Rigo, M.; Franceschi, M.; Preto, N. Carbonate Platform Crisis in the Carnian (Late Triassic) of Hanwang (Sichuan Basin, South China): Insights from Conodonts and Stable Isotope Data. *J. Asian Earth Sci.* **2018**, *164*, 104–124. [CrossRef]

12. Bernecker, M. Late Triassic Reefs from the Northwest and South Tethys: Distribution, Setting, and Biotic Composition. *Facies* **2005**, *51*, 442–453. [CrossRef]

13. Schäfer, P.; Senowbari-Daryan, B. Facies Development and Paleoecologic Zonation of Four Upper Triassic Patch-Reefs, Northern Calcareous Alps near Salzburg, Austria. In *European Fossil Reef Models*; Toomey, D.F., Ed.; SEPM Society for Sedimentary Geology: Tulsa, OK, USA, 1981; Volume 30, pp. 241–259.

14. Senowbari-Daryan, B.; Rashidi, K.; Torabi, H. Foraminifera and Their Associations of a Possibly Rhaetian Section of the Nayband Formation in Central Iran, Northeast of Esfahan. *Facies* **2010**, *56*, 567–596. [CrossRef]

15. Ziegler, A.M.; Eshel, G.; McAllister Rees, P.; Rothfus, T.A.; Rowley, D.B.; Sunderlin, D. Tracing the Tropics across Land and Sea: Permian to Present. *Lethaia* **2003**, *36*, 227–254. [CrossRef]

16. Flügel, E. Triassic Reef Patterns. In *Phanerozoic Reef Patterns*; Kiessling, W., Flugel, E., Golonka, J., Eds.; Society of Economic Paleontologists and Mineralogists: Tulsa, OK, USA, 2002; pp. 391–464.

17. Peyrotty, G.; Rigaud, S.; Kemkin, I.; Martini, R. Sedimentology and Biostratigraphy of Upper Triassic Atoll-Type Carbonates from the Dalnegorsk Area, Taukha Terrane, Far East Russia. *Glob. Planet. Chang.* **2020**, *184*, 103072. [CrossRef]

18. Peybernes, C.; Chablais, J.; Onoue, T.; Martini, R. Mid-Oceanic Shallow-Water Carbonates of the Panthalassa Domain: New Microfacies Data from the Sambosan Accretionary Complex, Shikoku Island, Japan. *Facies* **2016**, *62*, 1–27. [CrossRef]

19. Mitchell, A.H.G. Facies of an Early Miocene Volcanic Arc, Malekula Island, New Hebrides. *Sedimentology* **1970**, *14*, 201–243. [CrossRef]

20. Hamilton, W.B. Plate Tectonics and Island Arcs. *Geol. Soc. Am. Bull.* **1988**, *100*, 1503–1527. [CrossRef]

21. Peyrotty, G.; Brigaud, B.; Martini, R. Δ18O, Δ13C, Trace Elements and REE in Situ Measurements Coupled with U–Pb Ages to Reconstruct the Diagenesis of Upper Triassic Atoll-Type Carbonates from the Panthalassa Ocean. *Mar. Pet. Geol.* **2020**, *120*, 104520. [CrossRef]

22. Peybernes, C.; Chablais, J.; Onoue, T.; Escarguel, G.; Martini, R. Paleoecology, Biogeography, and Evolution of Reef Ecosystems in the Panthalassa Ocean during the Late Triassic: Insights from Reef Limestone of the Sambosan Accretionary Complex, Shikoku, Japan. *Palaeogeogr. Palaeoclimatol. Palaeoecol.* **2016**, *457*, 31–51. [CrossRef]

23. Chablais, J.; Martini, R.; Onoue, T. Aulotortus Friedli from the Upper Triassic Gravitational Flow Deposits of the Kumagawa River (Kyushu, Southwest Japan). *Paleontol. Res.* **2010**, *14*, 151–160. [CrossRef]

24. Chablais, J.; Onoue, T.; Martini, R. Upper Triassic Reef-Limestone Blocks of Southwestern Japan: New Data from a Panthalassan Seamount. *Palaeogeogr. Palaeoclimatol. Palaeoecol.* **2010**, *293*, 206–222. [CrossRef]

25. Chablais, J.; Martini, R.; Samankassou, E.; Onoue, T.; Sano, H. Microfacies and Depositional Setting of the Upper Triassic Mid-Oceanic Atoll-Type Carbonates of the Sambosan Accretionary Complex (Southern Kyushu, Japan). *Facies* **2010**, *56*, 249–278. [CrossRef]

26. Chablais, J.; Martini, R.; Kobayashi, F.; Stampfli, G.M.; Onoue, T. Upper Triassic Foraminifers from Panthalassan Carbonate Buildups of Southwestern Japan and Their Paleobiogeographic Implications. *Micropaleontology* **2011**, *57*, 93–124. [CrossRef]

27. Peybernes, C.; Peyrotty, G.; Chablais, J.; Onoue, T.; Yamashita, D.; Martini, R. Birth and Death of Seamounts in the Panthalassa Ocean: Late Triassic to Early Jurassic Sedimentary Record at Mount Sambosan, Shikoku, Southwest Japan. *Glob. Planet. Chang.* **2020**, *192*, 103250. [CrossRef]

28. Peybernes, C.; Chablais, J.; Martini, R. Upper Triassic (Ladinian?-Carnian) Reef Biota from the Sambosan Accretionary Complex, Shikoku, Japan. *Facies* **2015**, *61*, 20. [CrossRef]

29. Peyrotty, G.; Ueda, H.; Peybernes, C.; Rettori, R.; Martini, R. Upper Triassic Shallow–Water Carbonates from the Naizawa Accretionary Complex, Hokkaido (Japan): New Insights from Panthalassa. *Palaeogeogr. Palaeoclimatol. Palaeoecol.* **2020**, *554*, 109832. [CrossRef]
30. Rigaud, S.; Blau, J.; Martini, R.; Rettori, R. Taxonomy and Phylogeny of the Trocholinidae (Involutinina). *J. Foraminifer. Res.* **2013**, *43*, 317–339. [CrossRef]
31. Rigaud, S.; Vachard, D.; Schlagintweit, F.; Martini, R. New Lineage of Triassic Aragonitic Foraminifera and Reassessment of the Class Nodosariata. *J. Syst. Palaeontol.* **2016**, *14*, 919–938. [CrossRef]
32. Khalil, H.; Baumgartner, P.O.; Onoue, T.; Del Piero, N.; Stanley, G.; Rigaud, S.; Martini, R. Middle-Late Triassic Radiolarian Assemblages from Chert Clasts of the Excelsior Gulch Conglomerate (Wallowa Terrane, Oregon, U.S.A.). *Rev. Paleobiol.* **2020**, *39*, 565–579. [CrossRef]
33. Fucelli, A.; Golding, M.; Martini, R. Downslope Re-Sedimentation from a Short-Living Carbonate Platform: Record from the Upper Triassic Hosselkus Limestone (Northern California). *Sediment. Geol.* **2021**, *422*, 105967. [CrossRef]
34. Rigaud, S.; Martini, R.; Rettori, R.; Stanley, G.D.J. Stratigraphic Potential of the Upper Triassic Benthic Foraminifers. *Albertiana* **2010**, *38*, 34–39.
35. Rigaud, S.; Martini, R.; Rettori, R. Parvalamellinae, a New Subfamily for Triassic Glomospiroid Involutinidae. *J. Foraminifer. Res.* **2012**, *42*, 245–256. [CrossRef]
36. Rigaud, S.; Martini, R.; Rettori, R. A New Genus of Norian Involutinid Foraminifers—Its Morphological, Biostratigraphic, and Evolutionary Significance. *Acta Palaeontol. Pol.* **2013**, *58*, 391–405. [CrossRef]
37. Rigaud, S.; Martini, R.; Vachard, D. Early Evolution and New Classification of the Order Robertinida (Foraminifera). *J. Foraminifer. Res.* **2015**, *45*, 3–28. [CrossRef]
38. Rigaud, S.; Blau, J.; Martini, R.; Rettori, R. Taxonomy, Phylogeny, and Functional Morphology of the Foraminiferal Genus Involutina. *Acta Palaeontol. Pol.* **2015**, *60*, 235–244. [CrossRef]
39. Rigaud, S.; Vachard, D.; Martini, R. Agglutinated versus Microgranular Foraminifers: End of a Paradigm? *J. Syst. Palaeontol.* **2015**, *13*, 75–95. [CrossRef]
40. Rigaud, S.; Martini, R. Agglutinated or Porcelaneous Tests: Where To Draw the Line? *J. Foraminifer. Res.* **2016**, *46*, 333–344. [CrossRef]
41. Khalil, H.; McRoberts, C.A.; Del Piero, N.; Stanley, G.D.J.; Martini, R.; Rigaud, S. New Biostratigraphic Constraints for the Martin Bridge Formation (Upper Triassic, Wallowa Terrane, Oregon, U.S.A.). *Rev. Paléobiol.* **2018**, *37*, 109–119. [CrossRef]
42. Heerwagen, E.; Davies, J.H.F.L.; Schmidt, S.T.; Ulianov, A.; Martini, R. The Paleoposition of the Antimonio Depositional System (Sonora, Mexico): New Insights from Nonparametric and Multivariate Analysis of Detrital Zircon Data. *J. S. Am. Earth Sci.* **2020**, *105*, 102913. [CrossRef]
43. Heerwagen, E.; Martini, R. The Vizcaíno Terrane: Another Occurrence of Upper Triassic Shallow-Marine Carbonates in Mexico. *Facies* **2020**, *66*, 8. [CrossRef]
44. Heerwagen, E.; Martini, R. The Antimonio Ramp in Sonora, Mexico: A Shallow-Marine Upper Triassic Mixed Siliciclastic Carbonate Ramp System. *Facies* **2018**, *64*, 6. [CrossRef]
45. Del Piero, N.; Rigaud, S.; Takahashi, S.; Poulton, S.W.; Martini, R. Unravelling the Paleoecology of Flat Clams: New Insights from an Upper Triassic Halobiid Bivalve. *Glob. Planet. Chang.* **2020**, *190*, 103195. [CrossRef]
46. Del Piero, N.; Rigaud, S.; Martini, R. Taanella Yukonensis n. Gen. n. Sp., an Atypically Porous Ataxophragmiidae Foraminifera from the Upper Triassic of Panthalassa. *J. Foraminifer. Res.* **2022**, *52*, 99–107.
47. Forel, M.B.; Del Piero, N.; Rigaud, S.; Martini, R. Ostracods from the Late Triassic (Norian) of Yukon, Canada: New Taxonomic and Palaeogeographic Insights. *Riv. Ital. Paleontol. Stratigr.* **2022**, *128*, 325–328. [CrossRef]
48. Bucur, I.; Rigaud, S.; Del Piero, N.; Fucelli, A.; Heerwagen, E.; Peybernes, C.; Peyrotty, G.; Verard, C.; Chablais, J.; Martini, R. Upper Triassic Calcareous Algae from the Panthalassa Ocean. *Riv. Ital. Paleontol. Stratigr.* **2020**, *126*, 499–540. [CrossRef]
49. Tempelman-kluit, D.J. *Reconnaissance Geology, Laberge Map-Area*; Geological Survey of Canada: Ottawa, ON, Canada, 1978; pp. 61–66.
50. England, T.D.J. A Study of Upper Triassic Conodonts of the Intermontane Belt, Yukon Territory. Bachelor's Thesis, Department of Geological Sciences, The University of British Columbia, Vancouver, BC, Canada, 1980, Unpublished.
51. Reid, R.P. The Facies and Evolution of an Upper Triassic Reef Complex in Northern Canada. Ph.D. Thesis, University of Miami, Coral Gables, FL, USA, 1985.
52. Reid, R.P.; Tempelman-Kluit, D.J. Upper Triassic Tethyan-Type Reefs in the Yukon. *Bull. Can. Pet. Geol.* **1987**, *35*, 316–332.
53. Yarnell, J.M.; Stanley, G.D.J.; Hart, C.J.R. New Paleontological Investigations of Upper Triassic Shallow-Water Reef Carbonates (Lewes River Group) in the Whitehorse Area, Yukon. In *Yukon Exploration and Geology 1998*; Roots, J., Edmond, D.S., Eds.; Exploration and Geological Services Division: Yukon, Indian; Northern Affairs Canada: Gatineau, QC, Canada, 1999; pp. 179–184.
54. Yarnell, J.M. Paleontology of Two North American Triassic Reef Faunas: Implications for Terrane Paleontology. Master's Thesis, University of Montana, Missoula, MT, USA, 2000.
55. Reid, R.P.; Ginsburg, R.N. The Role of Framework in Upper Triassic Patch Reefs in the Yukon Canada. *Palaios* **1986**, *1*, 590–600. [CrossRef]
56. Reid, R.P. Discovery of Triassic Phylloid Algae: Possible Links with the Paleozoic. *Can. J. Earth Sci.* **1986**, *23*, 2068–2071. [CrossRef]

57. Reid, R.P. Nonskeletal Peloidal Precipitates in Upper Triassic Reefs, Yukon Territory (Canada). *J. Sediment. Res.* **1987**, *57*, 893–900. [CrossRef]

58. Reid, R.P. Lime Peak Reef Complex, Norian Age, Yukon. *Canada Adjac. Areas* **1989**, *13*, 758–765.

59. Senowbari-Daryan, B.; Reid, R.P. Upper Triassic Sponges (Sphinctozoa) from Southern Yukon, Stikinia Terrane. *Can. J. Earth Sci.* **1987**, *24*, 882–902. [CrossRef]

60. Gaździcki, A.; Reid, R.P. Upper Triassic Involutinidae (Foraminifera) of Lime Peak in Yukon, Canada. *Acta Geol. Pol.* **1983**, *33*, 99–106.

61. Hart, C.J.R. *A Transect across Northern Stikinia: Geology of the Northern Whitehorse Map Area, Southern Yukon Territory (105D/13-16)*; Indigenous and Northern Affairs Canada: Yellowknife, NT, Canada, 1997.

62. Coney, P.J.; Jones, D.L.; Monger, J.W.H. Cordilleran Suspect Terranes. *Nature* **1980**, *288*, 329–333. [CrossRef]

63. Jones, D.L.; Silberling, N.J.; Hillhouse, J. Wrangellia—A Displaced Terrane in Northwestern North America. *Can. J. Earth Sci.* **1977**, *14*, 2565–2577. [CrossRef]

64. Colpron, M.; Nelson, J.L.; Murphy, D.C. Northern Cordilleran Terranes and Their Interactions through Time. *GSA Today* **2007**, *17*, 4–10. [CrossRef]

65. Wheeler, J.O.; McFeeely, P. *Tectonic Assemblage Map of the Canadian Cordillera and Adjacent Part of the United States of America*; Geological Survey of Canada: Ottawa, ON, Canada, 1991.

66. Belasky, P.; Stevens, C.H.; Hanger, R.A. Early Permian Location of Western North American Terranes Based on Brachiopod, Fusulinid, and Coral Biogeography. *Palaeogeogr. Palaeoclimatol. Palaeoecol.* **2002**, *179*, 245–266. [CrossRef]

67. Beranek, L.P.; Mortensen, J.K. The Timing and Provenance Record of the Late Permian Klondike Orogeny in Northwestern Canada and Arc-Continent Collision along Western North America. *Tectonics* **2011**, *30*, TC5017. [CrossRef]

68. Aberhan, M. Terrane History of the Canadian Cordillera: Estimating Amounts of Latitudinal Displacement and Rotation of Wrangellia and Stikinia. *Geol. Mag.* **1999**, *136*, 481–492. [CrossRef]

69. Smith, P.L. Paleobiogeography and Early Jurassic Molluscs in the Context of Terrane Displacement in Western Canada. In *Paleogeography of the North American Cordillera: Evidence for and against Large-Scale Displacements*; Haggart, J.W., Enkin, R.J., Monger, J.W.H., Eds.; Geological Association of Canada: St. John's, NL, Canada, 2006; pp. 81–91.

70. Golding, M.L. Evaluating Tectonic Models for the Formation of the North American Cordillera Using Multivariate Statistical Analysis of Late Triassic Conodont Faunas. *Paleobiodivers. Paleoenviron.* **2019**, *100*, 135–149. [CrossRef]

71. Golding, M.L.; Mortensen, J.K.; Zonneveld, J.P.; Orchard, M.J. U-Pb Isotopic Ages of Euhedral Zircons in the Rhaetian of British Columbia: Implications for Cordilleran Tectonics during the Late Triassic. *Geosphere* **2016**, *12*, 1606–1616. [CrossRef]

72. Golding, M.L.; Mortensen, J.K.; Ferri, F.; Zonneveld, J.P.; Orchard, M.J. Determining the Provenance of Triassic Sedimentary Rocks in Northeastern British Columbia and Western Alberta Using Detrital Zircon Geochronology, with Implications for Regional Tectonics. *Can. J. Earth Sci.* **2016**, *53*, 140–155. [CrossRef]

73. Schroeder-Adams, C.; Haggart, J.W. Biogeography of Foraminifera in Tectonic Reconstructions; Imitations and Constraints on the Paleogeographic Position of Wrangellia. *Geol. Assoc. Canada Spec. Pap.* **2006**, *46*, 95–108.

74. Colpron, M.; Nelson, J.L. *A Digital Atlas of Terranes for the Northern Cordillera*; BCGS GeoFile; British Columbia Ministry of Energy and Mines: Victoria, BC, Canada, 2011.

75. Struik, L.C.; Schiarizza, P.; Orchard, M.J.; Cordey, F.; Sano, H.; MacIntyre, D.G.; Lapierre, H.; Tardy, M. Imbricate Architecture of the Upper Paleozoic to Jurassic Oceanic Cache Creek Terrane, Central British Columbia. *Can. J. Earth Sci.* **2001**, *38*, 495–514. [CrossRef]

76. Mihalynuk, M.G.; Nelson, J.A.; Diakow, L.J. Cache Creek Terrane Entrapment: Oroclinal Paradox within the Canadian Cordillera. *Tectonics* **1994**, *13*, 575–595. [CrossRef]

77. Bordet, E. *Bedrock Geology Map of the Teslin Mountain and East Lake Laberge Areas*; Parts of NTS 105E/2, 105E/3 and 105E/6; Yukon Geological Survey: Whitehorse, YT, Canada, 2016.

78. Bordet, E. Updates on the Middle Triassic-Middle Jurassic Stratigraphy and Structure of the Teslin Mountain and East Lake Laberge Areas, South-Central Yukon. In *Yukon Exploration and Geology 2016*; MacFarlane, K.E., Weston, L.H., Eds.; Yukon Geological Survey: Whitehorse, YT, Canada, 2017; pp. 1–24.

79. Tempelman-Kluit, D.J. *Geology, Laberge (105E) and Carmacks (115I)*; Yukon Geological Survey: Whitehorse, YT, Canada, 1984.

80. Monger, J.W.H.; Wheeler, J.O.; Tipper, H.W.; Gabrielse, H.; Harms, T.; Struik, L.C.; Campbell, R.B.; Dodds, C.J.; Gehrels, G.E.; O'Brien, J. Part B. Cordilleran Terranes, Upper Devonian to Middle Jurassic Assemblages. In *Geology of the Cordilleran Orogen in Canada*; Gabrielse, H., Yorath, C.J., Eds.; Geological Survey of Canada: Ottawa, ON, Canada, 1991; pp. 281–327.

81. Simmons, A.T.; Tosdal, R.M.; Awmack, H.J.; Wooden, J.L.; Friedman, R.M. *Early Triassic Stuhini Group and Tertiary Sloko Group Magmatism (NTS 104K/10W), Northwestern British Columbia: New U-Pb Geochronological Results*; British Columbia Geological Survey: Victoria, BC, Canada, 2007.

82. Bordet, E.; Crowley, J.L.; Piercey, S.J. *Geology of the Eastern Lake Laberge Area (105E), South-Central Yukon*; Yukon Geological Survey: Whitehorse, YT, Canada, 2019.

83. White, D.; Colpron, M.; Buffett, G. Seismic and Geological Constraints on the Structure and Hydrocarbon Potential of the Northern Whitehorse Trough, Yukon, Canada. *Bull. Can. Pet. Geol.* **2012**, *60*, 239–255. [CrossRef]

84. Bordet, E. Preliminary Results on the Middle Triassic-Middle Jurassic Stratigraphy and Structure of the Teslin Mountain Area, Southern Yukon. In *Yukon Exploration and Geology 2015*; MacFarlane, K.E., Nordling, M.G., Eds.; Yukon Geological Survey: Whitehorse, YT, Canada, 2016; pp. 43–61.

85. Morrison, G.W. Setting and Origin of Skarn Deposits in the Whitehorse Copper Belt, Yukom. Ph.D. Thesis, The University of Western Ontario, London, ON, Canada, 1981.

86. Lokier, S.W.; Al Junaibi, M. The Petrographic Description of Carbonate Facies: Are We All Speaking the Same Language? *Sedimentology* **2016**, *63*, 1843–1885. [CrossRef]

87. Burne, R.V.; Moore, L.S. Microbialites: Organosedimentary Deposits of Benthic Microbial Communites. *Palaios* **1987**, *2*, 241–254. [CrossRef]

88. Riding, R. Structure and Composition of Organic Reefs and Carbonate Mud Mounds: Concepts and Categories. *Earth-Sci. Rev.* **2002**, *58*, 163–231. [CrossRef]

89. Turnšek, D.; Ramovš, A. *Upper Triassic (Norian-Rhaetian) Reef Buildings in the Northern Julian Alps (NW Yugoslavia)*; Slovenian Academy of Sciences and Arts: Ljubljana, Slovenia, 1987.

90. Crasquin-Soleau, S.; Vaslet, D.; Le Nindre, Y.-M. Ostracods As Markers of the Permian/Triassic Boundary in the Khuff Formation of Saudi Arabia. *Paleontology* **2005**, *48*, 853–868. [CrossRef]

91. Lei, J.Z.X.; Golding, M.L.; Hussin, J.M. Paleoenvironmental Interpretation and Identification of the Norian-Rhaetian Boundary in the Whitehorse Trough (Stikine Terrane, Northern Canadian Cordillera). *Geol. Soc. Am. Programs* **2019**, *51*, 12–14. [CrossRef]

92. Golding, M.L.; Orchard, M.J.; Zagorevski, A. *Conodonts from the Stikine Terrane in Northern British Columbia and Southern Yukon*; Open File; Geological Survey of Canada: Ottawa, ON, Canada, 2017.

93. Reid, R.P.; Macintyre, I.G.; James, N.P. Internal Precipitation of Microcrystalline Carbonate: A Fundamental Problem for Sedimentologists. *Sediment. Geol.* **1990**, *68*, 163–170. [CrossRef]

94. Flügel, E. *Microfacies of Carbonate Rocks. Analysis, Interpretation and Application*, 2nd ed.; Springer: Berlin/Heidelberg, Germany, 2010; ISBN 9788578110796.

95. Keim, L.; Schlager, W. Automicrite Facies on Steep Slopes (Triassic, Dolomites, Italy). *Facies* **1999**, *41*, 15–25. [CrossRef]

96. Wolf, K.H. "Grain-Diminution" of Algal Colonies to Micrite. *J. Sediment. Petrol.* **1965**, *35*, 420–427. [CrossRef]

97. Russo, F.; Neri, C.; Mastandrea, A.; Baracca, A. The Mud Mound Nature of the Cassian Platform Margins of the Dolomites. A Case History: The Cipit Boulders from Punta Grohmann (Sasso Piatto Massif, Northern Italy). *Facies* **1997**, *36*, 25–36. [CrossRef]

98. McRoberts, C.A. Late Triassic Bivalvia (Chiefly Halobiidae and Monotidae) from the Pardonet Formation, Williston Lake Area, Northeastern British Columbia, Canada. *J. Paleontol.* **2011**, *85*, 613–664. [CrossRef]

99. Stanley, G.D.J.; Swart, P.K. Evolution of the Coral-Zooxanthellae Symbiosis during the Triassic: A Geochemical Approach. *Paleobiology* **1995**, *21*, 179–199. [CrossRef]

100. Muscatine, L.; Goiran, C.; Land, L.; Jaubert, J.; Cuif, J.P.; Allemand, D. Stable Isotopes (Δ13C and Δ15N) of Organic Matrix from Coral Skeleton. *Proc. Natl. Acad. Sci. USA* **2005**, *102*, 1525–1530. [CrossRef]

101. Stanley, G.D.J.; Helme, K.P. Middle Triassic Coral Growth Bands and Their Implication for Photosymbiosis. *Palaios* **2010**, *25*, 754–763. [CrossRef]

102. Kiessling, W. Reef Expansion during the Triassic: Spread of Photosymbiosis Balancing Climatic Cooling. *Palaeogeogr. Palaeoclimatol. Palaeoecol.* **2010**, *290*, 11–19. [CrossRef]

103. Flügel, E. Diversity and Environments of Permian and Triassic Dasycladacean Algae. In *Paleoalgology: Contemporary Research and Applications*; Toomey, D.F., Nitecki, M.H., Eds.; Springer: Berlin/Heidelberg, Germany, 1985; pp. 344–351.

104. Valet, G. Paleoecological Approach to Dasycladales from the Ecology of Recent Forms. *Bull. Cent. Rech. Explor. Elf-Aquitaine* **1979**, *3*, 859–866.

105. Reitner, J. Modern Cryptic Microbialite/Metazoan Facies from Lizard Island (Great Barrier Reef, Australia) Formation and Concepts. *Facies* **1993**, *29*, 3–40. [CrossRef]

106. Reolid, M.; Gaillard, C.; Olóriz, F.; Rodríguez-Tovar, F.J. Microbial Encrustations from the Middle Oxfordian-Earliest Kimmeridgian Lithofacies in the Prebetic Zone (Betic Cordillera, Southern Spain): Characterization, Distribution and Controlling Factors. *Facies* **2005**, *50*, 529–543. [CrossRef]

107. Gaillard, C. Les Biohermes à Spongiaires et Leur Environment Dans l'Oxfordien Du Jura Méridional. *Trav. Doc. Lab. Géol. Lyon* **1983**, *90*, 3–515.

108. Gaillard, C. Bioconstructions Jurassiques. *Mém. Bur. Rech. Géol. Min. Fr.* **1984**, *125*, 276–281.

109. Rodríguez-Martínez, M.; Heim, C.; Simon, K.; Zilla, T.; Reitner, J. Tolypammina Gregaria Wendt 1969-Frutexites Assemblage and Ferromanganese Crusts: A Coupled Nutrient-Metal Interplay in the Carnian Sedimentary Condensed Record of Hallstatt Facies (Austria). In *Advances in Stromatolite Geobiology*; Reitner, J., Quéric, N.-V., Arp, G., Eds.; Springer: Berlin/Heidelberg, Germany, 2011; pp. 409–434. ISBN 978-3-642-10415-2.

110. Keim, L.; Schlager, W. Quantitative Compositional Analysis of a Triassic Carbonate Platform (Southern Alps. Italy). *Sediment. Geol.* **2001**, *139*, 261–283. [CrossRef]

111. Tosti, F.; Mastandrea, A.; Guido, A.; Demasi, F.; Russo, F.; Riding, R. Biogeochemical and Redox Record of Mid-Late Triassic Reef Evolution in the Italian Dolomites. *Palaeogeogr. Palaeoclimatol. Palaeoecol.* **2014**, *399*, 52–66. [CrossRef]

112. Tinker, S.W. Shelf-to-Basin Facies Distributions and Sequence Stratigraphy of a Steep-Rimmed Carbonate Margin: Capitan Depositional System, Mckittrick Canyon, New Mexico and Texas. *J. Sediment. Res.* **1998**, *68*, 1146–1174. [CrossRef]

113. Kenter, J.A.M.; Harris, P.M.; Della Porta, G. Steep Microbial Boundstone-Dominated Platform Margins—Examples and Implications. *Sediment. Geol.* **2005**, *178*, 5–30. [CrossRef]
114. Reid, R.P.; Macintyre, I.G. Carbonate Recrystallization in Shallow Marine Environments: A Widespread Diagenetic Process Forming Micritized Grains. *J. Sediment. Res.* **1998**, *68*, 928–946. [CrossRef]
115. Reid, R.P.; Macintyre, I.G. Microboring versus Recrystallization: Further Insight into the Micritization Process. *J. Sediment. Res.* **2000**, *70*, 24–28. [CrossRef]
116. Kendall, C.G.S.C.; Alsharhan, A.S. Coastal Holocene Carbonates of Abu Dhabi, UAE: Depositional Setting, Geomorphology, and Role of Cyanobacteria in Micritization. *Int. Assoc. Sedimentol. Spec. Publ.* **2011**, *43*, 205–220.
117. Bathurst, R.G.C. Boring Algae, Micritic Envelopes and Lithification of Molluscan Biosparites. *Geol. J.* **1966**, *5*, 15–32. [CrossRef]
118. Davis, R.A.J.; Dalrymple, R.W. (Eds.) *Principles of Tidal Sedimentology*; Spinger: Berlin/Heidelberg, Germany, 2012; ISBN 9788578110796.
119. Shinn, E.A.; Michael, L.; Ginsburg, R.N. Anatomy of a Modern Carbonate Tidal-Flat, Andros Island, Bahamas. *J. Sediment. Petrol.* **1969**, *39*, 1202–1228.
120. Gischler, E. Sedimentary Facies of Bora Bora, Darwin's Type Barrier Reef (Society Islands, South Pacific): The Unexpected Occurrence of Non-Skeletal Grains. *J. Sediment. Res.* **2011**, *81*, 1–17. [CrossRef]
121. Hunter, A.W.; Underwood, C.J. Palaeoenvironmental Control on Distribution of Crinoids in the Bathonian (Middle Jurassic) of England and France. *Acta Palaeontol. Pol.* **2009**, *54*, 77–98. [CrossRef]
122. Mulder, T.; Alexander, J. The Physical Character of Subaqueous Sedimentary Density Flow and Their Deposits. *Sedimentology* **2001**, *48*, 269–299. [CrossRef]
123. Middleton, G.V.; Southard, J.B. *Mechanics of Sediment Transport. Eastern Section Short Course 3*, 2nd ed.; SEPM Society for Sedimentary Geology: Tulsa, OK, USA, 1984.
124. Mohrig, D.; Elverhoi, A.; Parker, G. Experiments on the Relative Mobility of Muddy Subaqueous and Subaerial Debris flows, and Their Capacity to Remobilize Antecedent Deposits. *Mar. Geol.* **1999**, *154*, 117–129. [CrossRef]
125. Mohrig, D.; Whipple, K.X.; Hondzo, M.; Ellis, C.; PArker, G. Hydroplaning of Subaqueous Debris Flows. *Geol. Soc. Am. Bull.* **1998**, *110*, 387–394. [CrossRef]
126. Iverson, R.M. Physics of Debris Flows. *Rev. Geophys.* **1997**, *35*, 245–296. [CrossRef]
127. Hampton, M.A. Competence of Fine-Grained Debris Flows. *J. Sediment. Petrol.* **1975**, *45*, 834–844. [CrossRef]
128. Hampton, M.A. The role of subaqueous debris flow in generating turbidity currents. *J. Sediment. Petrol.* **1972**, *42*, 775–793.
129. Rasser, M.W.; Riegl, B. Holocene Coral Reef Rubble and Its Binding Agents. *Coral Reefs* **2002**, *21*, 57–72. [CrossRef]
130. Beltrán, Y.; Cerqueda-García, D.; Taş, N.; Thomé, P.E.; Iglesias-Prieto, R.; Falcón, L.I. Microbial Composition of Biofilms Associated with Lithifying Rubble of Acropora Palmata Branches. *FEMS Microbiol. Ecol.* **2016**, *92*, 1–10. [CrossRef] [PubMed]
131. Camoin, G.F.; Gautret, P.; Montaggioni, L.F.; Cabioch, G. Nature and Environmental Significance of Microbialites in Quaternary Reefs: The Tahiti Paradox. *Sediment. Geol.* **1999**, *126*, 271–304. [CrossRef]
132. Piller, W. Involutinacea (Foraminifera) Der Trias Und Des Lias. *Beiträge Paläontol. Osterr.* **1978**, *5*, 1–164.
133. Sarg, J.F. Carbonate Sequence Stratigraphy. In *Sea-Level Changes: An Integrated Approach*; Wilgus, C.K., Hastings, B.S., Posamentier, H., Van Wagoner, J., Ross, C.A., Kendall, C.G.S.C., Eds.; Society for Sedimentary Geology: Tulsa, OK, USA, 1988; pp. 155–182.
134. Schmid, D.U. Marine Mikrobolithe Und Mikroinkrustierer Aus Dem Oberjura. *Profil* **1996**, *9*, 101–251.
135. Watkins, R. Volcaniclastic and Carbonate Sedimentation in Late Paleozoic Island-Arc Deposits, Eastern Klamath Mountains, California. *Geology* **1985**, *13*, 709–713. [CrossRef]
136. Watkins, R. Carboniferous and Permian Island-Arc Deposits of the Eastern Klamath Terrane, California. In *Paleozoic and Early Mesozoic Paleogeographic Relations: Sierra Nevada, Klamath Mountains, And Related Terranes*; Harwood, D.S., Meghan Miller, M., Eds.; Geological Society of America: Boulder, CO, USA, 1990; pp. 193–200.
137. Watkins, R. Carbonate Bank Sedimentation in a Volcaniclastic Arc Setting; Lower Carboniferous Limestones of the Eastern Klamath Terrane, California. *Geology* **1993**, *63*, 966–973.
138. Watkins, R.; Wilson, E.C. Paleoecologic and Biogeographic Significance of the Biostromal Organism Palaeoaplysina in the Lower Permian McCloud Limestone, Eastern Klamath Mountains, California. *Palaios* **1989**, *4*, 181–192. [CrossRef]
139. Hathway, B. Sedimentation and Volcanism in an Oligocene-Miocene Intra-Oceanic Arc and Fore-Arc, Southwestern Viti Levu, Fiji. *J. Geol. Soc. Lond.* **1994**, *151*, 499–514. [CrossRef]
140. Utami, D.A.; Reuning, L.; Cahyarini, S.Y. Satellite- and Field-Based Facies Mapping of Isolated Carbonate Platforms from the Kepulauan Seribu Complex, Indonesia. *Depos. Rec.* **2018**, *4*, 255–273. [CrossRef]
141. Anderson, O. Protozoa, Radiolarians. In *Encyclopedia of Ocean Sciences*; Steve, A.T., Turekian, K.K., Eds.; Academic Press: Oxford, UK, 2001; pp. 613–617. ISBN 978-0-12-374473-9.
142. Soja, C.M. Island-Arc Carbonates: Characterization and Recognition in the Ancient Geologic Record. *Earth-Sci. Rev.* **1996**, *41*, 31–65. [CrossRef]
143. Dorobek, S.L. Carbonate-Platform Facies in Volcanic-Arc Settings: Characteristics and Controls on Deposition and Stratigraphic Development. *Spec. Pap. Geol. Soc. Am.* **2008**, *436*, 55–90. [CrossRef]
144. Meltzner, A.J.; Sieh, K.; Chiang, H.W.; Wu, C.C.; Tsang, L.L.H.; Shen, C.C.; Hill, E.M.; Suwargadi, B.W.; Natawidjaja, D.H.; Philibosian, B.; et al. Time-Varying Interseismic Strain Rates and Similar Seismic Ruptures on the Nias-Simeulue Patch of the Sunda Megathrust. *Quat. Sci. Rev.* **2015**, *122*, 258–281. [CrossRef]

145. López, G. Walther's Law of Facies. In *Encyclopedia of Scientific Dating Methods*; Rink, W.J., Thompson, J.W., Eds.; Springer: Berlin/Heidelberg, Germany, 2015; pp. 957–958. Available online: http://link.springer.com/referenceworkentry/10.1007/978-94-007-6304-3_30 (accessed on 26 January 2022).

146. Frisia-Bruni, S.; Jadoul, F.; Weissert, H. Evinosponges in the Triassic Esino Limestone (Southern Alps): Documentation of Early Lithification and Late Diagenetic Overprint. *Sedimentology* **1989**, *36*, 685–699. [CrossRef]

147. Russo, F.; Gautret, P.; Mastandrea, A.; Perri, E. Syndepositional Cements Associated with Nannofossils in the Marmolada Massif: Evidences of Microbially Mediated Primary Marine Cements? (Middle Triassic, Dolomites, Italy). *Sediment. Geol.* **2006**, *185*, 267–275. [CrossRef]

148. Emmerich, A.; Zamparelli, V.; Bechstädt, T.; Zühlke, R. The Reefal Margin and Slope of a Middle Triassic Carbonate Platform: The Latemar (Dolomites, Italy). *Facies* **2005**, *50*, 573–614. [CrossRef]

149. Stoppani, A. Les Petrifications d'Esino Ou Description Des Fossiles Appartenans Au Depot Superieur Des Environs d'Esino En Lombardie. *Paleontol. Lomb.* **1858**, *1*, 360.

150. German, K. Calcite and Dolomite Fibrous Cements (Grossoolith) in the Reef Rocks of the Wettersteinkalk (Ladinian, Middle Trias), Northern Limestone Alps, Bavaria and Tyrol. In *Carbonate Cements*; Bricker, O.P., Ed.; Johns Hopkins Press: Baltimore, MA, USA, 1971; pp. 185–188.

151. McKenzie, J.A.; Lister, G. Origin of Alternating Calcite and Dolomite Void Filling Cements (Grossoolites)in Middle Triassic Reefs of the Northern Limestone Alps near Innsbruck, Austria. In *I.A.S. 4th European Regional Meeting Abstracts Book*; International Association of Sedimentologists: Split, Yugoslavia, 1983; pp. 156–157.

152. Cosjin, J. De Geologie van the Valle Di Olmo Al Brembo. *Leid. Geol. Med.* **1928**, *2*, 251–324.

153. Hofsteenge, L. La Geologie de La Valee Du Brembo et de Ses Affluents Entre Lenna et San Pellegrino. *Leid. Geol. Med.* **1932**, *4*, 25–82.

154. Russo, F.; Mastandrea, A.; Stefani, M.; Neri, C. Carbonate Facies Dominated by Syndepositional Cements: A Key Component of Middle Triassic Platforms. The Marmolada Case History (Dolomites, Italy). *Facies* **2000**, *42*, 211–226. [CrossRef]

155. Gale, L.; Rigaud, S.; Gennari, V.; Blau, J.; Rettori, R.; Martini, R.; Gaetani, M. Recognition of Upper Triassic Temperate Foraminiferal Assemblages: Insights from the Khodz Group (NW Caucasus, Russia). *Glob. Planet. Chang.* **2020**, *188*, 103152. [CrossRef]

156. Opdyke, B.N.; Wilkinson, B.H. Paleolatitude Distribution of Phanerozoic Marine Ooids and Cements. *Palaeogeogr. Palaeoclimatol. Palaeoecol.* **1990**, *78*, 135–148. [CrossRef]

157. Manzello, D.P.; Kleypas, J.A.; Budd, D.A.; Eakin, C.M.; Glynn, P.W.; Langdon, C. Poorly Cemented Coral Reefs of the Eastern Tropical Pacific: Possible Insights into Reef Development in a High-CO2 World. *Proc. Natl. Acad. Sci. USA* **2008**, *105*, 10450–10455. [CrossRef]

158. Stoner, A.W.; Waite, J.M. Distribution and Behavior of Queen Conch Strombus Gigas Relative to Seagrass Standing Crop. *Fish. Bull. US* **1990**, *88*, 451–460.

159. Stephenson, S.P.; Sheridan, N.E.; Geiger, S.P.; Arnold, W.S. Abundance and Distribution of Large Marine Gastropods in Nearshore Seagrass Beds along the Gulf Coast of Florida. *J. Shellfish Res.* **2013**, *32*, 305–313. [CrossRef]

160. Yancey, T.E.; Stanley, G.D.J. Giant Alatoform Bivalves in the Upper Triassic of Western North America. *Palaeontology* **1999**, *42*, 1–23. [CrossRef]

161. Stanley, G.D.J.; Yancey, T.E.; Shepherd, H.M.E. Giant Upper Triassic Bivalves of Wrangellia, Vancouver Island, Canada. *Can. J. Earth Sci.* **2013**, *50*, 142–147. [CrossRef]

162. Smith, S.V.; Kimmerer, W.J.; Laws, E.A.; Brock, R.E.; Walsh, T.W. Kaneohe Bay Sewage Diversion Experiment: Perspectives on Ecosystem Responses to Nutritional Perturbation. *Pacific Sci.* **1981**, *35*, 279–395.

163. Hallock, P.; Schlager, W. Nutrient Excess and the Demise of Coral Reefs and Carbonate Platforms. *Palaios* **1986**, *1*, 389–398. [CrossRef]

164. Hallock, P. The Role of Nutrient Availability in Bioerosion: Consequences to Carbonate Buildups. *Palaeogeogr. Palaeoclimatol. Palaeoecol.* **1988**, *63*, 275–291. [CrossRef]

165. Hallock, P. Coral Reefs, Carbonate Sedimentation, Nutrients, and Global Change. In *The History and Sedimentology of Ancient Reef Ecosystems*; Stanley, G.D.J., Ed.; Kluwer Academic/Plenum Publishers: New York, NY, USA, 2001; pp. 387–427.

166. Mutti, M.; Hallock, P. Carbonate Systems along Nutrient and Temperature Gradients: Some Sedimentological and Geochemical Constraints. *Int. J. Earth Sci.* **2003**, *92*, 465–475. [CrossRef]

167. Camoin, G.F.; Cabioch, G.; Eisenhauer, A.; Braga, J.C.; Hamelin, B.; Lericolais, G. Environmental Significance of Microbialites in Reef Environments during the Last Deglaciation. *Sediment. Geol.* **2006**, *185*, 277–295. [CrossRef]

168. Elliott, G.F. Ecologic Significance of Post-Palaeozoic Green Calcareous Algae. *Geol. Mag.* **1978**, *115*, 437–442. [CrossRef]

169. Ott, E. Die Gesteinsbildenden Kalkalgen Im Schlauchkar (Karwendelgebirge). *Jb. Ver. Schutze Alpenpfl.* **1966**, *31*, 1–8.

170. Ott, E. Dasycladaceen (Kalkalgen) Aus Der Nordalpinen Obertrias. *Mitt. Bayer. Staatssamml. Palaont. Hist. Geol.* **1967**, *7*, 205–226.

171. Ott, E. Mitteltriadischen Riffe Der Nördlichen Kalkalpen Und Altersgleiche Bildungen Auf Karaburun Und Chios (Ägäis). *Mitt. Ges. Geol. Bergbaustud.* **1972**, *21*, 251–276.

172. Di Stefano, P.; Senowbari-Daryan, B. Upper Triaissic Dasycladales (Green Algae) from the Palermo Mountains (Sicily, Italy). *Geol. Rom.* **1985**, *24*, 189–220.

173. Bodeur, Y. Le Complexe Récifal Jurassique Supérieur Au Sud Des Cévennes: Architecture Sédimentologique. *C. R. Acad. Sc.* **1976**, *282*, 835–837.

174. Rigaud, S. The Late Triassic Martin Bridge Carbonate Platform (Wallowa Terrane, NW U.S.A.): Sedimentology, Biostratigraphy, and Contribution to the Understanding of Aragonitic and Microgranular Foraminifers. Ph.D. Thesis, University of Geneva, Geneva, Switzerland, 2012.

175. Zorn, H. Über Den Lebensraum Fossiler Wirtelalgen in Der Trias Der Alpen. *Naturwissenschaften* **1976**, *63*, 426–429. [CrossRef]

176. Zorn, H. Del Einfluss Der Umwelt Auf Die Variation Fossiler Arten. *Nat. Mus.* **1977**, *107*, 1–5.

177. Payne, J.L. Evolutionary Dynamics of Gastropod Size across the End-Permian Extinction and through the Triassic Recovery Interval. *Paleobiology* **2005**, *31*, 269–290. [CrossRef]

178. Ketwetsuriya, C.; Nose, M.; Charoentitirat, T.; Nützel, A. Microbial-, Fusulinid Limestones with Large Gastropods and Calcareous Algae: An Unusual Facies from the Early Permian Khao Khad Formation of Central Thailand. *Facies* **2020**, *66*, 21. [CrossRef]

179. Stanton, R.J.; Flügel, E. Problems with Reef Models: The Late Triassic Steinplatte " Reef " (Northern Alps, Salzburg/Tyrol, Austria). *Facies* **1989**, *33*, 1. [CrossRef]

180. Connolly, M.W.; Lambert, L.L.; Stanton, R.J. Paleoecology of Lower and Middle Pennsylvanian (Middle Carboniferous) Chaetetes in North America. *Facies* **1989**, *20*, 139–168. [CrossRef]

181. Heindel, K.; Birgel, D.; Peckmann, J.; Kuhnert, H.; Westphal, H. Formation of Deglacial Microbialites in Coral Reefs off Tahiti (IODP 310) Involving Sulfate-Reducing Bacteria. *Palaios* **2010**, *25*, 618–635. [CrossRef]

182. Sánchez-Beristain, F.; Reitner, J. Paleoecology of Microencrusters and Encrusting "Coralline" Sponges in Cipit Boulders from the Cassian Formation (Upper Ladinian-Lower Carnian, Dolomites, Northern Italy). *Palaontol. Z.* **2012**, *86*, 113–133. [CrossRef]

183. Monty, C.L. Cavity or Fissure Dwelling Stromatolites (Endostromatolites) from Belgian Devonian Mud Mounds (Exteded Abstracts). *Ann. Soc Géol. Belg.* **1982**, *105*, 343–344.

184. Granier, B. The Biosignature of Sparite Permits the Distinction between Gravitational Cement and Endostromatolites. *Carnets Geol.* **2020**, *20*, 407–419. [CrossRef]

185. Schopf, W.J. The Fossil Record of Cyanobacteria. In *Ecology of Cyanobacteria II: Their Diversity in Space and Time*; Whitton, B.A., Ed.; Springer: Berlin/Heidelberg, Germany, 2012; pp. 15–36.

186. Hohenegger, J.; Piller, W. Ökologie Und Systematische Stellung Der Foraminiferen Im Gebankten Dachsteinkalk (Obertrias) Des Nördlichen Toten Gebirges (Oberösterreich). *Palaeogeogr. Palaeoclimatol. Palaeoecol.* **1975**, *18*, 241–276. [CrossRef]

187. Zaninetti, L.; Ciarapica, G.; Cirilli, S.; Cadet, J.-P. Miliolechina Stellata, n. Gen., n. Sp., et Hirsutospirella Pilosa, n. Gen., n. Sp. (Foraminifères), Dans Le Trias Supérieur (Norien) à Faciès Récifal Des Dinarides. *Rev. Paléobiol.* **1985**, *4*, 331–341.

188. Martini, R.; Zaninetti, L.; Ciarapica, G. Hirsutospirella Pilosa Zaninetti, Ciarapica, Cirilli et Cadet, 1985. (Foraminifère, Trias Supérieur), Morphologie et Paléobiologie. *Rev. Paléobiol.* **1986**, *5*, 193–196.

189. Márquez, L. Foraminiferal Fauna Recovered after the Late Permian Extinctions in Iberia and the Westernmost Tethys Area. *Palaeogeogr. Palaeoclimatol. Palaeoecol.* **2005**, *229*, 137–157. [CrossRef]

190. Martini, R.; Zaninetti, L.; Lathuilière, B.; Cirilli, S.; Cornée, J.J.; Villeneuve, M. Upper Triassic Carbonate Deposits of Seram (Indonesia): Palaeogeographic and Geodynamic Implications. *Palaeogeogr. Palaeoclimatol. Palaeoecol.* **2004**, *206*, 75–102. [CrossRef]

191. Jones, R.W. *Foraminifera and Their Applications*; Cambridge University Press: New York, NY, USA, 2014; ISBN 9781139567619.

192. Martindale, R.C.; Corsetti, F.A.; James, N.P.; Bottjer, D.J. Paleogeographic Trends in Late Triassic Reef Ecology from Northeastern Panthalassa. *Earth-Sci. Rev.* **2015**, *142*, 18–37. [CrossRef]

193. Sun, Y.; Orchard, M.J.; Kocsis, T.; Joachimski, M.M. Carnian–Norian (Late Triassic) Climate Change: Evidence from Conodont Oxygen Isotope Thermometry with Implications for Reef Development and Wrangellian Tectonics. *Earth Planet. Sci. Lett.* **2020**, *534*, 116082. [CrossRef]

194. Martindale, R.C.; Zonneveld, J.P.; Bottjer, D.J. Microbial Framework in Upper Triassic (Carnian) Patch Reefs from Williston Lake, British Columbia, Canada. *Palaeogeogr. Palaeoclimatol. Palaeoecol.* **2010**, *297*, 609–620. [CrossRef]

195. Martindale, R.C.; Bottjer, D.J.; Corsetti, F.A. Platy Coral Patch Reefs from Eastern Panthalassa (Nevada, USA): Unique Reef Construction in the Late Triassic. *Palaeogeogr. Palaeoclimatol. Palaeoecol.* **2012**, *313–314*, 41–58. [CrossRef]

196. Oldow, J.S. Structure and Stratigraphy of the Luning Allochthon and the Kinematics of Allochthon Emplacement, Pilot Mountains, West-Central Nevada. *Geol. Soc. Am. Bull.* **1981**, *92*, 888–911. [CrossRef]

197. Zonneveld, J.P.; Henderson, C.M.; Stanley, G.D.J.; Orchard, M.J.; Gingras, M.K. Oldest Scleractinian Coral Reefs on the North American Craton: Upper Triassic (Carnian), Northeastern British Columbia, Canada. *Palaeogeogr. Palaeoclimatol. Palaeoecol.* **2007**, *243*, 421–450. [CrossRef]

198. Vérard, C. Panalesis: Towards Global Synthetic Palaeogeographies Using Integration and Coupling of Manifold Models. *Geol. Mag.* **2019**, *156*, 320–330. [CrossRef]

199. Preto, N.; Kustatscher, E.; Wignall, P.B. Triassic Climates—State of the Art and Perspectives. *Palaeogeogr. Palaeoclimatol. Palaeoecol.* **2010**, *290*, 1–10. [CrossRef]

200. Buser, S.; Ramovš, A.; Turnšek, D. Triassic Reefs in Slovenia. *Facies* **1982**, *6*, 15–23. [CrossRef]

201. Gale, L. Rhaetian Foraminiferal Assemblage from the Dachstein Limestone of Mt. Begunjscica (Kosuta Unit, Eastern Southern Alps). *Geologija* **2012**, *55*, 17–44. [CrossRef]

202. Gale, L.; Kastelic, A.; Rozic, B. Taphonomic Features of Late Triassic Foraminifera from Mount Begunjscica, Karavanke Mountains, Slovenia. *Palaios* **2013**, *28*, 771–792. [CrossRef]

203. Senowbari-Daryan, B. Coralline Schwämme Aus Dem Norisch-Rhätischen Dachstein- Riff Des Gosaukammes (Nördliche Kalkalpen, Österreich). *Jahrb. Geol. Bundesanst.* **2009**, *149*, 111–166.

204. Senowbari-Daryan, B. Solenoporaceen Aus Den Obertriassischen (Nor) Riffkalken Des Taurusgebirges (Antalya-Gebiet, Südtürkei). *Palaontol. Z.* **2005**, *79*, 409–427. [CrossRef]
205. Senowbari-Daryan, B.; Reitner, J.; Neuweiler, F.; Gunkel, F. Upper Triassic Reefs and Reef Communities of Iran. *Gottinger Arb. Geol. Paläontol.* **1996**, *2*, 299–304.
206. Senowbari-Daryan, B.; Seyed-Emami, K.; Aghanabati, A. Some Inozoid Sponges from Upper Triassic (Norian-Rhaetian) Nayband Formation of Central Iran. *Riv. Ital. Paleontol. Stratigr.* **1997**, *103*, 293–322.
207. Senowbari-Daryan, B.; Hamadani, A. Thalamid Sponges from the Upper Triassic (Norian-Rhaetian) Nayband Formation near Wali-Abad, SE Abadeh, Central Iran. *Riv. Ital. Paleontol. Stratigr.* **1999**, *105*, 79–100.
208. Senowbari-Daryan, B. Peronidellen (Schwämme) Aus Der Trias Und Beschreibung von Peronidella Iranica n. Sp. Aus Der Obertrias (Nor-Rhät) Des Iran Und von Österreich. *Jahrb. Geol. Bundesanst.* **2003**, *143*, 63–72.
209. Senowbari-Daryan, B.; Hamadani, A. Obertriadische (Nor) Dasycladaceen Aus Der Nayband-Formation Vom Zentraliran. *Rev. Paléobiol.* **2000**, *19*, 97–121.
210. Senowbari-Daryan, B.; Amirhassankhani, F. Lovcenipora Iranica Nov. Sp., an Unusually Large Chaetetid Sponge from the Upper Triassic (Howz-e Khan Member, Nayband Formation) of Northeast Iran. *Zitteliana* **2013**, *53*, 15–22.
211. Senowbari-Daryan, B.; Rashidi, K.; Amirzadeh, M.; Saberzadeh, B.; Talebi, A. Sponges from the Upper Triassic (Norian–Rhaetian) Nayband Formation, Northeast Iran. *Jb. Geol. B.A. Wien* **2011**, *113A*, 347–355.
212. Senowbari-Daryan, B.; Schäfer, P.; Abate, B. Obertdadische Rifle Und Rifforganismen in Sizilien (Beiträge Zur Paläontologie Und Mikrofazies Obertriadischer Riffe Im Alpin-Mediterranen Raum, 27). *Facies* **1982**, *6*, 165–183. [CrossRef]
213. Senowbari-Daryan, B. Mikroproblematika Aus Den Obertriadischen Riffkalken von Sizilien. *Münster. Forsch. Geol. Paläont.* **1984**, *61*, 1–181.
214. Stanley, G.D.J.; Senowbari-Daryan, B. Upper Triassic, Dachstein-Type, Reef Limestone from the Wallowa Mountains, Oregon: First Reported Occurrence in the United States. *Palaios* **1986**, *1*, 172–177. [CrossRef]
215. Senowbari-Daryan, B. Die Systematische Stellung Der Thalamiden Schwämme Und Ihre Bedeutung in Der Erdgeschichte. *Münchner Geowiss. Abh.* **1990**, *A-21*, 5–326.
216. Zaninetti, L. Orthotrinacria, n. Gen.,(Protista: Foraminiferida) from Upper Triassic (Norian) Reefs of Sicily. *Rev. Paléobiologie* **1985**, *4*, 297–300.
217. Di Stefano, P.; Gullo, M.; Senowbari-Daryan, B. The Upper Triassic Reef of Monte Genuardo (Southwestern Sicily). *Boll. della Soc. Geol. Ital.* **1990**, *109*, 103–114.
218. Senowbari-Daryan, B.; Di Stefano, P.; Abate, B. *Hypercalcified Sponges from the Upper Triassic (Norian-Rhaetian) Reefs of Sicily*; Quaderni del Museo Geologico: Palermo, Italy, 2015; pp. 1121–1415.
219. Senowbari-Daryan, B.; Link, M. Hypercalcified Segmented Sponges ("sphinctozoans") from the Upper Triassic (Norian) Reef Boulders of Taurus Mountains (Southern Turkey). *Facies* **2011**, *57*, 663–693. [CrossRef]
220. Senowbari-Daryan, B.; Link, M. A New Thalamid Sponge from the Upper Triassic (Norian) Reef Limestones of the Antalya Region (Turkey). *Acta Geol. Hung.* **1998**, *42*, 343–354.
221. Senowbari-Daryan, B.; Link, M.; Garcia-Bellido, D.C. Fanthalamia Kadiri n. Sp., a New "Sphinctozoan" Sponge from the Triassic (Carnian) of Turkey. *Stud. UBB Geol.* **2003**, *48*, 125–131. [CrossRef]
222. Okay, A.I.; Altiner, D. Uppermost Triassic Limestone in the Karakaya Complex- Stratigraphic and Tectonic Significance. *Turk. J. Earth Sci.* **2004**, *13*, 187–199.
223. Senowbari-Daryan, B.; Link, M. Bicoelia Corticifera, a New Inozoid Sponge from the Upper Triassic (Norian) Reef Boulders of the Central Taurids (Southern Turkey). *Turk. J. Earth Sci.* **2014**, *23*, 575–579. [CrossRef]
224. Martindale, R.C.; Corsetti, F.A.; Bottjer, D.J.; Senowbari-Daryan, B. Microbialite Fabrics and Diminutive Skeletal Bioconstructors in Lower Norian Summit Point Reefs, Oregon, United States. *Palaios* **2012**, *27*, 489–508. [CrossRef]
225. Wood, R. *Reef Evolution*; Oxford University Press: New York, NY, USA, 1999.
226. Nakazawa, T.; Ueno, K.; Wang, X. Sedimentary Facies of Carboniferous-Permian Mid-Oceanic Carbonates in the Changning-Menglian Belt, West Yunnan, Southwest China: Origin and Depositional Process. *Isl. Arc* **2009**, *18*, 94–107. [CrossRef]
227. Milliman, J.D. *Marine Carbonates*; Springer: New York, NY, USA, 1974.
228. Milliman, J.D. Four Southwestern Caribbean Atolls: Courtown Cays, Albuquerque Cays, Roncador Bank and Serrana Bank. *Atoll Res. Bull.* **1969**, *129*, 1–26. [CrossRef]
229. Rankey, E.C.; Reeder, S.L. Holocene Ooids of Aitutaki Atool, Cook Islands, South Pacific. *Geology* **2009**, *37*, 971–974. [CrossRef]
230. Caggiati, M.; Gianolla, P.; Breda, A.; Celarc, B.; Preto, N. The Start-up of the Dolomia Principale/Hauptdolomit Carbonate Platform (Upper Triassic) in the Eastern Southern Alps. *Sedimentology* **2018**, *65*, 1097–1131. [CrossRef]
231. Haas, J.; Piros, O.; Budai, T.; Gorog, A.; Mandl, W.G.; Loobitzer, H. Transition Between the Massive Reef-Backreef and Cyclic Lagoon Facies of the Dachstein Limestone in the Southern Part of the Dachstein Plateau. *Abh. der Geol. Bundesanst.* **2010**, *65*, 35–56.